MAGNETIC PROPERTIES OF CONTINUOUS AND PATTERNED FEPT FILMS

QIU LEIJU

NATIONAL UNIVERSITY OF SINGAPORE

2008

MAGNETIC PROPERTIES OF CONTINUOUS AND PATTERNED FEPT FILMS

QIU LEIJU

(B. SCI., NANJING UNIVERSITY)

A THESIS SUBMITTED

FOR THE DEGREE OF MASTER OF ENGINEERING

DEPARTMENT OF MATERIALS SCIENCE AND ENGINEERING

NATIONAL UNIVERSITY OF SINGAPORE

2008

Acknowledgements

I would like to express my sincere thanks to my supervisor Dr. Ding Jun for his endless guidance and encouragement towards the completion of this thesis. I am really grateful for his efforts in imparting knowledge and experience on magnetic materials, and also for his inspirational advice and expertise to my master project.

My deep appreciation also goes to Dr. Shi Jianzhong and Dr. Chen Jingsheng in Data Storage Institute and Dr. Adekunle Olusola Adeyeye in the Department of Electrical and Computer Engineering, for their support throughout my research.

I wish to give my truly thanks to all of my group members and my colleagues, especially Mr. Liu Binghai, Mr. Yi Jiabao, Mr. Yin Jianhua, Miss. Sirikanjana Thongmee, Mr. Feng Yang, Miss. Zhang Lina, Dr. Tan Mei Chee, and Mr. Yuan Du, from the Department of Materials Science and Engineering, and Mr. Sarjoosing Goolaup from the Department of Electrical and Computer Engineering. All of them were extremely helpful with their assistance and friendship.

The financial support provided by National University of Singapore is gratefully acknowledged.

Last but not least, heartfelt thanks will be given to my family for their kind understanding and unconditional support.

Table of Contents

Abstract

Due to increasing demand in high density recording media, magnetic thin films with high magnetic anisotropy are widely studied to overcome the superparamagnetic effect. Iron-platinum (FePt) thin films with the ordered face-centered tetragonal (fct) phase have drawn significant attention towards high density magnetic recording. The objectives of this project were to fabricate continuous and patterned FePt thin films.

FePt thin films were deposited by pulsed laser deposition (PLD). Post-annealing was carried out. Different underlayers (or substrates): amorphous MgO, crystalline Ag, and (100) textured MgO, were studied. Crystalline Ag and textured MgO underlayers were found more effective to improve magnetic properties. Magnetic properties were also studied in the dependence of post-annealing temperature and FePt film thickness. With the post-annealing temperature ranging from 300 to 800 °C, coercivity of 40 nm thick FePt films grown on all those underlayers increased with the post-annealing temperature until 700 °C. To study the FePt film thickness effects, magnetic properties of FePt thin films with different thicknesses grown on textured MgO underlayer were characterized. It was found that the ordering temperature decreased with the increase of the FePt film thickness. Furthermore, perpendicular magnetic anisotropy was formed in FePt films with thickness less than 10 nm, while the FePt film thickness under study ranged from 5 to 40 nm.

Large area of patterned FePt films were fabricated on Si (100) substrates using deep

ultraviolet lithography with the wavelength of 248 nm, followed by PLD at room temperature, lift-off, and post-annealing in vacuum. Underlayers of Ag or MgO were deposited between Si substrates and FePt films to prevent the chemical reaction between Si and FePt. Phase transformation from the disordered face-centered cubic (fcc) phase to the ordered fct phase started after post-annealing at 500 °C for the patterned FePt films, which was higher than that for the continuous FePt films. However, high coercivity of 10-15 kOe has also been achieved in the patterned FePt films after post-annealing at 700 °C or higher. In addition, effects of Ag or MgO top layers on patterned structure were investigated. It should be noted that the MgO top layer could result in the enhancement of coercivity of the patterned FePt films with a well maintained patterned structure.

List of Figures

List of Tables

List of Publications

1. **Leiju Qiu**, Jun Ding, Adekunle Olusola Adeyeye, Jianhua Yin, Jingsheng Chen, Sarjoosing Goolaup, and Navab Singh. "FePt Patterned Media Fabricated by Deep UV Lithography Followed by Sputtering or PLD", IEEE Trans. Magn. 43, 2157 (2007).

2. **Leiju Qiu**, Jianzhong Shi, S.N. Piramanayagam, Jingsheng Chen, Jun Ding. "Nanocomposite Magnetic Films for High-density Perpendicular Magnetic Recording Media", Thin Solid Films 516, 5381 (2008).

3. **Leiju Qiu**, Jun Ding, Jianzhong Shi, S.N. Piramanayagam, Jingsheng Chen. "Exchange Coupling Effects in CoCrPt–SiO_2/FeCoTaCr Composite Media for Perpendicular Recording", Phys. Scr. T 129, 140 (2007).

CHAPTER 1

Introduction and Literature Review

1.1 Magnetic Recording Media

1.1.1 Principle of Magnetic Recording

Magnetic recording is the dominant storage method in modern computers, because of its competing combination of areal density (the number of bits per unit area on a disk surface) and access time of the hard disk. Figure 1-1 schematically shows the basic working principle of hard disk drive. By switching the direction of the write field generated by the write head, magnetization domains as bits can be written in media. For the reading process, the magnetic flux is then sensed by the read-back head [1].

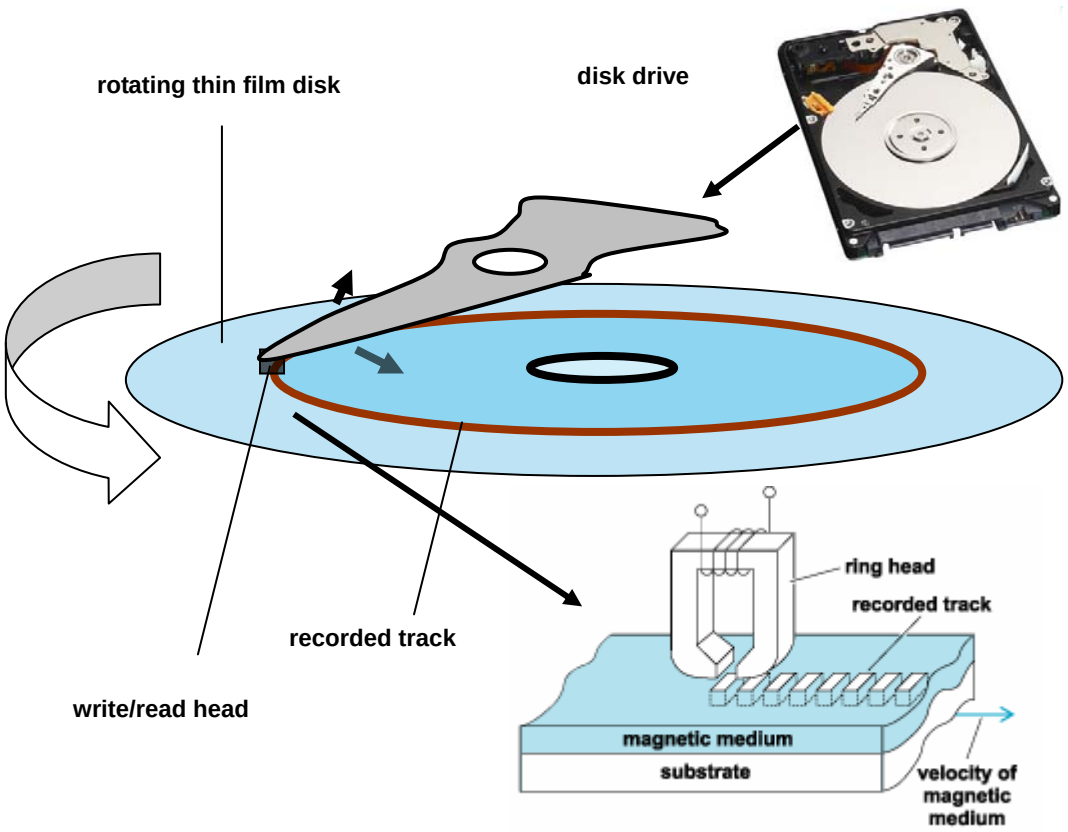

Figure 1-1 Schematic working principle of magnetic recording.

1.1.2 Development Trends of Hard Disk Drive

In today's information explosion era, hard disk has played a key role in data storage. In 1956, IBM built the first magnetic hard disk drive featuring a total storage capacity of 5 MB at a recording density of 2 Kbit/in^2. Since then, the areal density has been increasing at a fast pace, as shown graphically in Figure 1-2 [2,3].

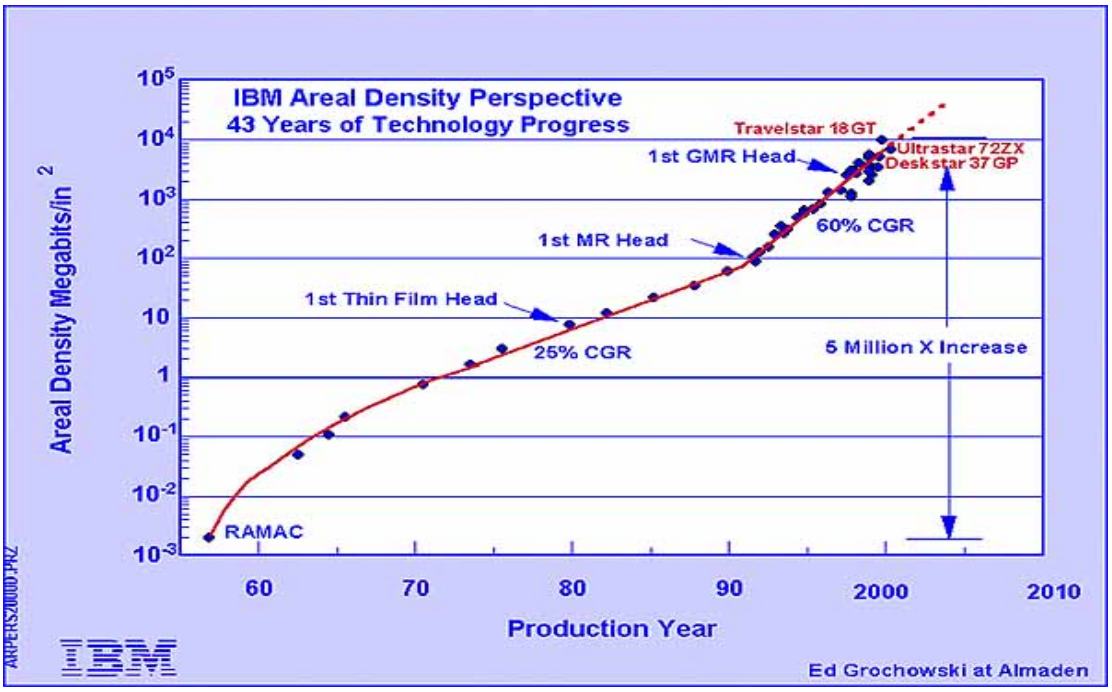

Figure 1-2 Areal density progress in IBM hard disks. (Courtesy of E. Grochowski and R. D. Halem, IBM Systems Journal 42, 338 (2003) Ref. 2)

In the 1970s and 1980s, the areal density underwent an annual compound growth at a rate of ~30%. It should be noted that the significant improvement came in 1991 with the introduction of thin film media as well as the magneto-resistive head. This accelerated the areal density growth from 30% to 60% per annum. Magnetic recording with an areal density up to 10 Gbit/in^2 was demonstrated in 1997. Since then, the

growth rate has been further accelerated to more than 100% per year [4,5]. Theoretical simulation on the other hand shows that the traditional hard disk recording will be limited within ~40 Gbits/in^2 by the superparamagnetic effect [6]. However, the pursuit of higher areal densities still continues by using different methods in manipulating and developing the hard disk media.

1.1.3 Continuous Thin Film Magnetic Recording Media

At present, the commercial magnetic recording system adopts continuous polycrystalline thin film media [7]. As shown in Figure 1-3, the recorded bits in the continuous thin film media are stored in the form of magnetic domains, which consist of several grains. A magnetic transition results in magnetic flux and thus a voltage pulse during the read process, representing a "1", while the absence of the transition represents a "0".

As shown in Figure 1-3, the inevitable existence of the zigzag shape of the transitions between two magnetic domains leads to the read-back noise. To obtain a narrow zigzag-like transition region in continuous thin film recording media, small grain size is required. Furthermore, small gain size reduces the bit size and in turn increases the areal density, which is the main driving force of magnetic recording. However, smaller grains become thermally unstable, which results in the decay of written information in short time-spans [6,8]. When the grain volume decreases to the point where magnetic energy per activation grain K_uV (K_u and V are the magnetic anisotropy energy density

and magnetic switching volume, respectively) becomes comparable with thermal energy K_BT (K_BT is the product of the Boltzman constant and temperature), the grain becomes thermally unstable. The stability factor, K_uV/K_BT can be used to express the thermal stability. A minimal stability factor of 60 is required for maintaining stability of signals for 10 years [9].

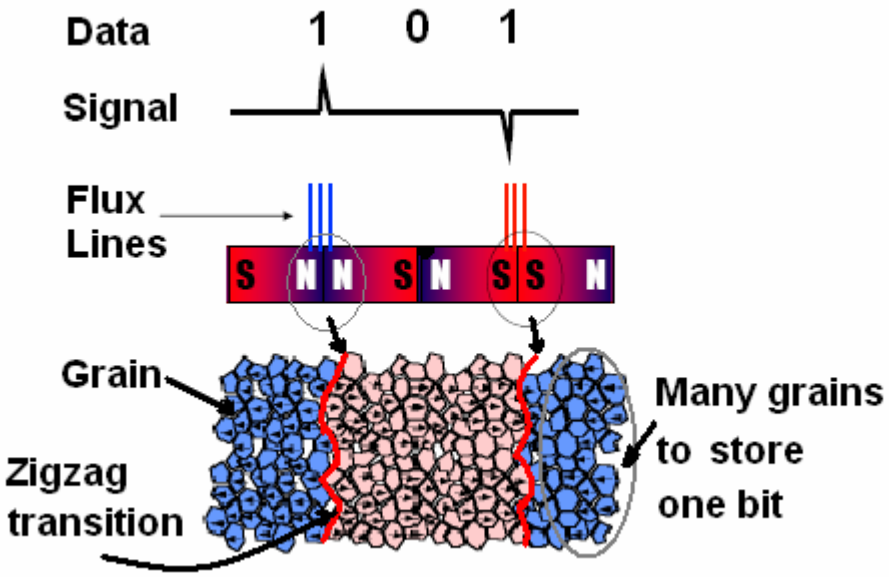

Figure 1-3 Schematic diagram for grains and recorded bits in continuous thin film magnetic recording media.

The volume V of grains typically decreases with the increase of areal density. In order to compensate for a decrease in V, higher K_u materials are needed to maintain sufficient stability [10]. However, at the superparamagnetic limit [11], the scaling of the grain size necessary to maintain the sufficient signal-to-noise ratio (SNR) can no longer be compensated by increasing K_u, due to the limited write fields achievable with

today's write head. The predicted superparamagnetic limit for conventional longitudinal recording is the areal density of 150 Gbit/in^2 [12].

One of the solutions to postpone the superparamagnetic limit is perpendicular recording [13- 16], where recorded information can be packed with greater density and larger write fields enable the enhancement of the thermal stability [17]. However, perpendicular recording has its own superparamagnetic limit and is expected to run out of steam at 1000 Gbit/in^2 [18]. Once perpendicular recording reaches its superparamagnetic limit, new technological innovations will have to occur. For example, patterned media can be utilized to further increase the areal density to well over 1 Tbit/in^2 [19].

1.1.4 Patterned Magnetic Recording Media

Recently, patterned media are regarded as one of the most promising candidates for the next generation of magnetic recording media [20- 22]. As shown in Figure 1-4, the patterned media consist of physically and exchange-isolated nanometer-scaled magnets with a periodicity (magnetic particle arrays). The direction of magnetization in each particle (left-or-right in Figure 1-4 (a) or up-or-down in Figure 1-4 (b)) corresponds to the digital signal of "0" or "1".

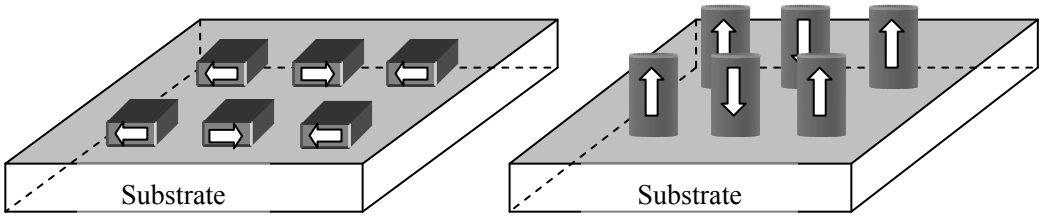

Figure 1-4 Schematic diagram for patterned magnetic recording media (a) longitudinal and (b) perpendicular.

Instead of statistically averaging the signal of many independent grains forming a bit in the continuous thin film media, this single-particle-per-bit recording paradigm in patterned media allows an increase in the thermal activation volume, thus, enhancing the thermal stability. Consequently, ultra-high recording density well beyond 1 Tbit/in^2 is expected to be achieved [4, 23]. Furthermore, patterned recording media can eliminate transition noise, since there are no irregular or zigzag transition regions in patterned media.

The patterned media can provide a higher areal density and lower noise than the continuous thin film recording media. However, the patterning presents a considerable challenge for the manufacturing process. Significant effort [24,25] is devoted to the fabrication of patterned media, the emphasis being on large area preparation, precise position control of particles, mass productivity and low cost. For example, magnetic patterned media have been prepared previously by self-assembled structures [26], the

use of nanotemplates [27], electron beam or focused ion beam lithography [28-30], X-ray lithography [31], interference lithography [32], and nanoimprint lithography [33] etc. Self-assembly methods are suitable for preparing small nanostructures at a low cost. However, precise position control is not achieved. Electron beam lithography is able to control the particle position, while its disadvantage is the small area size patternable in a reasonably short time. It is unlikely to have the low cost and throughput required for patterned media for electron beam lithography.

Deep ultraviolet (DUV) lithography has been successfully used in fabrication of various semiconductor electronic devices and different magnetic films at the submicron and/or nanometer level [34]. DUV light with wavelengths of 248 and 193 nm is ubiquitously used in the current state-of-the-art photolithography tools in the semiconductor manufacturing, which allows minimum feature sizes down to 50 nm [35]. Recently, DUV lithography can be extended to feature sizes below 50 nm using 193 nm light and liquid immersion techniques. For example, in 2006, feature sizes less than 30 nm were demonstrated by IBM using high-index immersion DUV lithography [36]. Although DUV lithography system costs increase as minimum feature size decreases, DUV lithography still remains attractive, because of its high throughput. Therefore, in this work, DUV lithography was used to fabricate the patterned thin films, which have potential application in patterned recording media.

1.1.5 Magnetic Materials for Recording Media

Different recording modes have been proposed to meet the challenges of signal-to-noise-ratio (*SNR*) and thermal stability for high density recording media. Magnetic materials with high coercivity (H_c) and adequate remanent magnetization (M_r) are required to improve the performance of magnetic recording media.

The first electrochemically deposited cobalt thin films for magnetic recording had a coercivity of less than 300 Oe [37]. The addition of nickel and phosphorus to cobalt leads to films with smaller and better isolated grains, thus higher coercivity. Co, Co-P, Co-Ni and Co-Ni-Cr have also been studied to improve the recording density. Currently used longitudinal thin film media are based on Co-Cr with Pt and Ta additions, which show an enhancement of H_c and grain isolation. Pt seems to play a role in increasing the magnetic anisotropy of the cobalt-based thin film and improving the epitaxial relation between the recording layer and the underlayer. Cr and Ta are used to isolate the magnetic grains.

To further increase the coercivity of recording layers, future media, especially the perpendicular recording media, may involve higher anisotropy materials such as CoPt, FePt, and $SmCo_5$. Table 1-1 summarizes the intrinsic magnetic properties of a number of potential alternative media alloys [10,38].

Table 1-1 Intrinsic magnetic properties of the potential alternative media alloys. (Courtesy of D. Weller et al., IEEE Trans. Magn. 36, 10 (2000) Ref. 10)

alloy system	material	K_u (10^7erg/cm^3)	M_s (emu/cm^3)	H_k (kOe)	T_c (K)	δ_w (A)	γ (erg/cm^3)
Co-alloys	CoPtCr	0.20	298	13.7	--	222	5.7
	Co	0.45	1400	6.4	1404	148	8.5
	Co_3Pt	2.0	1100	36	--	70	18
$L1_0$ phases	FePd	1.8	1100	33	760	75	17
	FePt	6.6-10	1140	116	750	39	32
	CoPt	4.9	800	123	840	45	28
	MnAl	1.7	560	69	650	77	16
rare-earth transition metals	$Fe_{14}Nd_2B$	4.6	1270	73	585	46	27
	$SmCo_5$	11-20	910	240-400	1000	22-30	42-57

The table includes the information of the first order magnetocrystalline anisotropy constant K_u, which is K_1 for uniaxial systems; the saturation magnetization M_s; the anisotropy field H_k=2K_u/M_s; the Curie temperature T_C; the intrinsic domain wall width δ_w and the wall energy γ. Many of the Co-alloys are well known bulk hard magnets, which have been extensively studied [39-41]. There is no distinction for the easy axis orientation in these bulk materials. Easy axis alignment is assumed either in-plane for longitudinal recording or out-of-plane for perpendicular recording, depending on the choice of substrates and/or underlayers/seedlayers. Compared to Co-alloys, $SmCo_5$ and FePt systems have anisotropies of ~10^8 erg/cm^3. This offers smaller stable grains. Hence, ultra-high densities, in the Tbit/in^2 regime, would be possible if only stability against thermal agitation is considered [42-45]. Besides high magnetocrystalline anisotropy and high magnetization, face-centered tetragonal (fct) FePt has a better chemical stability than $SmCo_5$. Thus, FePt is a promising candidate for the future perpendicular recording media.

1.2 General Properties of Iron-Platinum

Systematic study on the properties of Fe-Pt alloys started in 1907 [46]. As shown in the phase diagram (Figure 1-5), three intermediate crystal structures have been found: $FePt_3$, FePt, and Fe_3Pt [47].

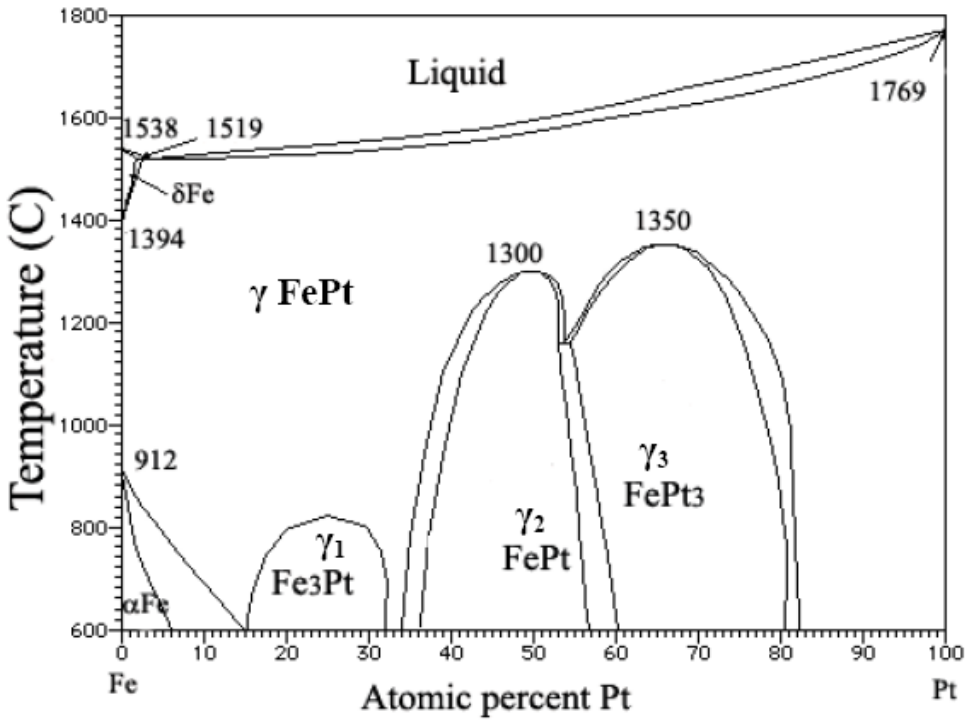

Figure 1-5 Phase diagram for Fe-Pt alloys. (Courtesy of K. Watanabe and H. Masumoto, Trans. Jap. Inst. Met 24, 627 (1983) Ref. 47)

1.2.1 Crystallography of Equiatomic FePt Alloy

The γ phase FePt has a face-centered cubic (fcc) structure, in which Fe and Pt atoms randomly occupy the crystallographic sites (Figure 1-6) [48,49]. The fcc FePt is a disordered phase. The lattice parameter a of γ phase FePt unit cell is 3.878 Å. The γ_2 phase FePt has a face-centered tetragonal (fct) superstructure with Pt atoms at (0 0 0)

and (½ ½ 0) sites and Fe atoms at (½ 0 ½) and (0 ½ ½) sites (Figure 1-6). The fct FePt is an ordered structure. The unit cell of the fct phase FePt has the lattice parameters a = 3.838 Å and c =3.715 Å [44]. In metallurgical nomenclature, this ordered fct structure is also known as the $L1_0$ phase.

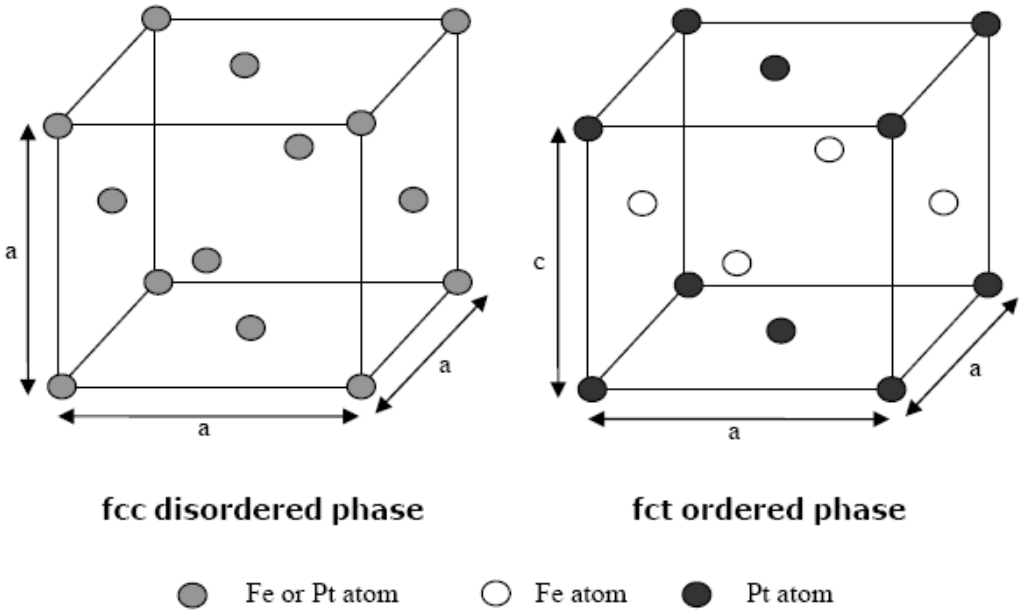

Figure 1-6 Crystal structures for the disordered and ordered phases of the FePt equiatomic alloy.

In general, the disordered fcc phase is formed in the as-prepared state. Phase transformation from disordered fcc FePt to ordered fct FePt occurs, when the fcc phase solid solution is annealed at a relative high temperature. Because the phase transformation is from the disordered structure to the ordered structure, it is also called the ordering process. Consequently, the transformation temperature is called the ordering temperature. During the ordering process, alternative Fe and Pt layers are

formed. The formation of the repeated multilayer structure leads to a slight constriction of lattice in the c-axis direction, and also a decrease in the symmetry of lattice. The ordered structure is often termed as superlattice in literatures [50,51].

1.2.2 Magnetic Properties

The equiatomic FePt alloy is ferromagnetic with a Curie temperature of 670 K [52]. The disordered fcc structure alloy is soft magnetic with $K_1 = 6 \times 10^3$ J/m^3. The ordered fct FePt alloy is hard magnetic, and K_1 has been measured as 7.0×10^6 J/m^3 for bulk alloy. A similar value, $K_1 = 6.0 \times 10^6$ J/m^3, has been reported for thin films of fct phase FePt [53,54]. The saturation magnetization of the ordered phase FePt is slightly lower than that of the disordered fcc phase FePt [55].

Because of its high magnetocrystalline anisotropy and large saturation magnetization, the ordered fct FePt is considered as a promising candidate for hard magnetic applications, especially for high density magnetic recording. However, the disordered fcc phase is usually the major phase in the as-prepared FePt alloy [56]. Therefore, for application as recording media it is necessary to transform the disordered phase into the ordered phase.

1.2.3 Disordered to Ordered Phase Transformation

In 1965, a coercivity of over 7 kOe for the FePt equiatomic alloy was achieved by the formation of the ordered phase via heat treatment to the initially prepared disordered

phase FePt [57]. Since then, heat treatment has always been used as the major method to drive the ordering. As reported, a high temperature above 1000 ^{o}C is required to obtain the phase transformation in bulk FePt alloy [58].

In the early days, research on FePt was concentrated on bulk alloy. Today, with the development of the thin film technology (sputtering, CVD etc), the FePt study is focused on thin films and nanostructures [59- 62]. Generally in FePt bulk alloy, annealing can cause an increase in grain size, which can lead to a decrease in coercivity (H_c) [63]. In thicker films, 300 - 400 nm, the structural and magnetic properties are similar to those of the bulk FePt [64]. It has been reported that relatively lower ordering temperatures (~600 ^{o}C) are found in thinner FePt films [65].

1.2.4 FePt Continuous Thin Films

For commercial application, continuous polycrystalline thin film recording media require high coercivity, as well as small and uniform grains. Generally, the as-prepared FePt thin films at ambient temperature have the disordered fcc phase with low coercivity. To transform the magnetically soft fcc phase to the magnetically hard fct phase, in-situ or post-annealing at a temperature of ~600 ^{o}C or higher is necessary for FePt thin films [65- 68]. Unfortunately, the high temperature annealing may result in the formation of large grains and surface roughness. Thus, it is important to develop methods to reduce the ordering temperature of FePt thin films.

Another key property of the films for high density magnetic recording is that the easy axis should be either in-plane for longitudinal recording media or out-of-plane for perpendicular recording media. However, it is a challenge to develop methods for the preparation of anisotropic FePt films.

It has been reported that using proper underlayers or substrates could be the most effective way to enhance both the phase transformation from disordered fcc phase to ordered fct FePt phase and crystallographic alignment texture in continuous FePt thin films. Ag [69,70], MgO [71-73], CrRu [74,75], AuCu [76], Ti [77], PtMn [78], and silicides [79] underlayers or substrates have been reported to reduce the ordering temperature by inducing strain in the FePt films, originating from the lattice misfit between the underlayers and the FePt films.

With a similar fcc lattice structure to FePt, MgO substrates [71-73] and Ag [69,70] underlayers have received considerable attention in recently years. They were found effective not only in reducing the FePt ordering temperature, but also in inducing the out-of-plane magnetic anisotropy of FePt films. Strain from lattice misfit of the underlayers and FePt films helps expand a-axis and shrink c-axis in the FePt unit cell. Hence, the fct ordered FePt (001) texture can be obtained at relatively low temperatures. Figure 1-7 shows an example of the epitaxial growth of FePt (200) film on MgO (200) underlayer or substrate.

Until now, in most studies single crystal MgO substrates are used to grow epitaxial FePt (001) thin films [80,81]. However, a single crystal MgO substrate is costly, which makes it unattractive for the magnetic recording industry. The unique feature in the present study stems from the usage of single crystal Si (100) substrates. Si substrates are cost-effective and readily available. Moreover, by using Si (100) substrates, integration with the present day microelectronic devices can be achieved. Therefore, Si (100) substrates with MgO underlayers become attractive for the deposition of FePt thin films. It has been reported that textured MgO thin films can be grown on Si (100) substrates using pulsed laser deposition (PLD) [82].

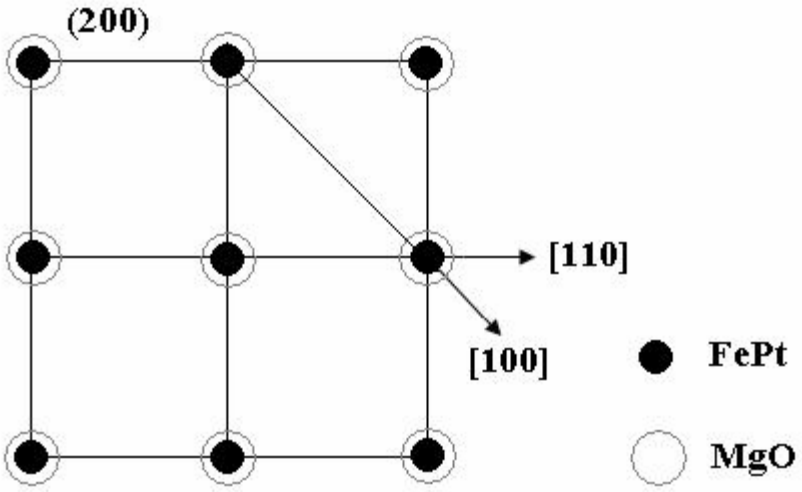

Figure 1-7 Schematic of the epitaxial growth of FePt on MgO underlayer.

1.2.5 FePt Patterned Thin Films

A lot of effort has been done on nanometer-sized patterned structures of magnetic materials, such as CoCrX alloys (where X refers to various additives such as Pt, Ta, Nb, and B) [83,84], CoPt [85-87], CoPd [88] etc, for patterned magnetic recording. However, limitations on the achievable high coercivity leave open questions whether CoCrX alloys are appropriate for patterned magnetic recording [9], as the high coercivity usually requires an energetic process involving deposition at high temperature and/or substrate bias. Such deposition conditions always result in Cr segregation at grain boundaries and exchange decoupling of magnetic gains, which is undesirable in the case of patterned media. This kind of problem does not occur in CoPt and CoPd alloy. However, CoPt and CoPd alloys have lower achievable coercivity than FePt. With high coercivity, patterned FePt thin films seem attractive for the high density patterned magnetic recording.

Studies on self-assembled FePt nanostructures have been carried out [89,90]. However, for patterned FePt nanostructures synthesized by self-assembly, both the shape and the position of the particles are not precisely controlled. To my knowledge, only a few investigations on large areas of uniform patterned FePt structures have been reported [91,92]. In those works, the patterned FePt structures were prepared by fabricating continuous FePt thin films with the ordered fct phase on single crystal MgO substrates followed by microfabrication including electron beam lithography and ion etching. As discussed before, both single crystal MgO substrates and electron beam lithography are

costly. Moreover, it has been reported that the maximum area of the patterned structures by electron beam lithography and etching in reasonable long time is $750 \times 750\,\mu m^2$ [93]. Furthermore, it was stated by Seki *et al*. [92] that the subsequent microfabrication on the as-prepared continuous FePt thin films would degrade the chemical order, which thus would degrade the magnetic properties. Therefore, it is essential to develop a proper preparation process to fabricate large areas of patterned FePt thin films.

1.3 Research Motivation

Due to their excellent magnetic properties, patterned FePt thin films with the ordered fct phase have drawn significant interest for high density patterned magnetic recording. The reported patterned FePt thin films [91,92] fabricated with electron beam lithography and etching on the as-prepared continuous FePt thin films have small area or degraded magnetic properties. Thus, the objective of this project was to develop a process to fabricate large area patterned FePt thin films without reducing the chemical order. Deep ultraviolet (DUV) lithography is efficient to fabricate large areas of patterned structures, so this technology was chosen in my fabrication method. The microfabrication after the as-prepared continuous FePt thin films may degrade the magnetic properties of FePt. If the disordered fcc FePt phase to ordered fct FePt phase transformation occurrs after microfabrication, rather than before microfabrication, the chemical order of the patterned FePt thin films would not be degraded. Hence, our fabrication process consisted of the following steps: coating photo-resist, deep ultraviolet (DUV) exposure to fabricate patterned templates, depositing FePt onto the patterned templates at room temperature, lift-off, and post-annealing. Reasons for post-annealing lay in both the enhancement of the formation of ordered fct phase and the avoidance of damage to the photo-resist.

Though the ordered fct FePt thin films have great magnetic properties, the high ordering temperature for the formation of the fct phase makes it unsuitable for industrial application, because the high temperature heat treatment causes grain growth

and surface roughness. Underlayers are effective in reducing the ordering temperature. In this work, the fabrication of patterned FePt films was on silicon (100) substrates. Si is cost-effective and widely used in industry, but it has a chemical reaction with FePt. So underlayers as buffer layers are necessary to avoid the chemical reaction between FePt and Si. As reported previously, Ag [69] and MgO [71-73] can reduce the ordering temperature of the fct phase and enhance the coercivity. Thus, in this work, Ag and MgO were selected to be underlayers. As pulsed laser deposition (PLD) is efficient in deposition of both metals and oxides, all the films in this work were deposited by PLD.

There are two steps to realize our objective of fabrication of a large area of patterned FePt thin films with the ordered fct phase. To find an optimized condition and also to compare with the pattern FePt thin films, continuous FePt thin films should also be studied. Therefore, the objective of the first part of this project was to fabricate continuous FePt thin films and to improve their magnetic properties by varying the type of underlayers (or substrates), temperature of post-annealing and thickness of FePt films.

The main objective of the second part of this work was to fabricate patterned FePt films and to improve coercivity. However, Based on the reported results of Ishikawa *et al*. [94], thermal agglomeration of the patterned structures at high temperature is severe. So another objective of this work was using top layers to maintain the FePt patterned structures after post-annealing, particularly after annealing at higher

temperatures for the formation of the ordered fct phase with high coercivity.

References:

[1] S. X. Wang and A. M. Taratorin, *Magnetic Information Storage Technology*, Academic Press, Boston (1998).
[2] E. Grochowski and R. D. Halem, IBM Systems Journal 42, 338 (2003).
[3] B. Hayes, Am. Sci. 90, 212 (2002).
[4] D. E. Speliotis, J. Magn. Magn. Mater. 193, 29 (1999).
[5] J. Li, M. Mirzamaani, X. Bian, M. Doerner, S. Duan, et. al., J. Appl. Phys. 85, 4286 (1999).
[6] S. H. Charap, P. L. Lu, and Y. He, IEEE Trans. Magn. 33, 978 (1997).
[7] W. Grogger, K. M. Krishnan, R. A. Ristau, T. Thomson, S. D. Harkness, and R. Ranjan, Appl. Phys. Lett. 80, 1165 (2002).
[8] A. Moser, K. Takano, D. T. Margulies, M. Albrecht, Y. Sonobe, et. al., J. Phys. D: Appl. Phys. 35, R157 (2002).
[9] D. Weller and A. Moser, IEEE Trans. Magn. 35, 4423 (1999).
[10] D. Weller, A. Moser, L. Folks, M. E. Best, et al., IEEE Trans. Magn. 36, 10 (2000).
[11] D. Litvinov, M. H. Kryder, and S. Khizroev, J. Magn. Magn. Mater. 241, 453 (2002).
[12] N. H. Bertram and M. Williams, IEEE Trans. Magn. 36, 4 (1999).
[13] S. Iwasaki and Y. Nakamura, IEEE Trans. Magn. 13, 1272 (1977).
[14] S. Iwasaki, IEEE Trans. Magn. 235, 227 (2001).
[15] R. Wood, Y. Sonobe, Z. Jin, and B. Wilson, J. Magn. Magn. Mater. 235, 1 (2001).
[16] W. Cain, A. Payne, M. Baldwinson, and R. Hempstead, IEEE Trans. Magn. 32, 97 (1996).
[17] S. Khizroev and D. Litvinov, *Perpendicular Magnetic Recording*, Kluwer Academic, London (2004).
[18] R. Wood, J. Miles, and T. Olson, IEEE Trans. Magn. 38, 1711 (2002).
[19] N. Honda, S. Takahashi, K. Ouchi, J. Magn. Magn. Mater. 320, 2195 (2008).
[20] D. A. Thompson and J. S. Best, IBM Journal of Research and Development 44, 311 (2000).
[21] R. L. White, R. M. H. New, and R. F. W. Pease, IEEE Trans. Magn. 33, 990 (1997).
[22] S. Y. Chou, Proc. IEEE 85, 652 (1997).
[23] N. Honda, K. Yamakawa, and K. Ouchi, IEEE Trans. Magn. 43, 2142 (2007).
[24] J. I. Martin, J. Nogues, K. Liu, J. L. Vicent, and I. K. Schuller, J. Magn. Magn. Mater. 256, 449 (2003).
[25] B. D. Terris and T. Thomson, J. Phys. D: Appl. Phys. 38, R199 (2005).
[26] X. M. Yang, C. Liu, J. Ahner, J. Yu, T. Klemmer, E. Johns, and D. Weller, J. Vac. Sci. Technol. B22, 31 (2004).
[27] A. I. Gapin, X. R. Ye, J. F. Aubuchon, L. H. Chen, Y. J. Tang, and S. Jin, J. Appl. Phys. 99, 08G902 (2006).
[28] J. Moritz, B. Dieny, J. P. Nozieres, R. J. M. van de Veerdonk, T. M. Crawford, D. Weller and S. Landis, Appl. Phys. Lett. 86, 063512 (2005).
[29] V. Parekh, E. Chunsheng1, D. Smith, A. Ruiz, J. C. Wolfe, P. Ruchhoeft, E. Svedberg, S. Khizroev, and D. Litvinov, Nanotechnology 17, 2079 (2006).

[30] C. R. Rettner, M. E. Best, and B. D. Terris, IEEE Trans. Magn. 37, 1649 (2001).
[31] C. Miramond, C. Fermon, F. Rousseaux, D. Decanini, and F. Carcenac, J. Magn. Magn. Mater. 165, 500 (1997).
[32] M. Farhoud, M. Hwang, H. I. Smith, M. L. Schattenburg, J. M. Bae, K. Youcef-Toumi, and C. A. Ross, IEEE Trans. Magn. 34, 1087 (1998).
[33] B. Cui, W. Wu, L. Kong, X. Sun, and S. Y. Chou, J. Appl. Phys. 85, 5534 (1999).
[34] C. C. Wang, A. O. Adeyeye, N. Singh, Nanotechnology, 17, 1629 (2006).
[35] M. M. Alkaisi, R. J. Blaikie, and S. J. McNab, Microelectron. Eng. 53, 237 (2000).
[36] A. Hand, Semiconductor International, 29, 24 (2006).
[37] R. C. O'Handley, *Modern Magnetic Materials: Principles and Applications*, John Wiley & Sons, Inc., USA (2000).
[38] T. Klemmer, D. Hoydick, H. Okumura, B. Zhang, and W. A. Soffa, Scripta Metallurgica et Materialia, 33, 1793 (1995).
[39] K. H. J. Buschow, Rep. Prog. Phys. 54, 1123 (1991).
[40] Y. Kubota, L. Folks, and E. E. Marinero, J. Appl. Phys. 84, 6202 (1998).
[41] Y. Yamada, T. Suzuki, H. Kanazawa, and J. C. Österman, J. Appl. Phys. 85, 5094 (1999).
[42] B. Zhang, and W. A. Soffa, Scripta Metallurgica et Materialia, 30, 683 (1994).
[43] L. Graf and A. Kussman, Physik. Z. 36, 544 (1935).
[44] H. Lipson, D. Schoenburg, and G. V. Stupart, J. Inst. Metals. 67, 333 (1941).
[45] J. Sayama, T. Asahi, K. Mizutani, and T. Osaka, J. Phys. D: Appl. Phys. 37, L1 (2004).
[46] E. Isaac and G. Tammann, Z. Anorg. Chem. 55, 63 (1907).
[47] K. Watanabe and H. Masumoto, Trans. Jap. Inst. Met 24, 627 (1983).
[48] T. Goto, H. Utsugi, and K. Watanabe, J. Alloys and Compounds, 204, 173 (1994).
[49] T. Goto, H. Utsugi, and A. Kashiwakara, J. Magn. Magn. Mater. 104, 2051 (1992).
[50] D. E. Laughlin, Encyclopedia of Materials Science and Engineering Supp. Vol. 1, 263 (1988).
[51] D. McKie and M. McKie, *Crystalline Solids*, Thomas Nelson & Sons, London (1974).
[52] M. Fallot, Ann. phys. 10, 291 (1938).
[53] O. A. Ivanov, L. V. Solina, V. A. Demshina, and L. M. Magat, Fiz. metal. metalloved. 35, 92 (1973).
[54] V. G. Pynko, A. S. Komalov, and L. V. Ivaeva, Phys. Stat. Sol., 63a, 127 (1981).
[55] A. Kussman and G. V. Rittberg, Z. Metallkunde 42, 470 (1950).
[56] S. Stavroyiannis, I. Panagiotopoulos, D. Niarchos, J. A. Christodoulides, Y. Zhang, and G. C. Hadjipanayis, J. Appl. Phys. 85, 4304 (1999).
[57] S, Shimizu, and K, Watai, J. Jap. Inst. Met, 29, 822 (1965).
[58] M. H. Hong, K. Hono, and M. Watanabe, J. Appl. Phys. 84, 4403 (1998).
[59] C. H. Lai, C. H. Yang, and C. C. Chiang, Appl. Phys. Lett. 83, 4550 (2003).
[60] T. Maeda, T. Kai, A. Kikitsu, T. Nagase, and J. Akiyama, Appl. Phys. Lett. 80, 2147 (2002).
[61] M. Muller and K. Albe, Acta. Mater. 55, 6617 (2007).
[62] D. J. Sellmyer, Y. F. Xu, M. L. Yan, Y. C. Sui, J. Zhou, R. Skomski, J. Magn. Magn. Mater. 303, 302 (2006).

[63] S. W. Yung, Y. H. Chang, T. J. Lin, and M. P. Hung, J. Magn. Magn. Mater. 116, 411 (1992).
[64] J. A. Aboaf, T. R. McGuire, S. R. Herd, and E. Klokholm, IEEE Trans. Mag. 20, 1642 (1984).
[65] C. P. Luo, S. H. Liou, L. Gao, Y. Liu, and D. J. Sellmyer, Appl. Phys. Lett. 77, 2225 (2000).
[66] T. Suzuki, N. Honda, and K. Ouchi, J. Appl. Phys. 85, 4301 (1999).
[67] C. M. Kuo, P. C. Kuo, H. C. Wu, Y. D. Yao, and C. H. Lin, J. Appl. Phys. 85, 4886 (1999).
[68] M. R. Visokay, and R. Sinclair, Appl. Phys. Lett, 66, 1692 (1995).
[69] Y. Hsu, S. Jeong, D. E. Laughlin, and D. N. Lambeth, J. Magn. Magn. Mater. 260, 282 (2003).
[70] K. Kang, Z. G. Zhang, C. Papusoi, and T. Suzuki, Appl. Phys. Lett. 82, 3284 (2003).
[71] Z. L. Zhao, J. S. Chen, J. Ding, J. B. Yi, B. H. Liu, and J. P. Wang, Appl. Phys. Lett. 88, 052503 (2006).
[72] B. M. Lairson, M. R. Visokay, R. Sinclair, and B. M. Clemens, Appl. Phys. Lett. 62, 639 (1993).
[73] T. Shima, T. Moriguchi, S. Mitani, and K. Takanashi, Appl. Phys. Lett. 80, 288 (2002).
[74] J. S. Chen, B. C. Lim, and T. J. Zhou, J. Vac. Sci, Technol. A, 23, 184 (2005).
[75] Y. F. Xu, J. S. Chen, and J. P. Wang, Appl. Phys. Lett. 80, 3325 (2002).
[76] Y. Zhu and J. W. Cai, Appl. Phys. Lett. 87, 032540 (2005).
[77] S. C. Chen, P. C. Kuo, S. T. Kuo, A. C. Sun, C. Y. Chou, and Y. H. Fang, IEEE Trans. Magn. 41, 915 (2005).
[78] C. C. Chiang, C. H. Lai, and Y. C. Wu, Appl. Phys. Lett. 88, 152508 (2006).
[79] C. H. Lai, C. C. Chiang, and C. H. Yang, J. Appl. Phys. 97, 10H310 (2005).
[80] K. Barmak, J. Kim, L. H. Lewis, K. R. Coffey, M. F. Toney, A. J. Kellock, and J. U. Thiele, J. Appl. Phys. 98, 033904 (2005).
[81] F. Casoli, F. Albertini, L. Pareti, S. Fabbrici, L. Nasi, C. Bocchi, and R. Ciprian, IEEE Trans. Magn. 41, 3223 (2005).
[82] X. Y. Chen, K. H. Wong, C. L. Mak, J. M. Liu, X. B. Yin, M. Wang, and Z. G. Liu, Appl. Phys. A 75, 545 (2002).
[83] M. Albrecht, S. Anders, T. Thomson, C. T. Rettner, M. E. Best, et. al., J. Appl. Phys. 91, 6845 (2002).
[84] C. Haginoya, S. Heike, M. Ishibashi, K. Nakamura, K. Koike, T. Yoshimura, J. Yamamoto, and Y. Hirayama, J. Appl. Phys. 85, 8327 (1999).
[85] T. Aoyama, S. Okawa, K. Hattori, H. Hatate, Y. Wada, et. al., J. Magn. Magn. Mater. 235, 174 (2001).
[86] A. I. Gapin, X. R. Ye, J. F. Aubuchon, L. H. Chen, Y. J. Tang, and S. Jin, J. Appl. Phys. 99, 08G902 (2006).
[87] N. Yasui, A. Imada, and T. Den, Appl. Phys. Lett. 83, 3347 (2003).
[88] V. Parekh, E. Chunsheng, D. Smith, A. Ruiz, J. C. Wolfe, et. al., Nanotechnology 17, 2079 (2006).
[89] N. Shukla, E. B. Svedberg, and J. Ell, Surf. Coat. Tech. 201, 3810 (2006).
[90] S. B. Darling, N. A. Yufa, A. L. Cisse, S. D. Bader, and S. J. Sibener, Adv. Mater. 17, 2446 (2005).
[91] O. Kazakova, M. Hanson, and E. B. Svedberg, IEEE Trans. Magn. 39, 2747 (2003).

[92] T. Seki, T. Shima, K. Yakushiji, and K. Takanashi, J. Appl. Phys. 100, 043915 (2006).
[93] S. M. Cherif and J. F. Hennequin, J. Magn. Magn. Mater. 165, 504 (1997).
[94] Y. Ishikawa, M. Kumezawa, R. Nuryadi, and M. Tabe, Appl. Surf. Sci. 190, 11 (2002).

CHAPTER 2

Synthesis and Characterization

2.1 Samples Fabrication

2.1.1 Continuous Films Fabrication

In this work, thin films were fabricated using pulsed laser deposition (PLD). PLD has drawn wide-spread interest in the past few years for its ease of use and success in depositing materials of complex stoichiometry [1]. As shown in Figure 2-1, a high power pulsed laser beam is focused inside a vacuum chamber to strike a target with desired composition. Materials are then vaporized from the target and deposited as thin films on substrates. Thin film formation process in PLD can be generally divided into four stages: (1) Laser ablation of target materials and creation of plasma; (2) Dynamic of ablation materials; (3) Deposition of ablation materials onto substrates; and (4) Nucleation and growth of thin films on substrate surface. Each stage is crucial for the crystallinity, uniformity and stoichiometry of the resultant films.

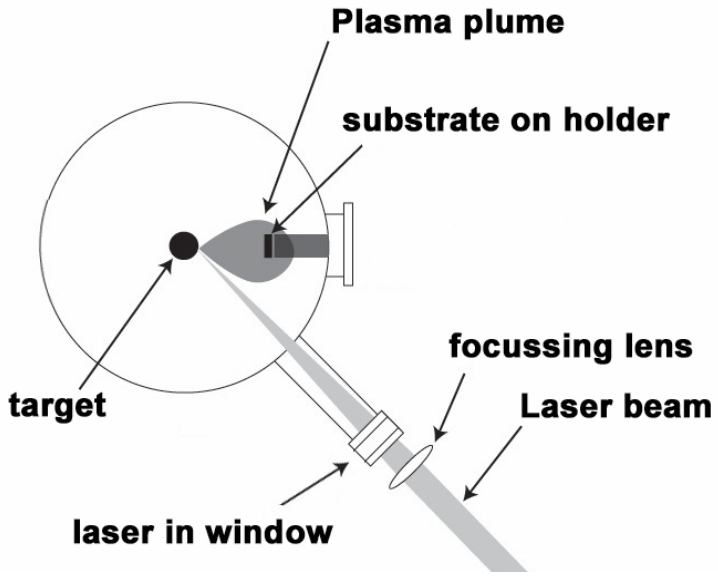

Figure 2-1 Schematic of pulsed laser deposition system.

In the first stage, laser beam is focused onto the surface of targets. At sufficiently high flux density and short pulse duration, all elements in the target are rapidly heated up to their evaporation temperature. Materials are dissociated from the target surface and ablated out with stoichiometry as in the target. The ablation mechanisms involve many complex physical phenomena such as collisional, thermal, and electronic excitation, exfoliation and hydrodynamics.

During the second stage, materials expand in the plasma normal to the target surface towards the substrate due to Coulomb repulsion and recoil from the target surface. Spatial distribution of the plume depends on the background pressure inside the PLD chamber. Density of the plume can be described by a $\cos^n(x)$ law with a shape similar to a Gaussian curve. Both the spot size of the laser and the temperature of the plasma have significant effects on the uniformity of deposited films. The target-to-substrate distance is another factor that governs the angular spread of the ablated materials.

The third stage is important to determine the quality of deposited films. The ejected high-energy species impinge onto the substrate surface and may induce various types of damage to the deposited film by sputtering off atoms from the surface. The sputtered species from the substrate and the particles emitted from the target form a collision region, which serves as a source for condensation of particles. Thus, films grow on the substrate surface at the expense of the direct flow of ablation particles.

Nucleation and growth of crystalline films on substrates depend on several factors, such as density, energy, ionization degree of the ablated materials and temperature, roughness and crystalline properties of substrates. For PLD, the critical nucleus radius is small and in the range of one or two atoms, and the nucleation site density is high, which increase the smoothness of deposited films.

The PLD used in our lab consists of a KrF exciter laser (Lamda Physik Compex 205: 248 nm wavelength, 1 – 50 Hz repetition, and 23 ns pulsed duration), a vacuum chamber with load lock system (~5×10^{-8} Torr optimal base pressure, six rotating targets). FePt thin films were deposited in the high vacuum of 5×10^{-8} Torr, using a FePt alloy target with FePt composition ratio of 1:1. The laser repetition rate and power were 10 Hz and 200 mJ, respectively. In addition, the distance between target and substrate was fixed during deposition at 55 mm.

2.1.2 Patterned Films Fabrication

In this work, the patterned film fabrication process consisted of the following steps: coating of photo-resist, DUV exposure for the fabrication of templates, deposition of FePt at room temperature, lift-off, and post-annealing. This is a typical photolithography process, which transfers a two-dimensional pattern that is formed on a mask into a three-dimensional patterned structure of required materials [2].

Figure 2-2 shows pattern definition in the photo-resist by selective exposure to a radiation source such as UV light. When the photo-resist is placed in a developer solution after selective exposure to a light source, one of the two regions (exposed or unexposed) will be etched away. If the exposed photo-resist is etched away by the developer and the unexposed region remains, it is called positive resist (Figure 2-2 (a)). If the exposed photo-resist remains after developer applied, it is called negative resist (Figure 2-2 (b)).

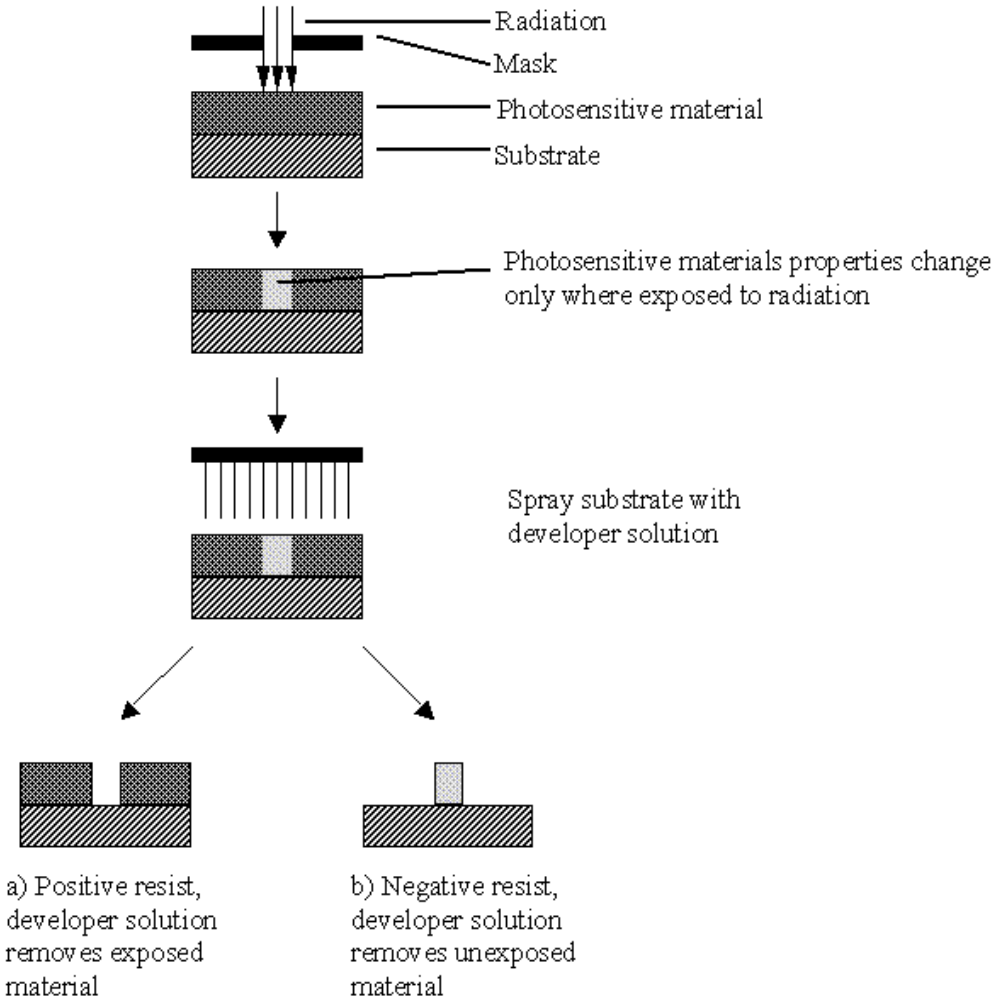

Figure 2-2 Pattern definition in (a) positive resist, and (b) negative resist.

Figure 2-3 shows pattern transfer from patterned photo-resist to required materials. Photo-resist can be used as a temporary mask when etching an underlying layer, so that the pattern can be transferred to the underlying layer. Once the pattern has been transferred to another layer, the resist is usually stripped. Patterned photo-resist can also be used as a template for depositing of required materials. After deposition, materials deposited on the resist and the resist are lifted off.

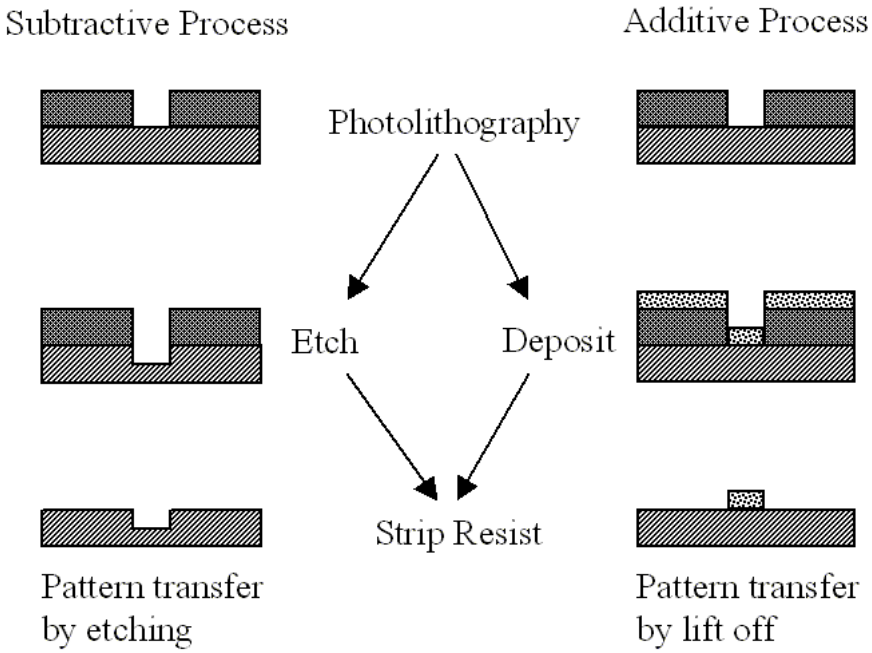

Figure 2-3 Pattern transfer from patterned photo-resist to underlying layer by etching or overlying layer by lift-off.

In this work, the patterned photo-resist templates were fabricated on Si (100) substrates using deep ultraviolet lithography with a wavelength of 248 nm. A 60 nm thick anti-reflective layer and a 480 nm thick positive deep ultraviolet (DUV) photo-resist on the anti-reflective layer were coated on the Si substrates. To prepare the

patterned templates, a Nikon lithography scanner with KrF exciter laser radiation was used to expose the resist. FePt layers and other layers (underlayers and top layers) were deposited by PLD on the patterned templates on Si (100) substrates. After the deposition, the films on patterned resist templates were soaked in an OK 73 thinner to achieve lift-off. After the lift-off, the samples were post-annealed from 300 °C to 800 °C for 30 min in the vacuum of 1×10^{-6} Torr. The procedure of the patterned FePt films fabrication is schematically shown in Figure 2-4.

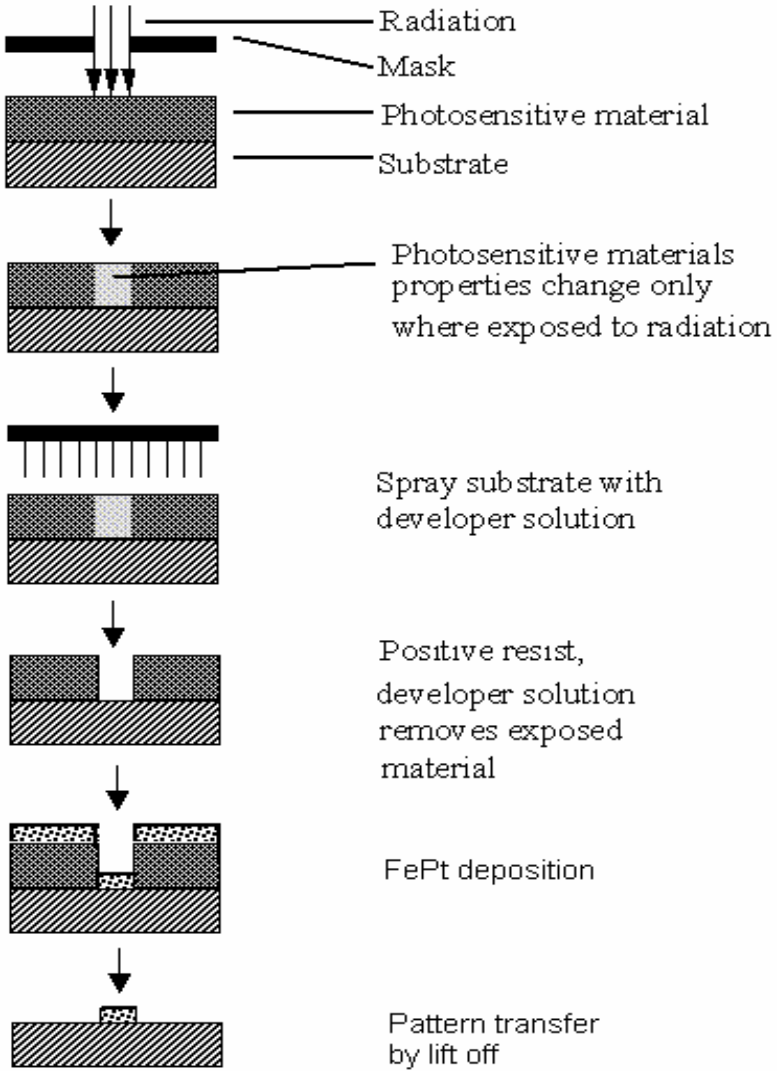

Figure 2-4 Schematic of patterned FePt film fabrication.

2.2 Samples Characterization

2.2.1 X-ray Diffractometer (XRD)

X-ray Diffractometer (XRD) is used to determine crystalline structures of materials. All the XRD results reported in this work were carried out on the Bruker D8 ADVANCE X-ray diffraction, with the monochromatic and Ni filtered Cu K_α radiation (λ=1.54056 Å).

The basic principle of XRD is Bragg's Law (Figure 2-5) [3], which is given by

$$n\lambda = 2d\sin\theta \qquad (2.1)$$

Where n is the integer representing the order of diffraction, λ the wavelength, d the interplanar spacing of the diffraction plane, and θ the angle between the incidence and the diffraction planes.

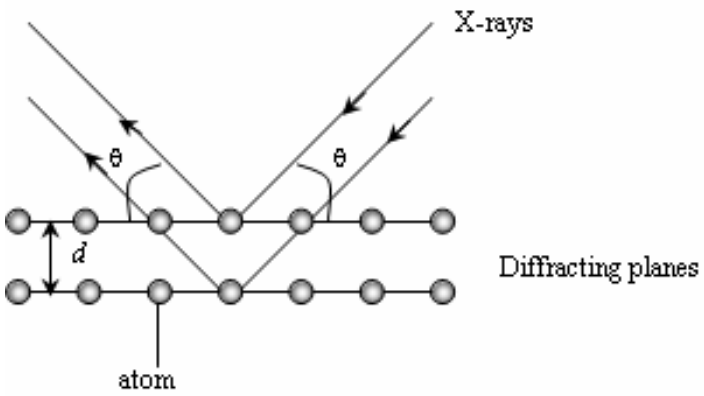

Figure 2-5 Schematic of X-ray diffraction.

For polycrystalline materials, when individual crystals are less than 100 nm in size, the crystallite size can be estimated using Scherrer equation [3]:

$$L = \frac{\kappa\lambda}{B\cos\theta} \qquad (2.2)$$

Where B is the peak width measured at half intensity, κ the particle shape factor (for spherical particles, κ=0.9), and L the diameter of crystallites.

Additionally, the technique of rocking curves was used to determine the crystalline orientation of thin films. The source and detector angles are synchronized to each other, so that Bragg condition is always satisfied for the plane parallel to the surface of the film. As the angle of the incident X-ray beam is varied, the detector will pick up the constructive interference of the reflected X-rays when an angle corresponding to the crystalline lattice spacing of any family planes in the sample is reached. C-axis orientated thin film corresponds to when only one family of planes, i.e. (00l), satisfies the Bragg condition during the θ-2θ scan. The degree of c-axis orientation can be determined with a rocking curve. By fixing the detector angle to the value for the (001) crystalline plane, the source angle can be varied by as much as two degrees around it. The full width at half maximum (FWHM) of the resulting peak thereby gives an indication of the degree c-axis orientation of the crystal.

2.2.2 Vibrating Sample Magnetometer (VSM)

Vibrating sample magnetometer (VSM) is one of the most commonly used equipments for measuring magnetic properties. The VSM used in this work was Lakeshore 7400, with the maximum applied field of 21 kOe at room temperature.

The principle of VSM is based on Faraday's Law [4] of electromagnetic induction, which states that the voltage induced in an electrical circuit is proportional to the rate of change of magnetic flux linking the circuit. The schematic of VSM is shown in Figure 2-6. The sample is mounted at the end of a rigid rod attached to a mechanical resonator, which oscillates the sample at a fixed frequency. The oscillation of the sample in the applied magnetic field alters the magnetic flux through the pick-up coils, which causes an induction voltage in the coils that is proportional to the magnetization of the sample. Thus, the output is proportional to the magnetic moment. In this work, the VSM was used to obtain hysteresis loops of continuous FePt films.

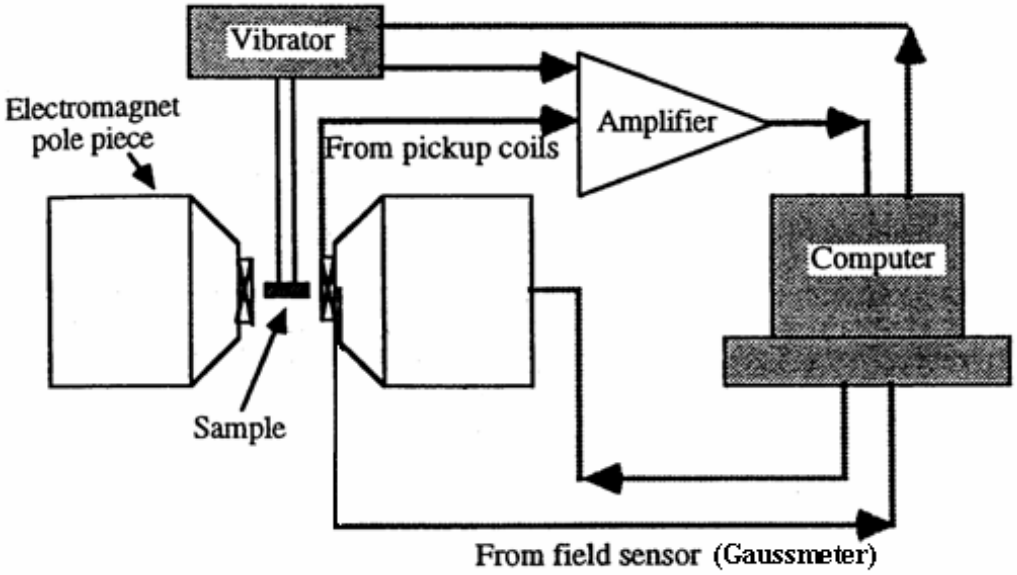

Figure 2-6 Schematic of Vibrating Sample Magnetometer.

2.2.3 Alternating Gradient Force Magnetometer (AGM)

Alternating gradient force magnetometer (AGM) is a useful instrument for measuring magnetic properties [5]. Extremely high sensitivity (10^{-8} emu) and rapid speed of measurement (100 ms per point), combined with compact design and ease of use make AGM a powerful instrument for measuring magnetic properties.

The sample is mounted on an extension rod attached to a piezoelectric element. The top end of the piezoelectric element is rigidly clamped. The force of the field gradient on the magnetized sample produces a bending moment on the piezoelectric element, which generates a voltage proportional to the force of the sample. The output signal from the piezoelectric element is synchronously detected at the operating frequency of the gradient field. The amplitude of this voltage is proportional to the magnetic moment of the sample, which can be varied by changing an applied dc field. The

built-in software automatically determines the mechanical resonance and sets the appropriate operating frequency for the sample under study. The AGM used in this work was in Data Storage Institute, with a maximum applied field of 20 kOe. Because of its high sensitivity, it was used to measure hysteresis loops of the patterned FePt films.

2.2.4 Scanning Electron Microscopy (SEM)

Philips XL30-FEG (Field Emission Gun) Scanning Electron Microscopy (SEM) was used to observe surface morphologies. In SEM, a fine beam of high energy electrons coming from an electron gun is scanned across the sample by the scan coils, while a detector counts the number of low energy secondary electrons or back-scattered electrons given off from each point on the scanned surface. The signal obtained from these types of electrons conveys information on the topology of the sample.

An energy dispersive X-ray (EDX) detector is used for the detection and identification of the X-ray produced by the impact of the electron beam on the sample surface, thus allowing qualitative and quantitative elemental analysis.

2.2.5 Atomic Force Microscopy (AFM)

Atomic force microscopy (AFM) is one of the most powerful tools for determining the surface topography of specimens at sub-nanometer resolution. It reproduces the image of the sample surface using a sharp tip as a probe which is commonly made from

silicon or silicon nitride which is attached to a flexible cantilever with a specific spring constant. The cantilever defects in the Z-direction due to the surface topography during tip scanning. A laser reflecting off the cantilever is tracked by a 4 segment photodiode. The computer processes the electrical differential signal of the photodiode obtained from each point of the surface and generate a feedback signal for a piezo-scanner to maintain a constant force on the tip. This information is then processed into a topographical image.

Based on the interaction between the tip and the sample surface, AFM can be classified as Contact mode, Noncontact mode, and Tapping mode. In the tapping mode AFM, the cantilever is oscillated typically with a frequency of 50 to 500 Hz. When the tip nears the surface, it “taps” the surface which leads to a reduction in oscillation amplitude. This reduction is used to identify and measure surface topographic features. The average cantilever deflections are used as an input signal into the feedback loop to maintain a constant applied force on the surface. In this work, Digital Instrument AFM, Tapping mode was used.

2.2.6 X-ray Photoelectron Spectroscopy (XPS)

Surface analysis by X-ray photoelectron spectroscopy (XPS) involves the irradiation of a solid in a vacuum with monoenergentic soft X-rays in a vacuum chamber and the analysis of the emitted electrons. These photons have limited penetrating power into a solid on the order of 1~10 nanometers. The photons interact with atoms in the surface

region. With the result that the kinetic energy of the electron can be measured as:

$$KE = h\nu - BE - \varphi_s \qquad (2.3)$$

where $h\nu$ is the energy of the photons. BE the binding energy of the atomic orbital from which the electron originates and φ_s the spectrometer work function [6].

The spectrum is obtained by a plot of the number of detected electrons per energy interval versus their kinetic energy. Each element has a characteristic spectrum. The spectrum of a mixture of elements may be considered as the sum of the peaks of the individual constituents. Identification of chemical states can be obtained from an accurate estimation of the separations and peak position, as well as from certain spectral features. In the XPS, the composition of the film can be measured by utilizing the peak area and peak height sensitivity factors.

In this investigation, surface analysis by XPS (PHI Quartera SXM) with a Al Kα (1486.6eV) X-ray source was performed by irradiating a sample with monoenergetic soft x-ray and analyzing the energy of the detected electrons.

References:

[1] D. B. Chrisey, and G. K. Hubler, *Pulsed Laser Deposition of Thin Films*, John Wiley, New York (1994).
[2] D. Banks, *Microengineering, MEMS, and Interfacing: a practical guide*, Dekker/CRC Press, Boca Raton, FL (2006).
[3] B. D. Cullity, *Elements of X-Ray Diffraction*, (International Edition) Addison-Wesley (1978).
[4] S. Foner, Rev. Sci. Instr. 30, 548 (1959).
[5] P. J. Flanders, J. Appl. Phys. 63, 3940 (1988).
[6] D. Briggs and J. T. Grant, *Practical Surface Analysis: By Auger and X-Ray Photoelectron Spectroscopy*, John Wiley & Sons, New York (2003).

CHAPTER 3

Magnetic Properties of Continuous FePt Films

3.1 Introduction

Though the final objective of this work was to fabricate large area of patterned FePt thin films with the ordered face-centered tetragonal (fct) phase, to find an optimized condition and also to compare with the pattern FePt thin films, continuous FePt thin films should be studied. In the literature review section, we note that Ag and MgO underlayers are effective in reducing the ordering temperature of the fct phase and enhance the coercivity. Furthermore, post-annealing temperature is also a vital factor for the formation of the fct phase. However, different groups have obtained different results regarding the different film deposition system. Therefore, it is necessary to obtain the post-annealing temperature dependence of the FePt magnetic properties. The FePt film thickness is another factor that affects the magnetic properties of FePt thin films. Hence, the objective of this part was to fabricate continuous FePt thin films and to improve their magnetic properties by varying type of underlayers (or substrates), temperature of post-annealing and thickness of FePt films.

3.2 Experimental Procedures

Continuous FePt thin films were deposited by pulsed laser deposition in a high-vacuum system with the base pressure of ~5×10^{-8} Torr at room temperature, using a rotating FePt alloy target with FePt composition ratio of approximately 1:1. Si (100) substrates were used. In order to avoid the chemical reaction between FePt and Si, underlayers (amorphous MgO, crystalline Ag or (100) textured MgO) were used. Amorphous MgO and crystalline Ag underlayers were deposited by PLD in the vacuum of ~5×10^{-8} Torr at room temperature. (100) textured MgO underlayer was achieved by PLD on the Si substrate heated up to 800 ^{o}C in the vacuum of ~5×10^{-8} Torr. FePt thin films deposited directly on pretreated natural-oxidized (100) Si substrates (SiO_x) were also prepared for comparison. SiO_x was obtained by annealing Si substrates at 1200 ^{o}C in air for 2 hours. Thus, four series of samples were fabricated (illustrated in Figure 3-1), namely SiO_x/FePt(40 nm), Si/MgO(20 nm, amorphous)/FePt(40 nm), Si/Ag(20 nm, crystalline)/FePt(40 nm), and Si/MgO(100 nm, textured)/FePt(40 nm). After the deposition, all the samples were post-annealed from 300 ^{o}C to 800 ^{o}C for 30 min in the vacuum of 1×10^{-6} Torr.

Generally for FePt thin films with the thickness less than 40 nm, the c-axis (easy axis) can be perpendicular to the plane, so that the films display out-of-plane anisotropy [1]. In this study, FePt films with a thickness of 5 nm, 10 nm, 15 nm, or 40 nm were prepared to study the thickness effect on the enhancement of anisotropy. The (100) textured MgO underlayer was deposited on Si substrates using the same conditions

stated in the last paragraph. The FePt films with the thickness of 5 nm, 10 nm, 15 nm, and 40 nm were deposited at room temperature, respectively. After the deposition, all the samples were post-annealed from 300 ^{o}C to 800 ^{o}C for 30 min in the vacuum of 1×10^{-6} Torr. As shown in Figure 3-2, the samples were named as Si/MgO(100 nm, textured)/FePt(5 nm), Si/MgO(100 nm, textured)/FePt(10 nm), Si/MgO(100 nm, textured)/FePt(15 nm), and Si/MgO(100 nm, textured)/FePt(40 nm), respectively.

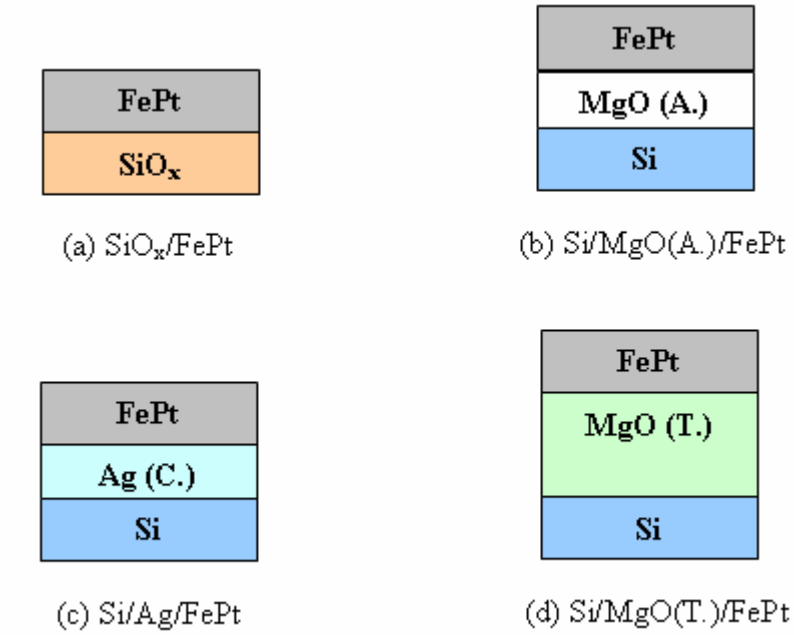

Figure 3-1 Illustration of film structures (a) *SiO_x/FePt(40 nm), (b) Si/MgO(20 nm, amorphous)/FePt(40 nm), (c) Si/Ag(20 nm, crystalline)/FePt(40 nm), and (d) Si/MgO(100 nm, textured)/FePt(40 nm).*

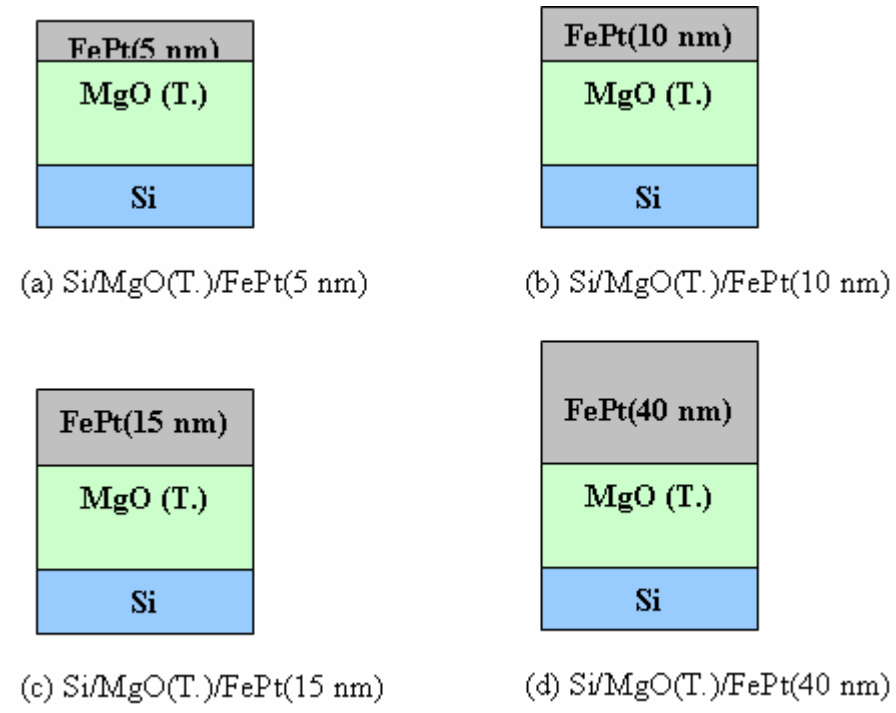

Figure 3-2 Illustration of film structures (a) Si/MgO(100 nm, textured)/FePt(5 nm), (b) Si/MgO(100 nm, textured)/FePt(10 nm), (c) Si/MgO(100 nm, textured)/FePt(15 nm), and (d) Si/MgO(100 nm, textured)/FePt(40 nm).

Composition of the FePt films was measured with SEM/EDX. Magnetic properties of the films were measured using VSM with a maximum applied field 21 kOe. Moreover, crystallographic texture of the films was studied by XRD.

3.3 Results and Discussion

Energy dispersive X-ray (EDX) spectra showed that the ratio of Fe to Pt was ~1:1 for all the FePt thin films. For example, Figure 3-3 (a) shows the EDX spectrum for the FePt film with amorphous MgO underlayer, which had the composition of $Fe_{50.2}Pt_{49.8}$. The inset (Figure 3-3 (b)) presents the scanning electron microscopy (SEM) image of the FePt films deposited by pulsed laser deposition on amorphous MgO underlayers. As SEM images look featureless for all the FePt films, it means that they all have the similar morphology.

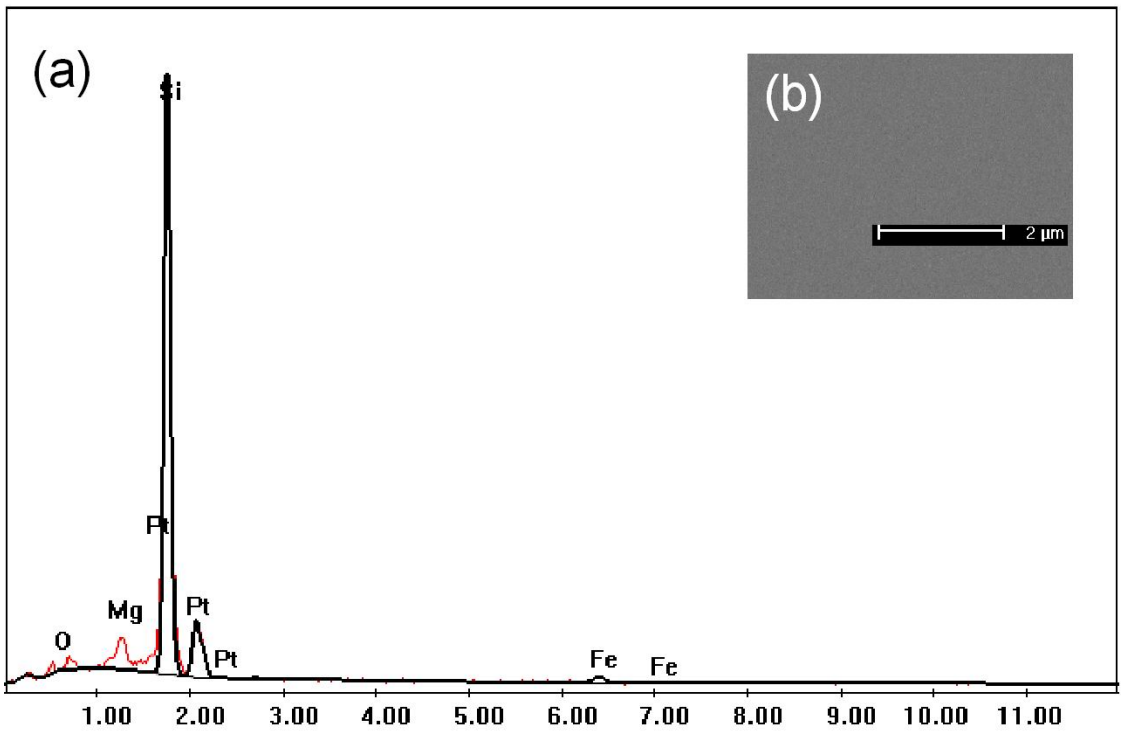

Figure 3-3 (a) EDX spectrum and (b) SEM image for the featherless FePt film with amorphous MgO underlayer.

3.3.1 Magnetic Properties of FePt Films with Different Underlayers

3.3.1.1 FePt Films on SiO_x Substrates

For comparison, FePt films were deposited directly on pretreated naturally-oxidized (100) Si substrates, namely SiO_x/FePt(40 nm).

The normalized magnetization hysteresis loops of the SiO_x/FePt samples post-annealed at different temperatures are shown in Figure 3-4. From the figure, the samples post-annealed at 300 °C or below were magnetically soft. With an increase of the post-annealing temperature from 400 °C, the samples showed the magnetically hard hysteresis loops. Furthermore, when the post-annealing temperature increased, the hysteresis loops became broader and broader, indicating the transformation from the magnetically soft phase to the magnetically hard phase was improved. There were steps in the in-plane hysteresis loops of the samples post-annealed at 700 °C and 800 °C. This result could be understood based on the existence of the magnetically soft phase in the dominant magnetically hard phase.

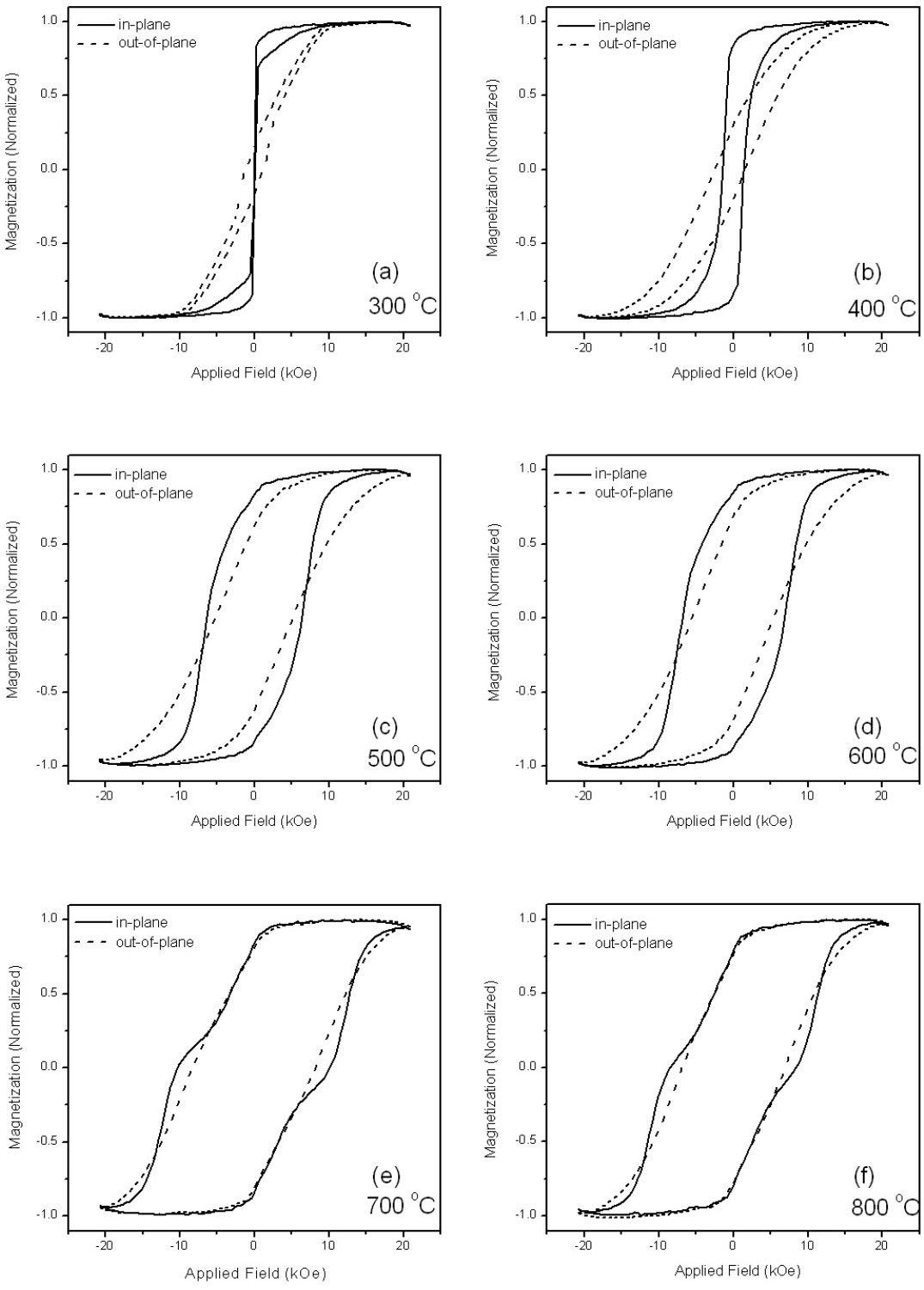

Figure 3-4 Magnetization hysteresis loops of the SiO_x/FePt samples post-annealed at (a) 300 °C, (b) 400 °C, (c) 500 °C, (d) 600 °C, (e) 700 °C, (f) 800 °C.

Figure 3-5 shows the in-plane and out-of-plane coercivity as a function of post-annealing temperature for the SiO_x/FePt samples (The values of the in-plane and out-of-plane coercivity for the SiO_x/FePt samples post-annealed at different temperatures are summarized in Table 3-1). The coercivity was low, when the post-annealing temperature was 300 °C or below, indicating the soft magnetic phase. When the hard magnetic phase was formed and began to be the dominant phase in the FePt films after post-annealing at 500 °C, the in-plane coercivity increased to 6 kOe. Coercivity increased gradually with the increase of the post-annealing temperature and achieved a maximum of 10 kOe after post-annealing at 700 °C. There was some weak in-plane magnetic anisotropy, as the coercivity measured out-of-plane was lower compared to the coercivity measured in-plane.

Table 3-1 In-plane and out-of-plane coercivity of the SiO_x/FePt samples.

Temperature (^{o}C)	**$H_{c\parallel}$ (kOe)**	**$H_{c\perp}$ (kOe)**
300	0.06	1.18
400	1.35	2.17
500	6.12	5.26
600	7.04	5.60
700	10.35	8.25
800	8.87	6.92

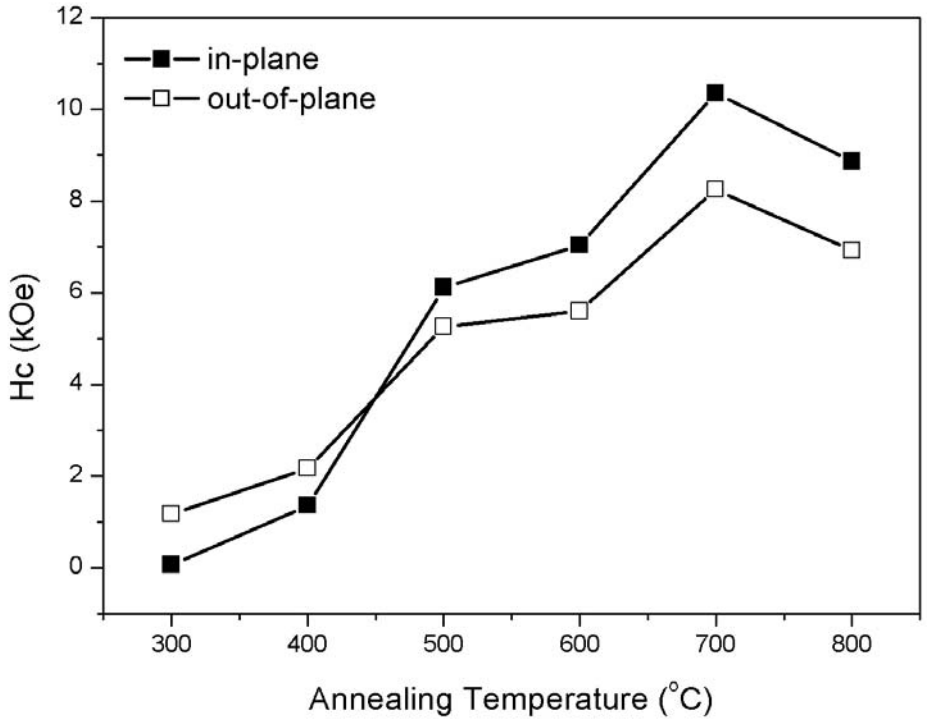

Figure 3-5 In-plane and out-of-plane coercivity of the SiO_x/FePt samples.

XRD patterns of the SiO_x/FePt samples after the post-annealing at different temperatures are shown in Figure 3-6. The FePt films post-annealed at 300 °C or below exhibited the disordered fcc phase with the soft magnetic property, which was consistent with the low coercivity shown in Figure 3-5 and Figure 3-4 (a). As shown in Figure 3-6, with the increase of the post-annealing temperature, the FePt (111) peak gradually shifted to higher angle, indicating the formation of the ordered fct phase with the hard magnetic property. The formation of the magnetically hard fct phase thus explained the increase in coercivity as the post-annealing temperature increased. After the post-annealing at 500 °C, the (001) peak of the FePt fct phase appeared. Moreover, the intensity of this (001) peak increased, as the post-annealing temperature further increased. In addition, the superlattice peak (002) of the fct phase appeared after

post-annealing at 700 °C, indicating the formation of the ordered fct phase was enhanced.

There was a weak and broad FePt (111) peak with the as-deposited film, indicating small grain size. With the increase of the annealing temperature, the peak became sharper, indicating the increase of the grain size. The grain size calculated from the Scherrer formula is plotted in Figure 3-7. The grain size was ~6 nm for the as-deposited sample, and increased continuously to ~32 nm after annealing at 800 °C.

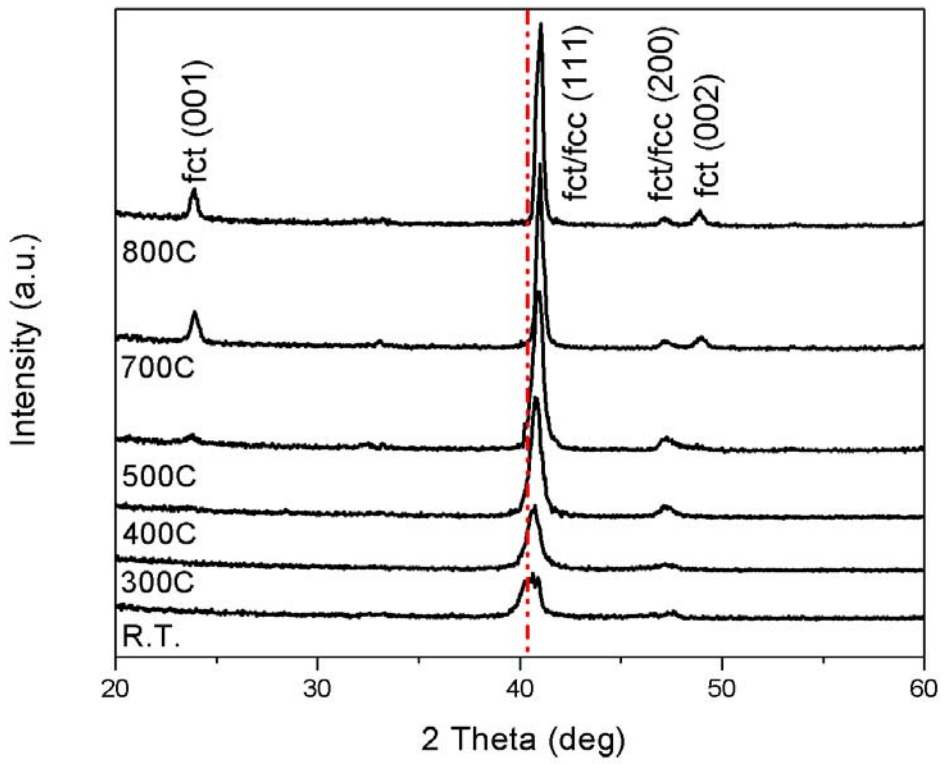

Figure 3-6 XRD patterns of the SiO_x/FePt samples with different annealing temperatures.

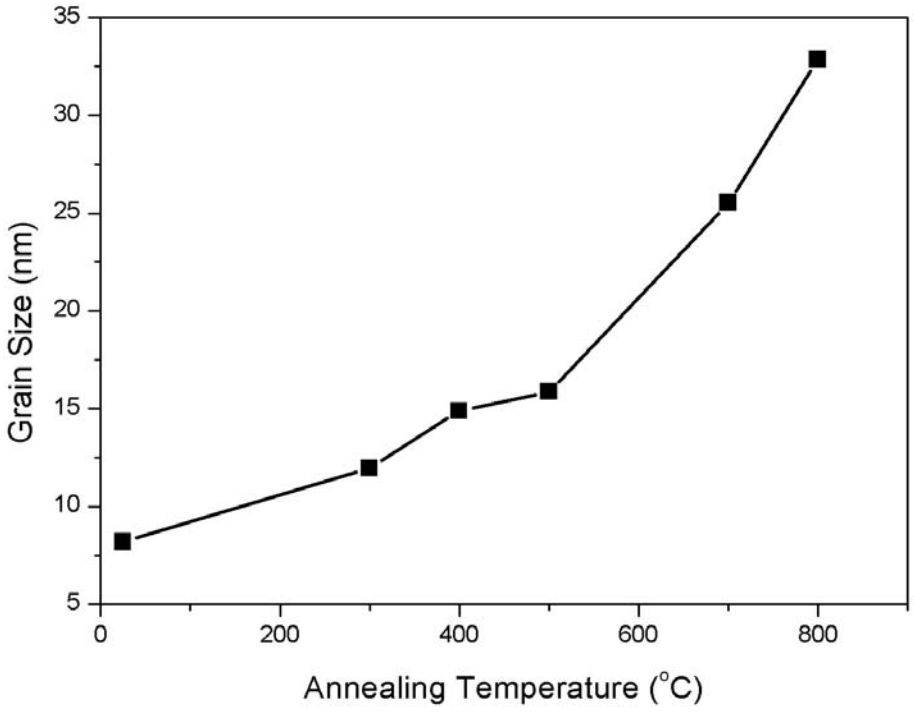

Figure 3-7 Temperature dependence of grain size in the SiO_x/FePt films.

3.3.1.2 FePt Films with Amorphous MgO Underlayers

The pretreated Si substrates (SiO_x substrates) were amorphous materials. Another amorphous underlayer, amorphous MgO underlayer was also studied. Subsequently, the samples were named as Si/MgO(20 nm, amorphous)/FePt(40 nm).

In Figure 3-8, the in-plane and out-of-plane normalized magnetization hysteresis loops of the Si/MgO(amorphous)/FePt samples post-annealed at different temperatures are plotted. Similar hysteresis phenomena as those of the SiO_x/FePt samples were observed in the Si/MgO(amorphous)/FePt samples. However, with the same post-annealing temperature, Si/MgO(amorphous)/FePt samples showed broader hysteresis loops than SiO_x/FePt samples.

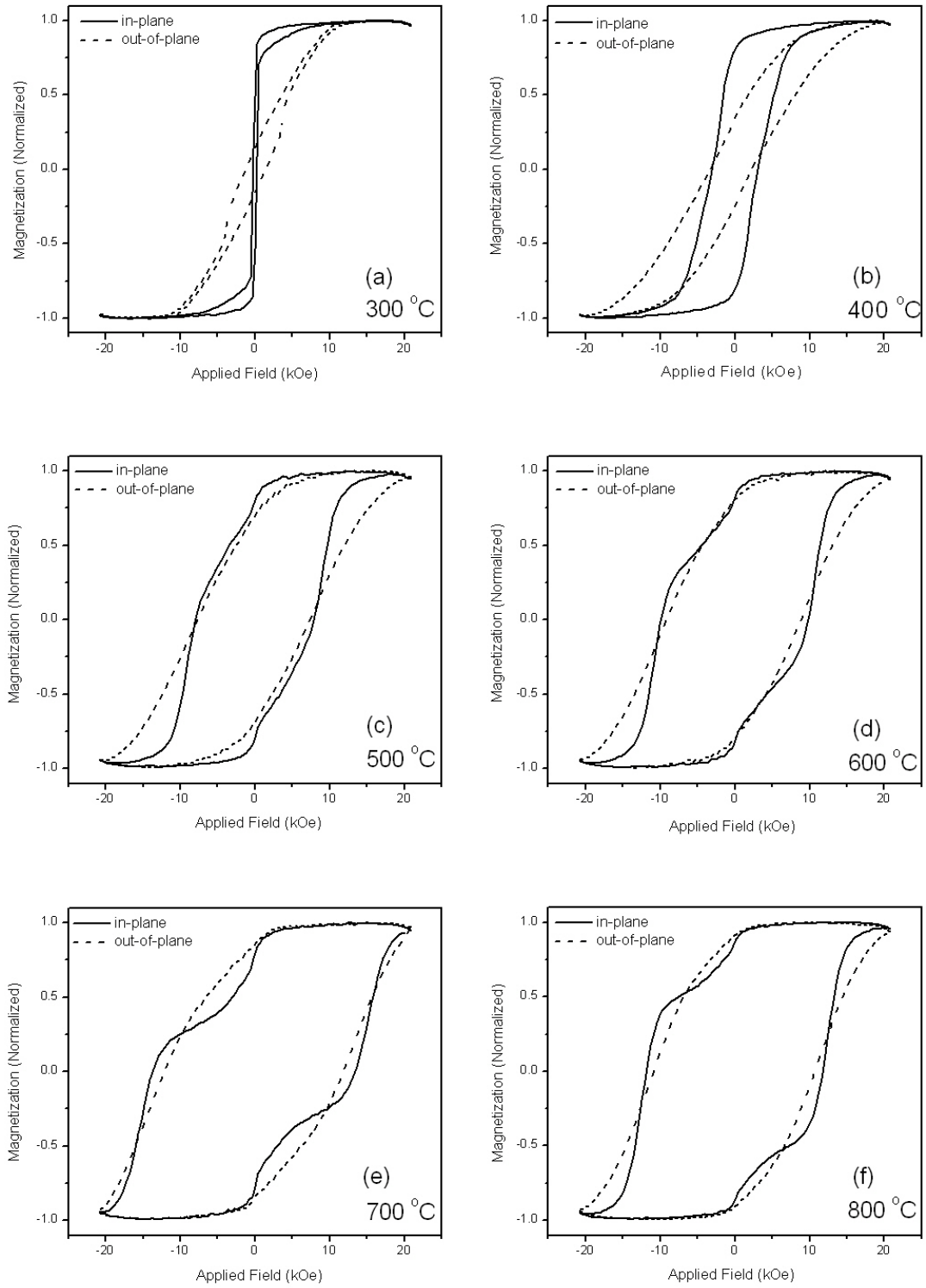

Figure 3-8 Magnetization hysteresis loops of the Si/MgO(amorphous)/FePt samples post-annealed at (a) 300 °C, (b) 400 °C, (c) 500 °C, (d) 600 °C, (e) 700 °C, (f) 800 °C.

In-plane and out-of-plane coercivity of the Si/MgO(amorphous)/FePt films after post-annealing at different temperatures are present in Table 3-2 and Figure 3-9. The sample post-annealed at 300 °C showed soft magnetic properties. With the increase of the post-annealing temperature, the change of coercivity of the Si/MgO(amorphous)/FePt films showed the similar trend as that of the SiO_x/FePt films, but higher coercivity. Moreover, the ordering temperature was lower than that of the SiO_x/FePt films, as the coercivity increased to 3 kOe after post-annealing at 400 °C, indicating the start of formation of the ordered fct phase. The maximum coercivity could reach 14 kOe after post-annealing at 700 °C.

Table 3-2 In-plane and out-of-plane coercivity of the Si/MgO(amorphous)/FePt samples.

Temperature (^{o}C)	**$H_{c\parallel}$ (kOe)**	**$H_{c\perp}$ (kOe)**
300	0.17	1.33
400	2.94	2.55
500	8.26	7.68
600	10.29	9.35
700	14.04	12.42
800	11.79	10.79

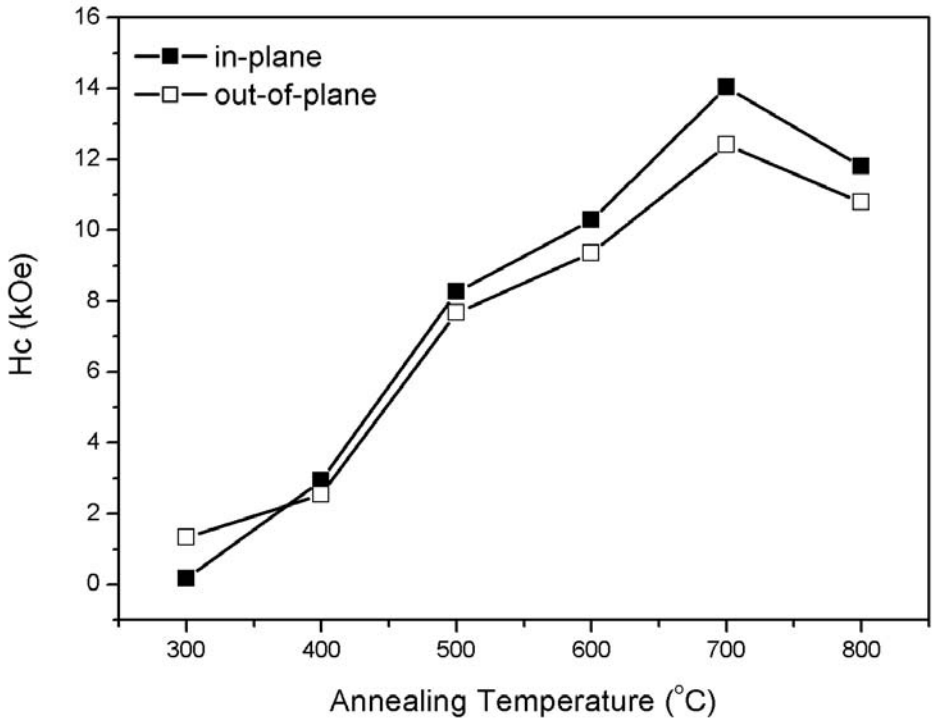

Figure 3-9 In-plane and out-of-plane coercivity of the Si/MgO(amorphous)/FePt films.

With the aid of the X-ray photoelectron spectrum (Figure 3-10), it was found that magnesium and oxygen were present in the Si/MgO underlayers. Structures of the Si/MgO(amorphous)/FePt films annealed at different temperatures were examined through XRD as shown in Figure 3-11. No MgO crystalline peaks were found in XRD patterns, which was indicative of amorphous phase of MgO. The as-deposited sample exhibited the disordered fcc phase. Similar as the SiO_x/FePt films in Figure 3-6, the FePt (111) peak gradually shifted to higher angle with the increase of the post-annealing temperature, indicating the formation of the ordered fct phase. The peaks (001) and (002) of the fct FePt phase appeared after post-annealing at 500 °C, indicating more ordering. This phase result matched with the coercivity result in Figure 3-9, which further indicated that the ordering temperature of the

Si/MgO(amorphous)/FePt films was lower than that of the SiO_x/FePt films.

XRD patterns revealed that the increase of the annealing temperature yielded sharper peaks, indicating an increase of the grain size. The grain size calculated from the Scherrer formula is plotted in Figure 3-12. The grain size was ~12 nm for the as-deposited sample. When the fct phase was formed after annealing at 400 °C, the grain size increased rapidly to ~22 nm and increased further to ~30 nm after annealing at 800 °C.

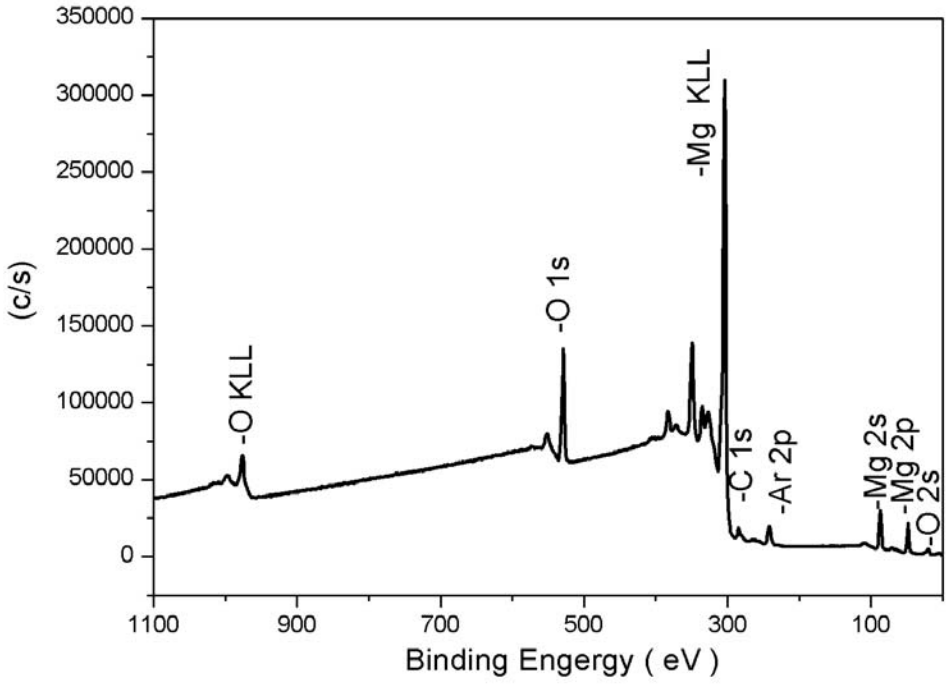

Figure 3-10 X-ray photoelectron spectrum for the Si/MgO(amorphous) film.

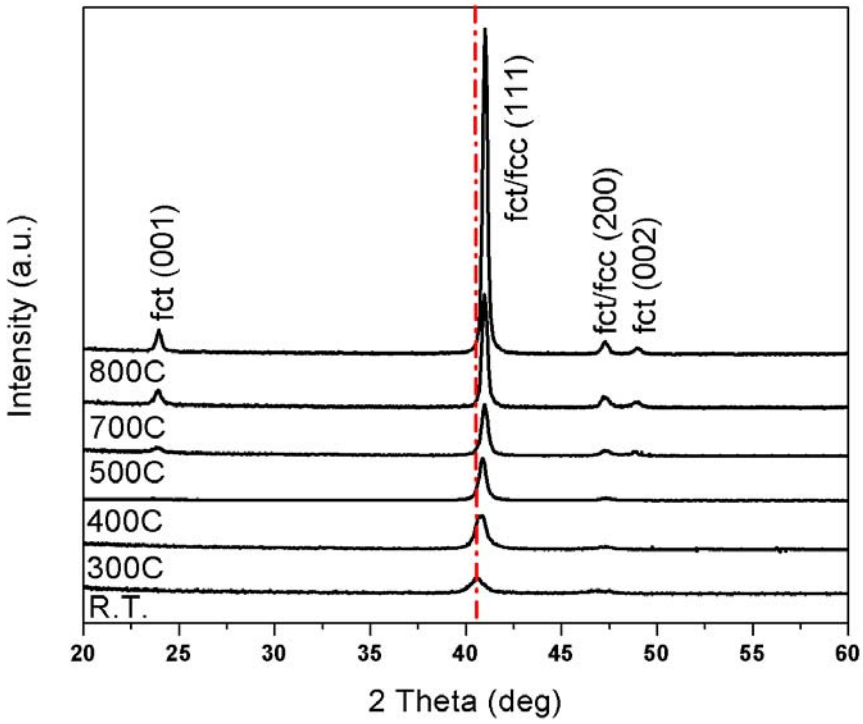

Figure 3-11 XRD patterns of the Si/MgO(amorphous)/FePt films with different annealing temperatures.

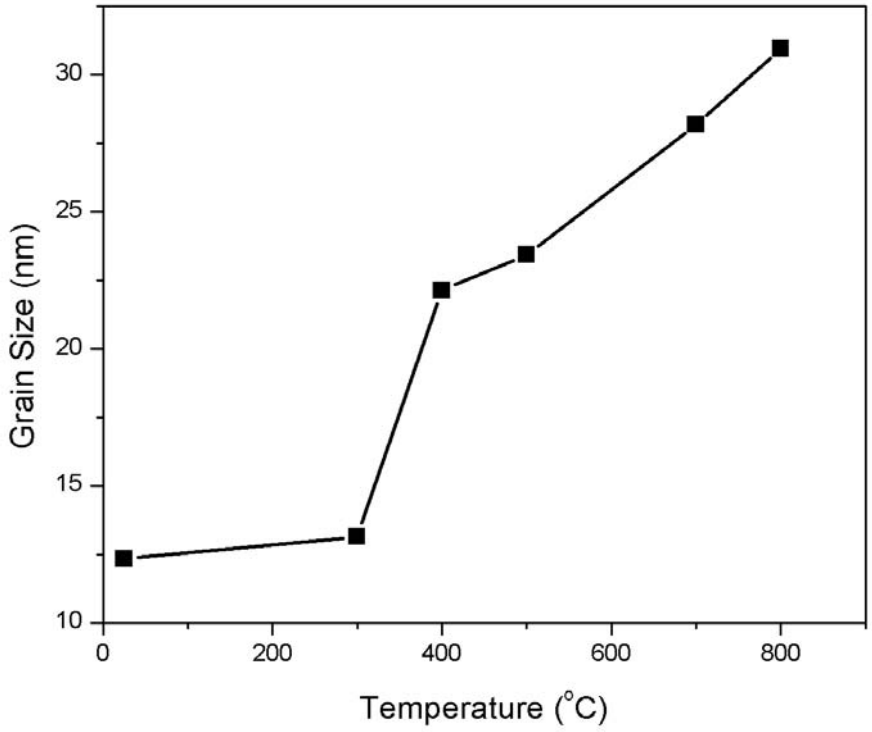

Figure 3-12 Temperature dependence of grain size in the Si/MgO(amorphous)/FePt films.

3.3.1.3 FePt Films with Crystalline Ag Underlayers

Two groups of samples with crystalline underlayers: Si/Ag(20 nm, crystalline)/FePt(40 nm), and Si/MgO(100 nm, textured)/FePt(40 nm) (Section 3.3.1.4) were studied.

Figure 3-13 shows the in-plane and out-of-plane normalized magnetization hysteresis loops of the Si/Ag/FePt samples post-annealed at different temperatures. The samples post-annealed at 300 °C or below exhibited the typical soft magnetic hysteresis loops, which were narrow. When the post-annealing temperature increased to 400 °C, the hysteresis loops in both of the in-plane and out-of-plane directions suddenly became broad, illustrating that the samples became magnetically hard. With the increase of the post-annealing temperature, the hysteresis loops became broader and broader until 700 °C, indicating that the hard magnetic property was enhanced, which further implied that the ordering of the FePt films was improved. There were steps in the hysteresis loops for the samples annealed at 400 °C and 500 °C. These steps were understandable because of the coexistence of the remaining soft magnetic phase and the dominant hard magnetic phase in the FePt films. Steps in the hysteresis loops for the samples post-annealed at 800 °C were also observed. Moreover, the coercivity of the samples post-annealed at 800 °C was smaller than those post-annealed at 600 °C and 700 °C. This result might be due to the oxidization of FePt at a high post-annealing temperature.

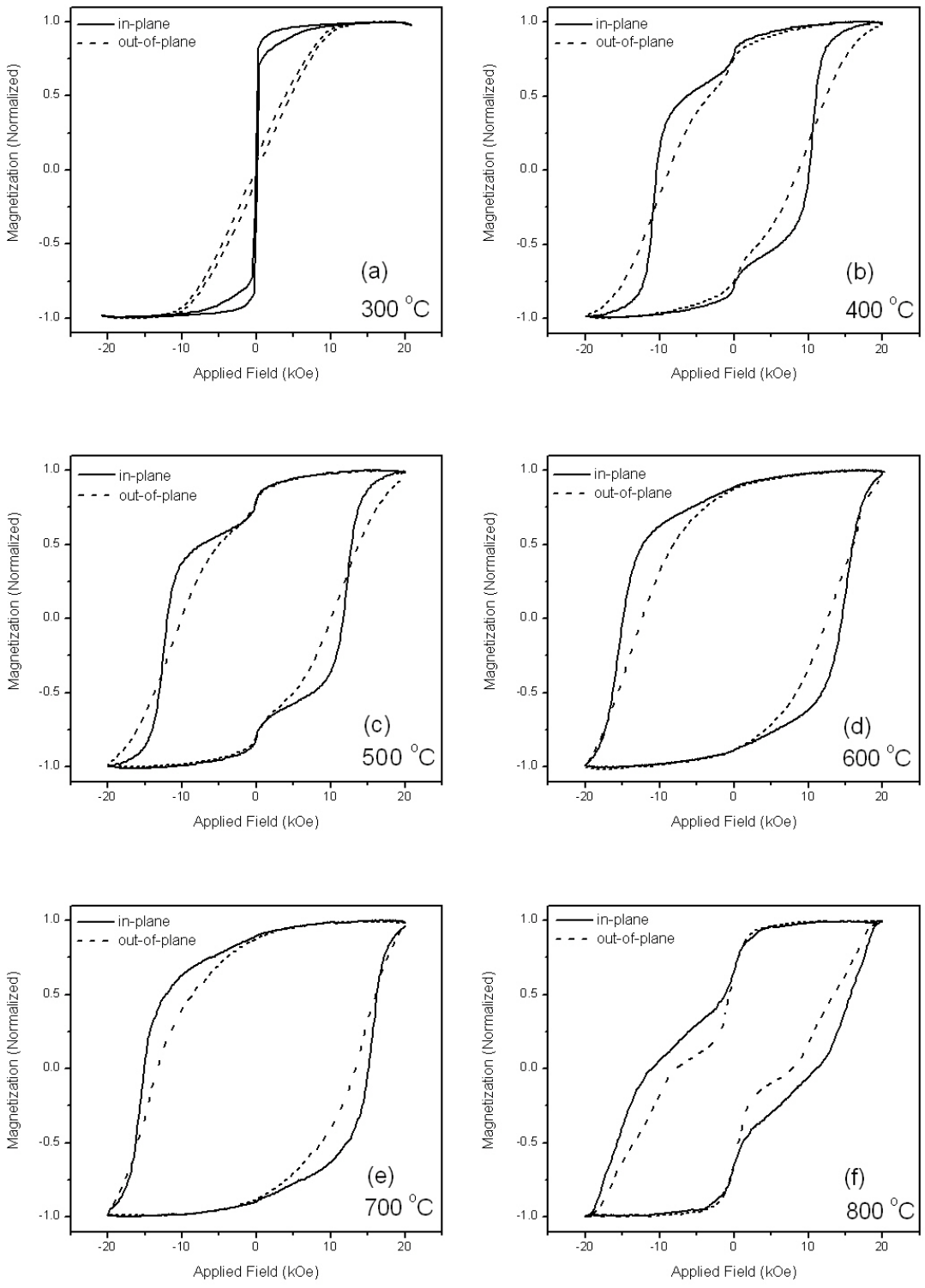

Figure 3-13 Magnetization hysteresis loops of the Si/Ag/FePt samples post-annealed at (a) 300 °C, (b) 400 °C, (c) 500 °C, (d) 600 °C, (e) 700 °C, (f) 800 °C.

In-plane and out-of-plane coercivity of the Si/Ag/FePt samples is shown in Figure 3-14 as a function of the post-annealing temperature (The values of the in-plane and out-of-plane coercivity for the samples post-annealed at different temperatures are summarized in Table 3-3). When the annealing temperature was 300 °C, the coercivity was around hundred Oe. However, after annealing at 400 °C, the coercivity as high as 10 kOe was suddenly achieved, which indicated that the ordered fct phase was formed to the great extent. As the post-annealing temperature increased above 400 °C, the coercivity gradually approached a maximum of 15 kOe when annealed at 700 °C. Compared to the FePt films deposited on amorphous underlayers, FePt samples with crystalline Ag underlayer showed much higher coercivity and lower ordering temperature. Furthermore, there was slightly in-plane magnetic anisotropy in the Si/Ag/FePt samples, as the coercivity measured out-of-plane was lower than the coercivity measured in-plane.

Table 3-3 In-plane and out-of-plane coercivity of the Si/Ag/FePt samples.

Temperature (^{o}C)	**$H_{c\parallel}$ (kOe)**	**$H_{c\perp}$ (kOe)**
300	0.15	0.56
400	10.27	8.70
500	11.79	9.98
600	14.72	12.48
700	15.12	13.34
800	11.06	7.85

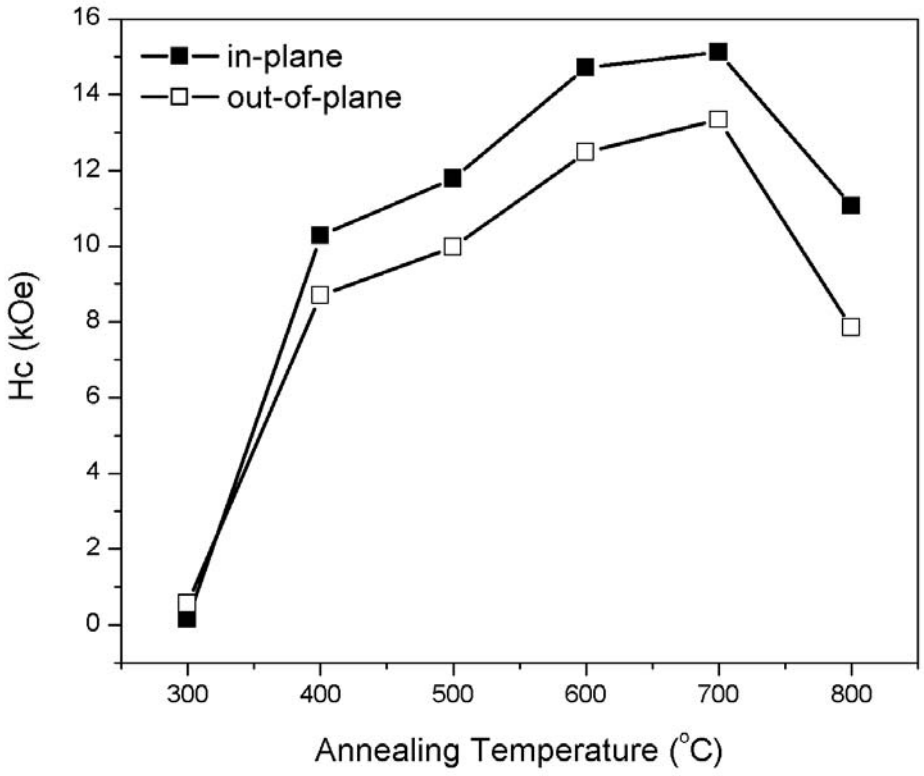

Figure 3-14 In-plane and out-of-plane coercivity of the Si/Ag/FePt samples.

Figure 3-15 shows the XRD patterns of the Si/Ag/FePt films with different annealing temperatures. After annealing above 500 °C, Ag showed the (111) and (200) crystalline peaks. There was only the disordered fcc FePt phase after annealing at 300 °C or below. After annealing at 400 °C, the FePt (001) and (002) peaks of the ordered fct phase appeared, indicating the formation of the ordered fct phase. This was the reason for the sudden increase in the coercivity of FePt films after annealing at 400 °C. With the increase of the temperature, the formation of the ordered fct phase was further strengthened, as the intensity of the (001) peak was increased and the (111) peak was shifted to higher angle. XRD patterns revealed that with the increase of the

post-annealing temperature, the FePt peaks became sharper and sharper, indicating the increase of the grain size at the higher temperature. Grain size calculated from the Scherrer formula is shown in Figure 3-16. The gain size was ~10 nm for the as-deposited film, and increased continuously with the increase of the temperature. It was ~27 nm for the film annealed at 800 °C.

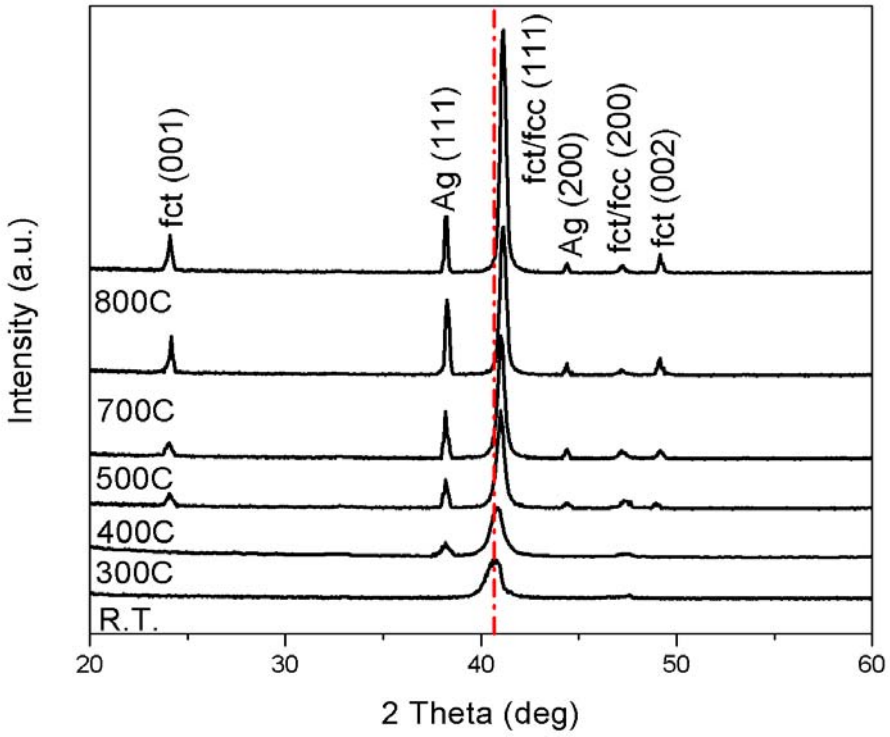

Figure 3-15 XRD patterns of the Si/Ag/FePt films with different annealing temperatures.

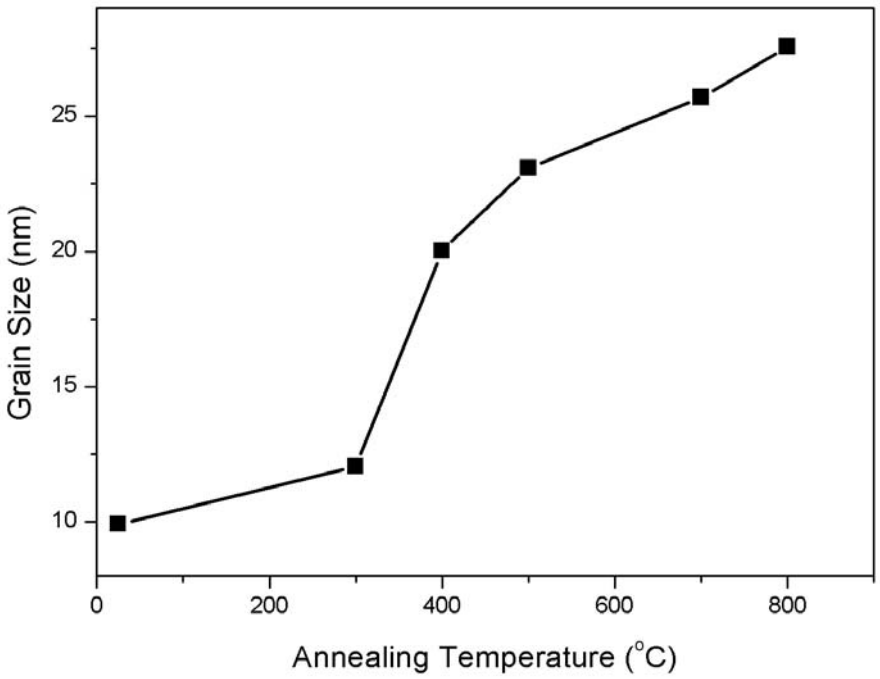

Figure 3-16 Temperature dependence of grain size in the Si/Ag/FePt films.

3.3.1.4 FePt Films with Textured MgO Underlayers

MgO single crystalline substrates have been intensively used to enhance the coercivity and to induce magnetic anisotropy in FePt films [2,3]. However, MgO single crystalline substrate was too expensive for the industry application. Thus, the objectives of this part were to fabricate the textured MgO thin films on Si substrates and to use them as underlayers to deposit FePt thin films. The textured MgO underlayer in this work was achieved by PLD on the Si substrate heated up to 800 °C in the vacuum of ~5×10^{-8} Torr. These textured MgO underlayers were relatively cost-effective, and thus possible for the industry application.

The XRD pattern of the 100 nm thick MgO on Si substrate is shown in Figure 3-17. Only the MgO (200) peak was observed. Even the second strongest MgO (220) peak was not detected. Furthermore, as shown in Figure 3-18, the Full Width at Half Maximum (FWHM) of this MgO (200) peak was obtained to be 5.14 ^{o} by applying rocking curve measurement of XRD. The small FWHM indicates well texture. Thus, the rocking curve study on MgO supported that the MgO film fabricated on Si substrate was well (100) textured with the [100] direction perpendicular to the film surface.

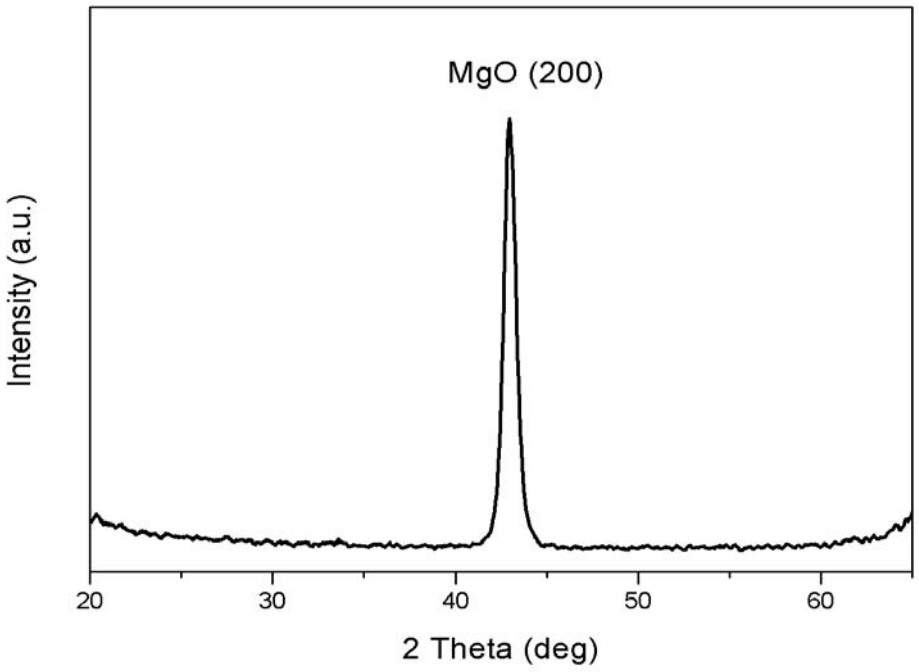

Figure 3-17 XRD pattern of Si/MgO(textured, 100 nm) sample.

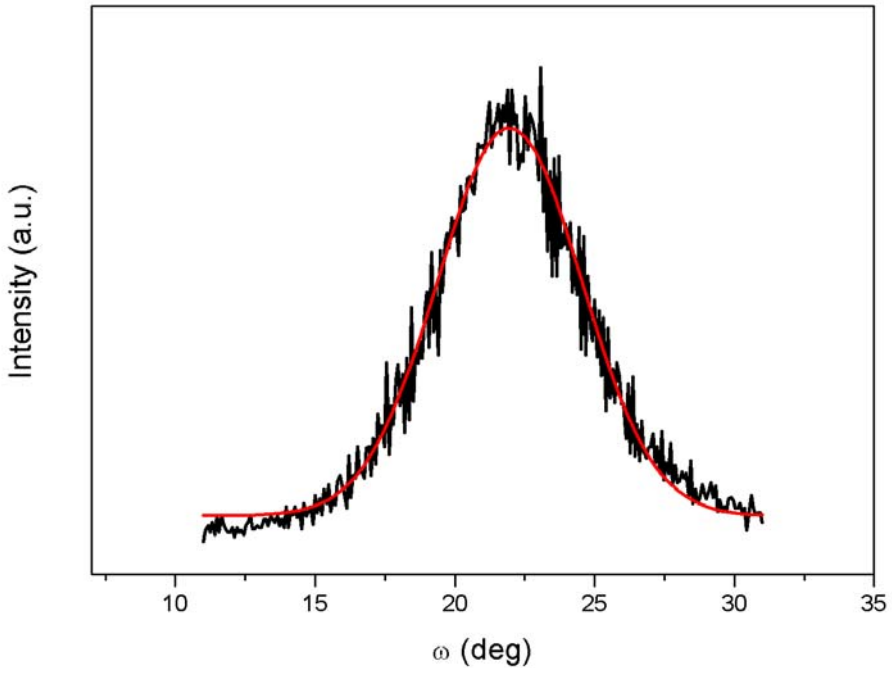

Figure 3-18 Rocking curve of MgO (200) peak.

The in-plane and out-of-plane normalized magnetization hysteresis loops of the Si/MgO(textured)/FePt samples post-annealed at different temperatures are plotted in Figure 3-19. Though the samples post-annealed at 300 °C exhibited narrow hysteresis loops, they still showed some weak hard magnetic properties, because the coercivity was higher than 1 kOe. As the post-annealing temperature increased above 400 °C, the hysteresis loops in both of the in-plane and out-of-plane directions became broader and broader until 700 °C. This variation illustrated that the hard magnetic phase was enhanced by the high temperature post-annealing. There were steps in the hysteresis loops for all the samples except the one annealed at 300 °C. This result indicated that there were still some part of soft magnetic phase, which further implied that the FePt films were partially ordered and some disordered fcc phase existed to contribute to the soft magnetic property.

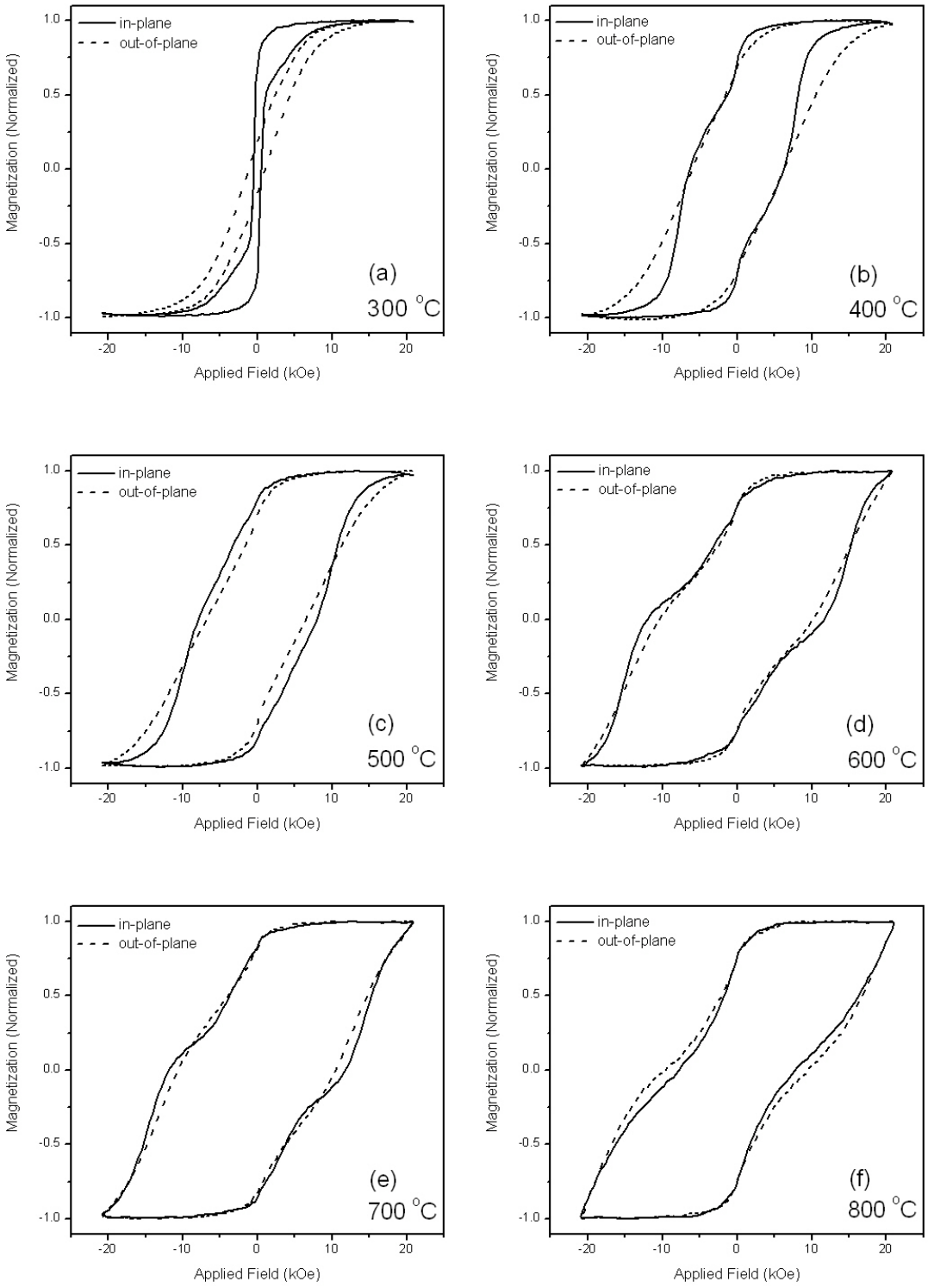

Figure 3-19 Magnetization hysteresis loops of the Si/MgO(textured)/FePt samples post-annealed at (a) 300 °C, (b) 400 °C, (c) 500 °C, (d) 600 °C, (e) 700 °C, (f) 800 °C.

Table 3-4 shows the values of the in-plane and out-of-plane coercivity of the Si/MgO(textured)/FePt films after post-annealing at different temperatures, while Figure 3-20 shows the in-plane and out-of-plane coercivity as a function of post-annealing temperature. As shown in Figure 3-20, FePt films deposited on 100 nm thick (100) textured MgO underlayers showed the similar trend of the in-plane and out-of-plane coercivity as those with crystalline Ag underlayers. The samples showed low coercivity, when post-annealed at 300 °C or lower temperature. As the post-annealing temperature increased to 400 °C, the coercivity rapidly increased to ~6 kOe, indicating the improved transformation from the disordered fcc phase to the ordered fct phase. When the post-annealing temperature increased from 300 °C to 600 °C, the coercivity increased gradually to a maximum value of ~12 kOe as the post-annealing temperature was 600 °C.

Table 3-4 In-plane and out-of-plane coercivity of the Si/MgO(textured)/FePt samples.

Temperature (^{o}C)	**$H_{c\parallel}$ (kOe)**	**$H_{c\perp}$ (kOe)**
300	0.57	1.39
400	6.51	6.13
500	7.71	6.92
600	12.06	10.46
700	12.03	10.87
800	7.85	10.82

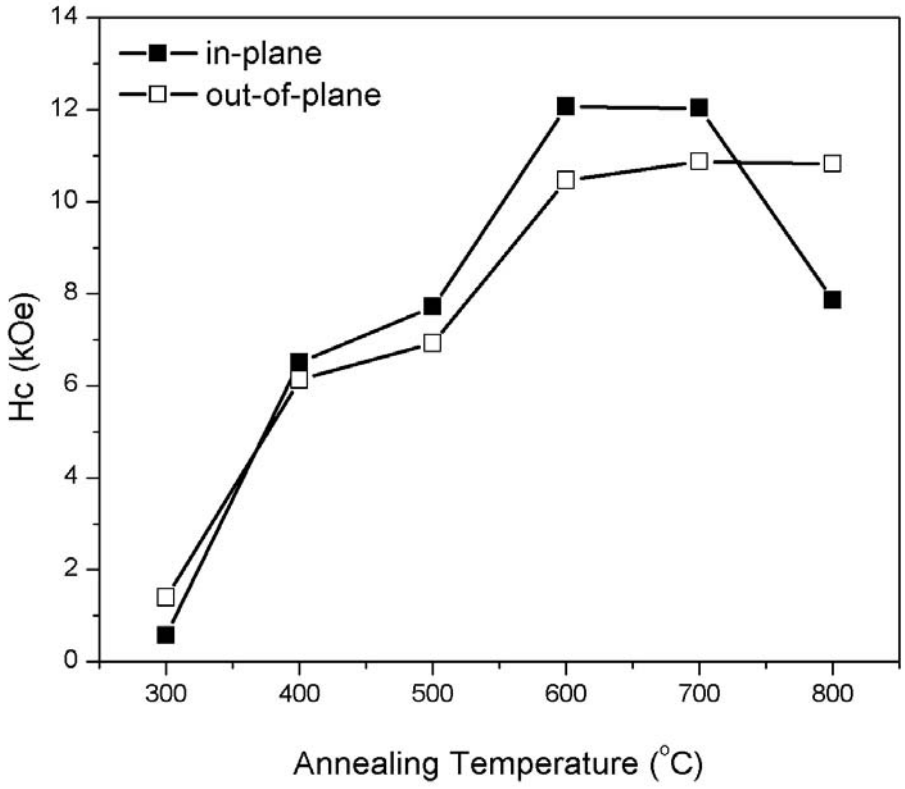

Figure 3-20 In-plane and out-of-plane coercivity of the Si/MgO(textured)/FePt films.

Figure 3-21 shows the XRD patterns of the Si/MgO(textured)/FePt films with different post-annealing temperatures. Similar as the samples with crystalline Ag underlayers, only the disordered fcc FePt phase was shown for the samples post-annealed at 300 °C or below. When the post-annealing temperature increased to 400 °C, the (001) and (002) peaks of the ordered fct phase appeared, indicating the formation of the ordered fct phase. This explained the rapid increase of coercivity for the samples post-annealed at 400 °C. With the increase of the temperature, the FePt (111) peak shifted to higher angle and the intensity of the FePt (001) peak increased, indicating the further enhancement of the ordered fct phase. Grain size calculated from the Scherrer formula is showed in Figure 3-22. The gain size was ~6 nm for the as-deposited FePt film, and

increased continuously with the increase of the post-annealing temperature. The grain size was ~22 nm for the Si/MgO(textured)/FePt films post-annealed at 800 °C. The FePt films deposited on textured MgO underlayers showed smaller grain size than the FePt films deposited on any other underlayer (substrate) in this study (SiO_x/FePt(40 nm), Si/MgO(20 nm, amorphous)/FePt(40 nm), Si/Ag(20 nm, crystalline)/FePt(40 nm))

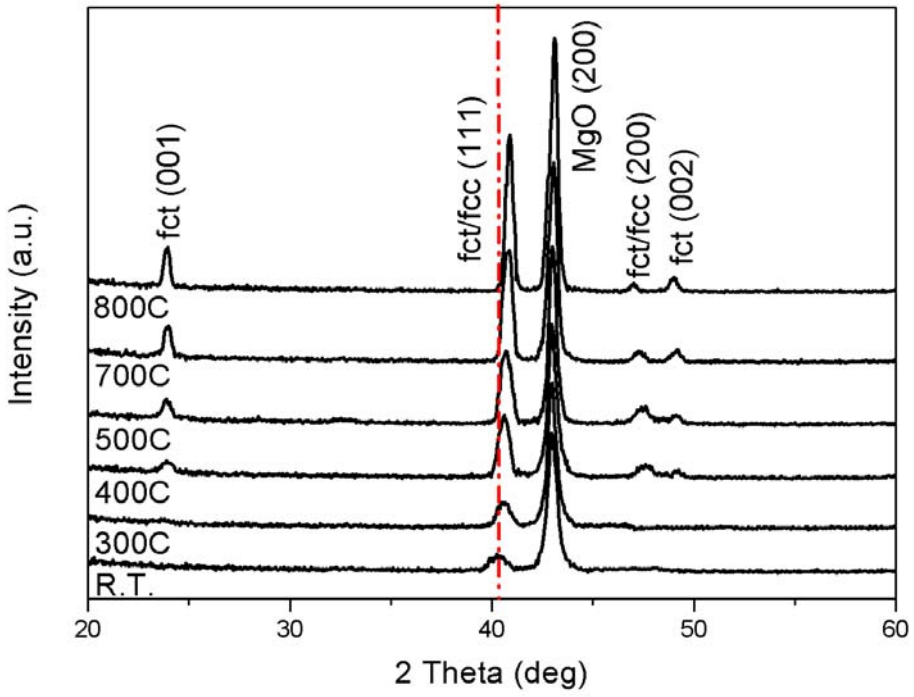

Figure 3-21 XRD patterns of the Si/MgO(textured)/FePt films with different annealing temperatures.

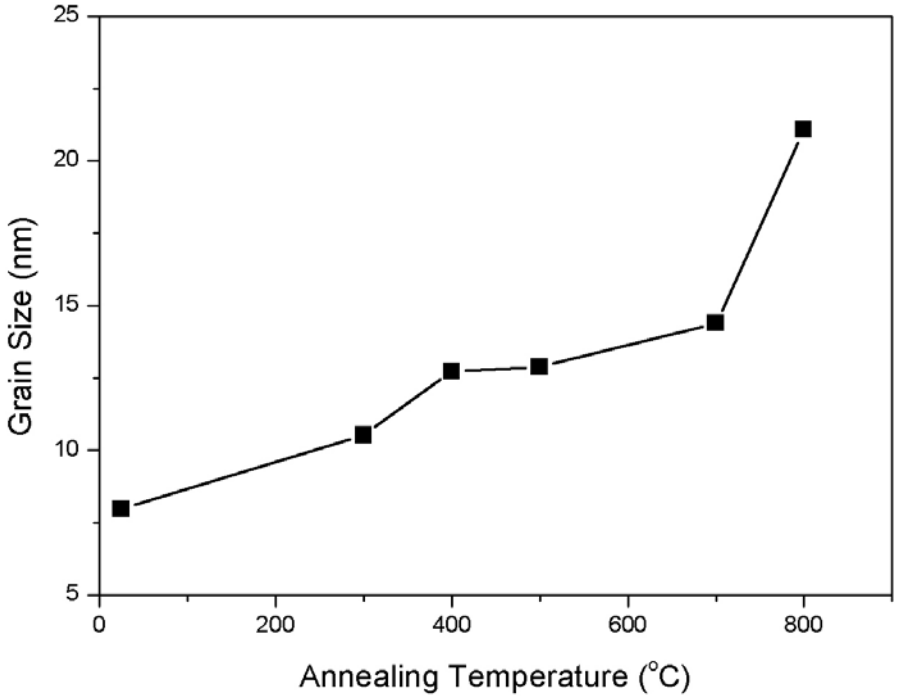

Figure 3-22 Temperature dependence of grain size in the Si/MgO(textured)/FePt films.

3.3.1.5 Summary

All the FePt films deposited on different underlayers showed maximum coercivity when post-annealed at 700 °C. Thus, the in-plane and out-of-plane coercivity and grain size of FePt samples with different underlayers post-annealed at 700 °C are summarized in Table 3-5. The FePt samples prepared using crystalline underlayers were found to have lower ordering temperature and higher coercivity than those with amorphous underlayers. Moreover, our results showed that both crystalline Ag and textured MgO underlayers were promising to reduce the ordering temperature, and to enhance the coercivity.

The FePt samples with textured MgO underlayers showed lower coercivity than those with crystalline Ag underlayers. However, the FePt samples with textured MgO underlayers had smaller grain size, which was also a key advantage for magnetic recording application. In addition, a textured MgO underlayer is relatively cost-effective compared to the MgO single crystalline substrate. Furthermore, FePt samples with crystalline Ag underlayers have been intensively studied previously by Zhao *et al.* [4,5]. Therefore, the textured MgO underlayer was chosen for further study on the FePt film thickness effects on the magnetic anisotropy.

Table 3-5 Summary of the in-plane and out-of-plane coercivity and grain size of FePt samples with different underlayers post-annealed at 700 ℃.

Samples (700 °C)	**$H_{c\parallel}$ (kOe)**	**$H_{c\perp}$ (kOe)**	**Grain size (nm)**	**Ordering Temperature (°C)**
SiO_x/FePt	10	8	25	500
Si/MgO(amorphous)/FePt	14	12	28	500
Si/Ag(crystalline)/FePt	15	13	25	400
Si/MgO(textured)/FePt	12	11	14	400

3.3.2 Thickness Effects on Magnetic Anisotropy

FePt films with nominal thicknesses of 5 nm, 10 nm, 15 nm, and 40 nm on (100) textured MgO (100 nm) underlayers were studied. The samples were named as Si/MgO(textured, 100 nm)/FePt(*t* nm), where *t* is the thickness of FePt films. The

effects of FePt film thickness on the ordering temperature, coercivity, and magnetic anisotropy were studied.

Si/MgO(textured)/FePt(5 nm)

Figure 3-23 shows the magnetization hysteresis loops of the Si/MgO(textured)/FePt(5 nm) samples post-annealed at different temperatures. The samples post-annealed at 300 °C - 500 °C were magnetically soft, due to the predominant disordered fcc FePt phase. With the increase of the post-annealing temperature above 500 °C, the hysteresis loops became broad, which meant the hard magnetic phase was formed. There were steps in both of the in-plane and out-of-plane hysteresis loops of the samples post-annealed at 700 °C and 800 °C, indicating that some magnetically soft phase still existed though the hard magnetic phase dominated. Perpendicular magnetic anisotropy was observed in the sample post-annealed at 700 °C, as the out-of-plane hysteresis loop was much broader than the in-plane hysteresis loop. When the post-annealing temperature increased to 800 °C, both the in-plane and out-of-plane hysteresis loops became narrow and the coercivity dropped dramatically. This might be due to the oxidization of the extremely thin FePt films at 800 °C. Thus XRD measurement was carried out to determine the phase. Unfortunately, except for the textured MgO (200) peak and Si (400) peak, no other peaks could be detected, which was probably due to the depression of the XRD signal from the extremely thin FePt film.

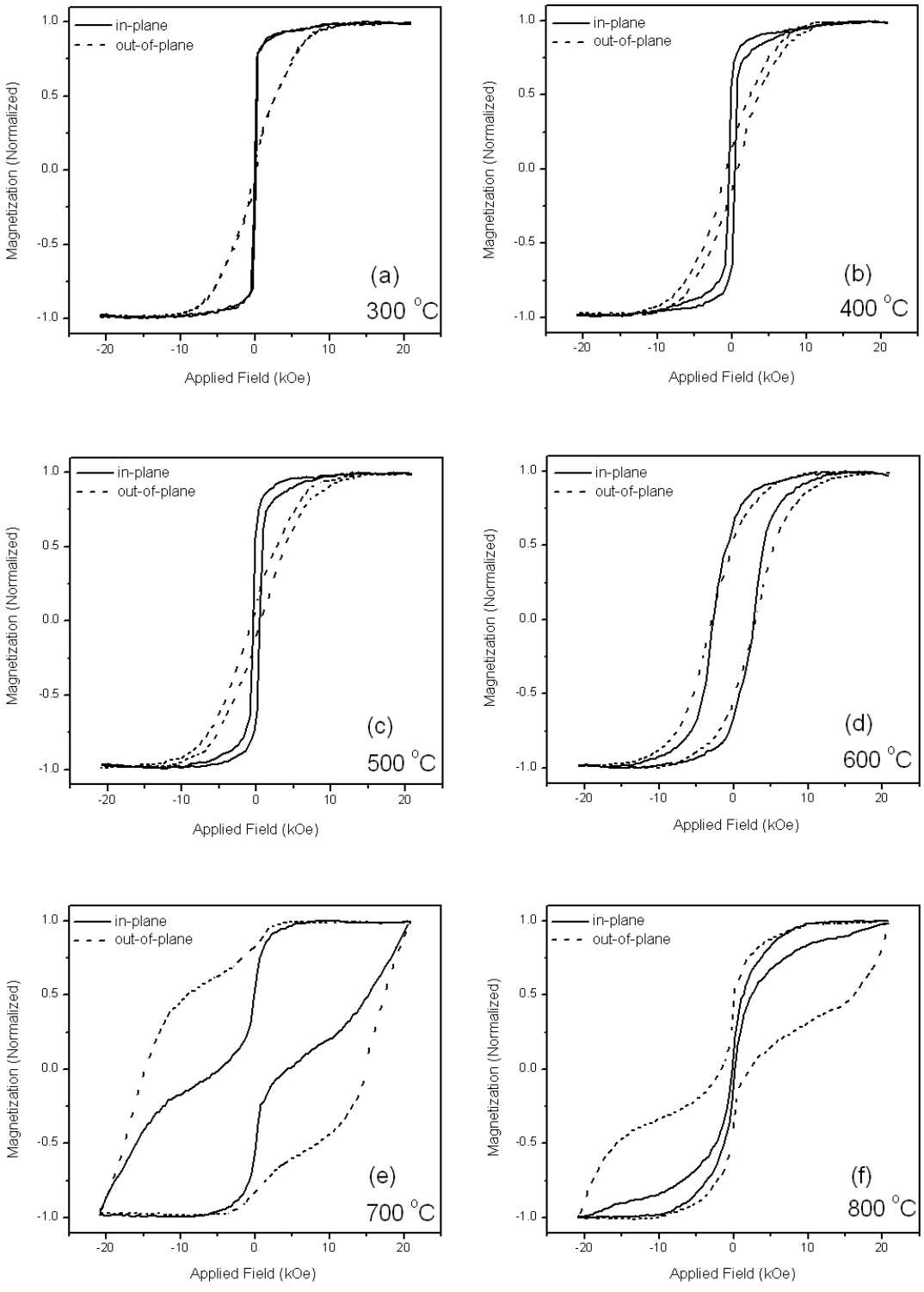

Figure 3-23 Magnetization hysteresis loops of the Si/MgO(textured)/FePt(5 nm) samples post-annealed at (a) 300 °C, (b) 400 °C, (c) 500 °C, (d) 600 °C, (e) 700 °C, (f) 800 °C.

Table 3-6 and Figure 3-24 show the in-plane and out-of-plane coercivity of the samples with the FePt thickness of 5 nm. For the samples post-annealed at 300 °C - 500 °C, both the in-plane and out-of-plane coercivity was about one or two hundred Oe. The low coercivity indicated the presence of the dominant disordered fcc phase while the lack of the ordered fct FePt phase in these samples post-annealed at 300 °C - 500 °C. When the sample was post-annealed at 600 °C, both the in-plane and out-of-plane coercivity increased to ~2.5 kOe, indicating the formation of the ordered fct FePt phase. The 5 nm thick FePt samples with the textured MgO underlayers showed a higher ordering temperature of ~600 °C, compared to the 40 nm thick FePt films on the textured MgO underlayers with the ordering temperature of ~ 400 °C (Figure 3-20). When the sample was post-annealed at 700 °C, the out-of-plane coercivity increased dramatically to ~15 kOe, indicating that the ordered fct FePt phase was to the great extent formed. However, the in-plane coercivity of this sample post-annealed at 700 °C slightly increased to ~4.5 kOe. This sample post-annealed at 700 °C showed the perpendicular magnetic anisotropy, as the out-of-plane coercivity (~15 kOe) was much higher than the in-plane coercivity (~4.5 kOe). When the post-annealing temperature increased to 800 °C, both the in-plane and out-of-plane coercivity dropped to some hundred Oe.

Table 3-6 In-plane and out-of-plane coercivity of the Si/MgO(textured)/FePt(5 nm) samples.

Temperature (^{o}C)	$H_{c\parallel}$ (kOe)	$H_{c\perp}$ (kOe)
300	0.18	0.26
400	0.39	0.58
500	0.47	0.59
600	2.73	2.91
700	4.92	14.82
800	0.22	1.37

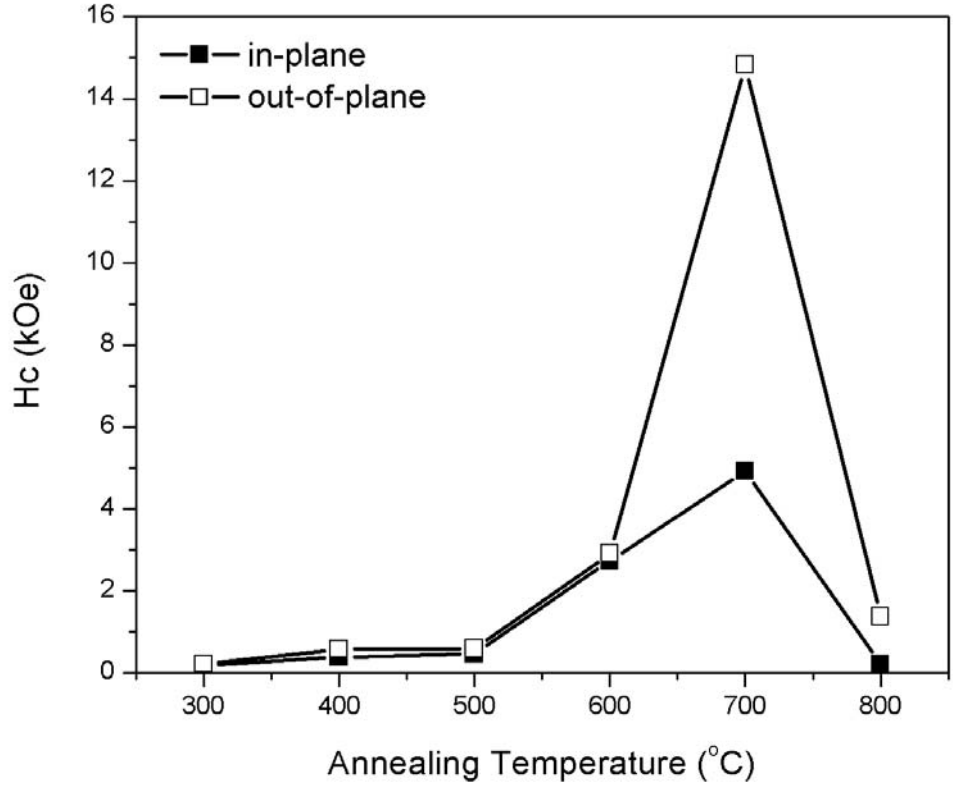

Figure 3-24 In-plane and out-of-plane coercivity of the Si/MgO(textured)/FePt(5 nm) samples post-annealed at different temperatures.

Si/MgO(textured)/FePt(10 nm)

The magnetization hysteresis loops of the Si/MgO(textured)/FePt(10 nm) samples post-annealed at different temperatures are shown in Figure 3-25. The trend of the variation of the hysteresis loops was almost the same as that of the Si/MgO(textured)/FePt(5 nm) samples. Perpendicular magnetic anisotropy was also observed in the Si/MgO(textured)/FePt(10 nm) samples post-annealed at 700 °C.

The values of the in-plane and out-of-plane coercivity of the Si/MgO(textured)/FePt(10 nm) samples post-annealed at different temperatures are shown in Table 3-7. Figure 3-26 shows how the in-plane and out-of-plane coercivity varied with different post-annealing temperatures for the Si/MgO(textured)/FePt(10 nm) samples. As similar trend as that of Si/MgO(textured)/FePt(5 nm) samples was found. Low in-plane and out-of-plane coercivity was observed, when the samples were post-annealed at 500 °C or below. When the post-annealing temperature increased to 600 °C, the in-plane coercivity increased to 2.3 kOe, while the out-of-plane coercivity increased to 4.1 kOe. This indicated that both the ordering and perpendicular magnetic anisotropy started to occur. Compared to 5 nm thick FePt samples, 10 nm thick FePt samples showed lower ordering temperature, since the out-of-plane coercivity at 600 °C was already 4.1 kOe. When the sample was post-annealed at 700 °C, the out-of-plane coercivity increased dramatically to ~8.5 kOe, while the in-plane coercivity even decreased to ~2.1 kOe. This result indicated that the perpendicular magnetic anisotropy was further enhanced after post-annealed at 700 °C. When the

post-annealing temperature increased to 800 °C, both the in-plane and out-of-plane coercivity dropped to some hundred Oe. This result might be due to the oxidization of FePt at a high post-annealing temperature.

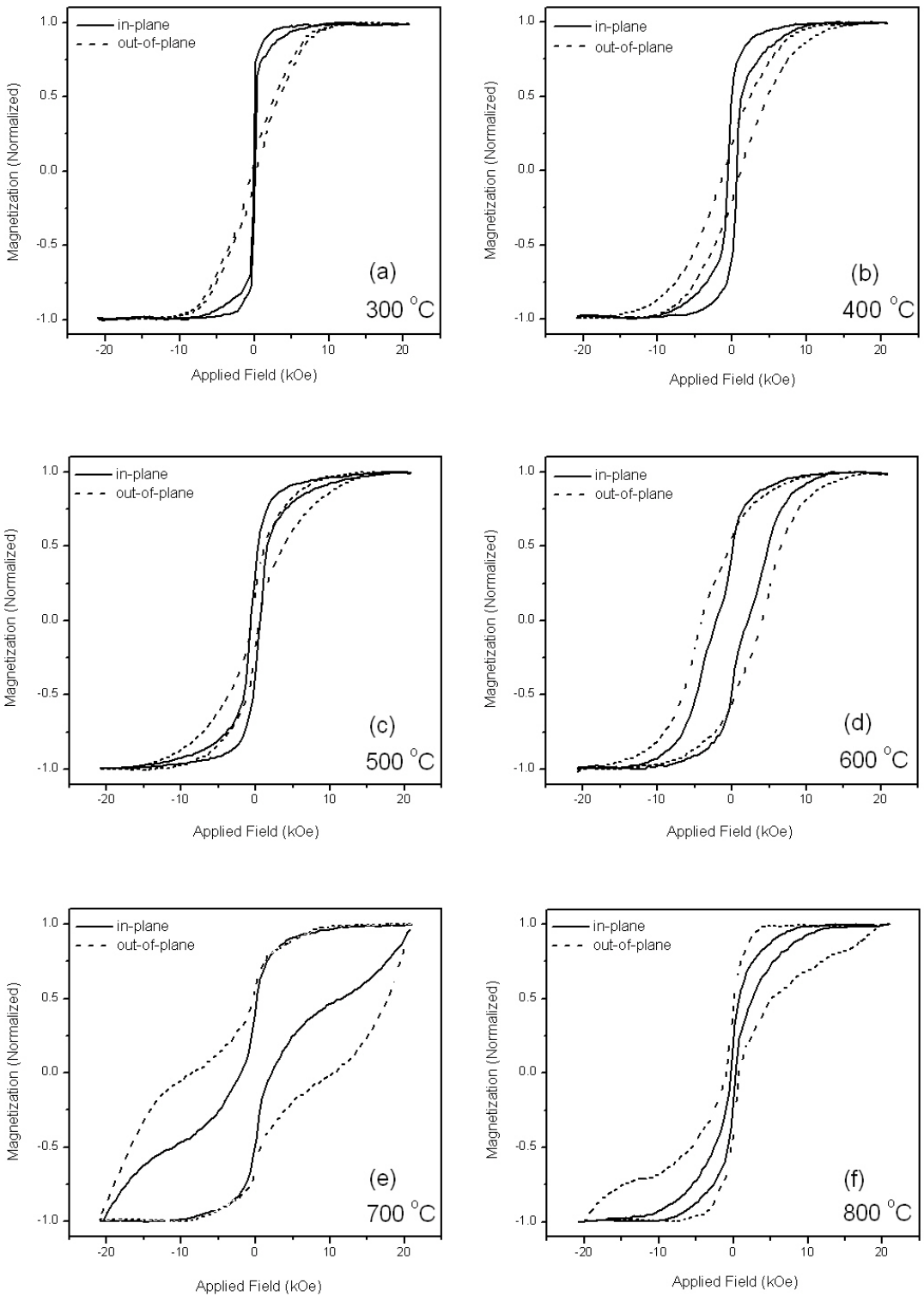

Figure 3-25 Magnetization hysteresis loops of the Si/MgO(textured)/FePt(10 nm) samples post-annealed at (a) 300 °C, (b) 400 °C, (c) 500 °C, (d) 600 °C, (e) 700 °C, (f) 800 °C.

Table 3-7 In-plane and out-of-plane coercivity of the Si/MgO(textured)/FePt(10 nm) samples.

Temperature (^{o}C)	$H_{c\parallel}$ (kOe)	$H_{c\perp}$ (kOe)
300	0.19	0.19
400	0.58	0.98
500	0.53	0.56
600	2.16	4.14
700	1.75	8.49
800	0.43	0.97

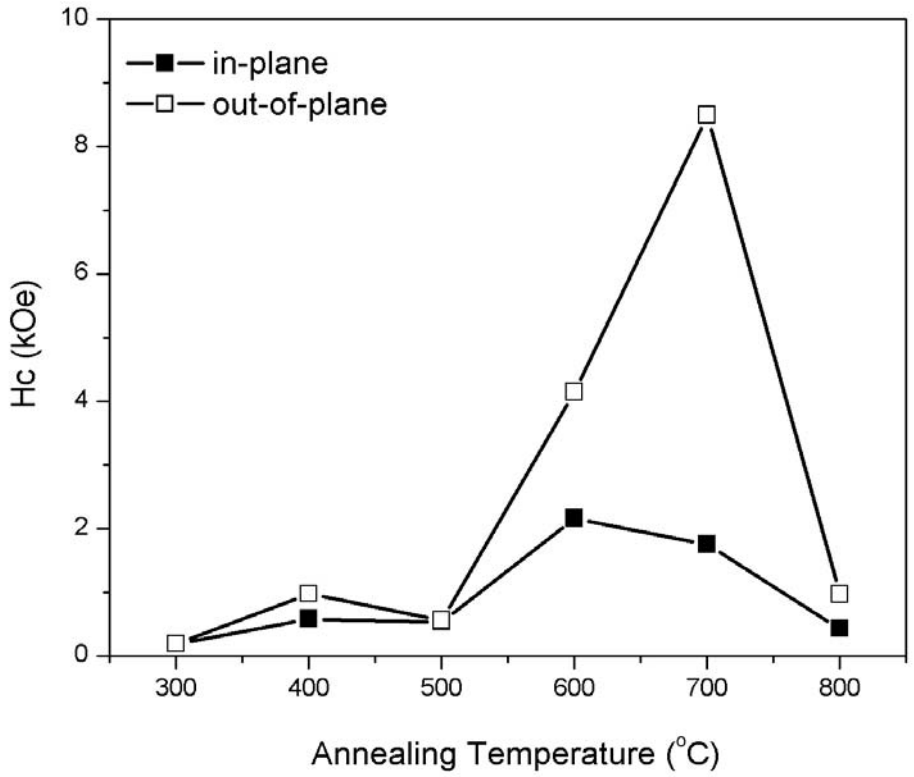

Figure 3-26 In-plane and out-of-plane coercivity of the Si/MgO(textured)/FePt(10 nm) samples post-annealed at different temperatures.

Si/MgO(textured)/FePt(15 nm)

Figure 3-27 shows the magnetization hysteresis loops of the 15 nm thick FePt samples post-annealed at different temperatures. The Si/MgO(textured)/FePt(15 nm) samples post-annealed at 300 °C was magnetically soft, due to the dominant disordered fcc FePt phase. With the increase of the post-annealing temperature, the hysteresis loops became broader, indicating the hard magnetic phase was forming.

Table 3-8 and Figure 3-28 show the in-plane and out-of-plane coercivity of the Si/MgO(textured)/FePt(15 nm) samples after post-annealing at different temperatures. The coercivity was low, when the sample was annealed at 300 °C. This low coercivity indicated the disordered fcc FePt phase dominated in the FePt film. The coercivity increased gradually with the increase of the post-annealing temperature. The coercivity increased to 4 kOe after post-annealing at 500 °C, indicating the ordering temperature was around 500 °C. This ordering temperature was lower than that of the 5 nm and 10 nm thick FePt films (600 °C), but higher than that of the 40 nm thick FePt films (400 °C). A maximum coercivity of 14 kOe was achieved after post-annealing at 800 °C. No obvious magnetic anisotropy was observed in the Si/MgO(textured)/FePt(15 nm) samples.

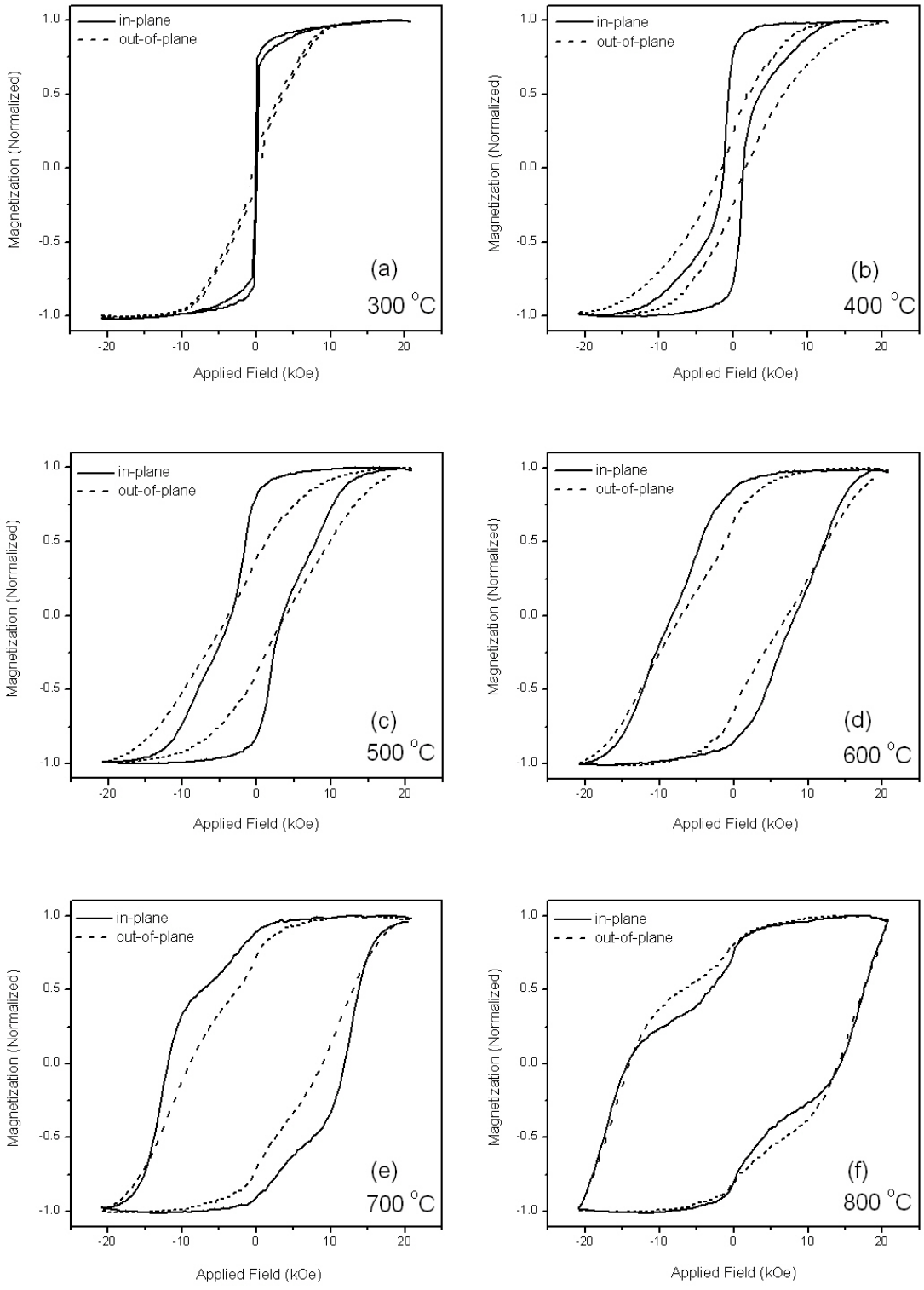

Figure 3-27 Magnetization hysteresis loops of the Si/MgO(textured)/FePt(15 nm) samples pos- annealed at (a) 300 °C, (b) 400 °C, (c) 500 °C, (d) 600 °C, (e) 700 °C, (f) 800 °C.

Table 3-8 In-plane and out-of-plane coercivity of the Si/MgO(textured)/FePt(15 nm) samples.

Temperature (^{o}C)	$H_{c\parallel}$ (kOe)	$H_{c\perp}$ (kOe)
300	0.04	0.32
400	1.38	1.77
500	3.36	3.76
600	7.30	8.21
700	12.00	9.28
800	14.06	14.03

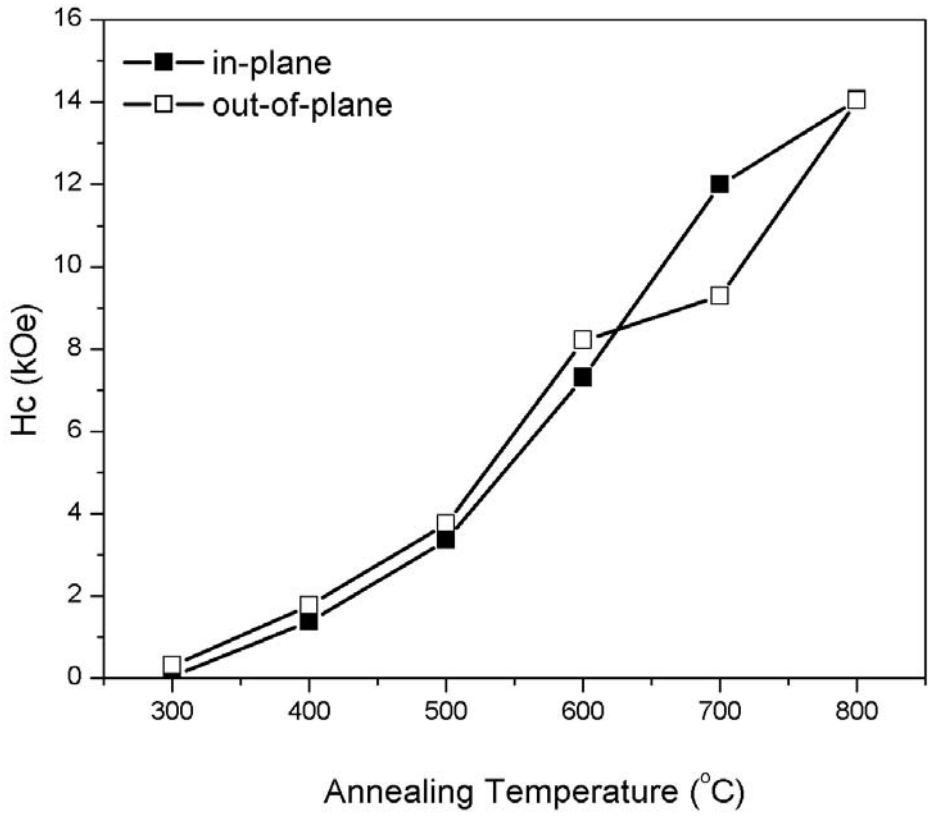

Figure 3-28 In-plane and out-of-plane coercivity of the Si/MgO(textured)/FePt(15 nm) samples post-annealed at different temperatures.

Si/MgO(textured)/FePt(40 nm)

Results of the Si/MgO(textured)/FePt(40 nm) samples were discussed in section 3.3.1.4 (Figure 3-19, Figure 3-20, Figure 3-21, and Figure 3-22).

Based on our study of the FePt films with different thicknesses deposited on the MgO textured underlayers, effects of FePt film thickness on ordering temperature, and magnetic anisotropy were as following:

- Firstly, the ordering temperature of the FePt films decreased with the increase of the FePt film thickness.

- Secondly, the perpendicular magnetic anisotropy was formed in FePt films with thickness below ~10 nm.

3.4 Summary

FePt thin films with a thickness of 40 nm were deposited on Si (100) substrates at room temperature by pulsed laser deposition, and post-annealed at different temperatures. Both amorphous underlayers and crystalline underlayers (or substrates): amorphous SiO_x, amorphous MgO, crystalline Ag, and (100) textured MgO, were studied. With the post-annealing temperature ranged from 300 °C to 800 °C, coercivity of 40 nm thick FePt films on all these underlayers increased as the annealing temperature increased until 700 °C. Moreover, crystalline Ag and textured MgO underlayers were found effective to promote the formation of the ordered fct FePt phase. High coercivity of 10-15 kOe has been achieved in the FePt samples with crystalline Ag underlayers or textured MgO underlayers. Furthermore, the FePt samples with textured MgO underlayers had smaller grain size, which was also a key advantage for magnetic recording application.

Therefore, the magnetic properties of FePt thin films with different thicknesses on the textured MgO underlayer were further studied. The ordering temperature of the FePt films decreased with the increase of the FePt film thickness. It was found that the perpendicular magnetic anisotropy was formed at thinner FePt films (5 nm and 10 nm) while the thicker films (15 nm and 40 nm) were magnetically isotropic. This may be related to the surface and interface energy [6] for the magnetic anisotropy only seen in the thinner FePt films.

References:

[1] V. G. Pynko, A. S. Komalov, and L. V. Ivaeva, Phys. Stat. Sol., 63a, 127 (1981).
[2] B. M. Lairson, M. R. Visokay, R. Sinclair, and B. M. Clemens, Appl. Phys. Lett. 62, 639 (1993).
[3] T. Shima, T. Moriguchi, S. Mitani, and K. Takanashi, Appl. Phys. Lett. 80, 288 (2002).
[4] Z. L. Zhao, J. Ding, K. Inaba, J. S. Chen, and J. P. Wang, Appl. Phys. Lett. 83, 2196 (2003).
[5] Z. L. Zhao, J. S. Chen, J. Ding, J. B. Yi, B. H. Liu, and J. P. Wang, Appl. Phys. Lett. 88, 052503 (2006).
[6] V. Novikov, *Grain Growth and Control of Microstructure and Texture in Polycrystalline Materials*, CRC Press, New York (1997).

CHAPTER 4

Magnetic Properties of Patterned FePt Films

4.1 Introduction

Besides the patterned magnetic recording media reviewed in Chapter 1, the patterned FePt films also have the potential in other applications, like Micro-Electro Mechanical Systems (MEMS). MEMS are the integration of mechanical elements, sensors, actuators, and electronics on a common silicon substrate through microfabrication technology. They are progressively permeating our everyday lives, mainly in the form of micro-sensors (pressure, temperature, contact, chemical, gyroscopes etc…) and have applications in many fields including automotive, air-and-space, industrial processing and biotechnology [1].

MEMS devices such as microactuators, sensors, micromotors, and frictionless microgears require the use of both hard and soft magnetic materials because electromagnetically actuated MEMS can be actuated with low voltage and power consumption, while more stable for large actuation forces over relatively long distances. Moreover, they are less susceptible to malfunction when subjected to adverse environments such as dust and humidity [2]. Magnetic MEMS is an emerging domain of applications for hard magnetic materials. For example, hard magnetic materials with a high remanence, B_r, are well suited for bidirectional microactuator applications [3]. In addition, microactuators driven by offchip coils can be activated with lower fields and hence lower power levels if a hard magnetic material is used instead of a soft magnetic material. As one kind of hard magnetic material, the ordered fct phase FePt is also receiving attention from the field of magnetic MEMS [4]. To

improve the magnetic properties like remanence and coercivity of the patterned FePt films, heat treatment is necessary. High temperature annealing may damage the patterned structures [5]. However, damage to the patterned structure is not wanted for both of the magnetic recording media and MEMS applications. In this thesis, a MgO top layer was found effective to maintain the patterned structures and the magnetic properties.

4.2 Experimental Procedures

The pre-patterned templates were fabricated on Si (100) substrates using deep ultraviolet lithography with a wavelength of 248 nm. A 60 nm thick anti-reflective layer and a 480 nm thick positive deep ultraviolet (DUV) photo-resist on the anti-reflective layer were coated on the Si substrates. To prepare the pre-patterned templates, a Nikon lithography scanner with KrF exciter laser radiation was used to expose the resist. The buffer layer and the FePt layer were deposited using PLD at room temperature on the pre-patterned templates on the Si (100) substrates. Ag* and MgO* were used as the buffer layer to separate Si substrate and FePt.

Two sets of samples were fabricated, namely Si/Ag(20nm)/FePt(40nm) and Si/MgO(20nm)/FePt(40nm) (illustrated in Figure 4-1 (a) and (b)). After the deposition, the films on pre-patterned resist templates were soaked in an OK 73 thinner to achieve lift-off. After the lift-off, the samples were post-annealed from 300°C to 800°C for 30 min in the vacuum of 1×10^{-6} Torr. In order to study the effects of top layers, Ag* and MgO* top layers with a nominal thickness of 20 nm was deposited on Si/MgO(20nm)/FePt(40nm) samples before the lift-off. As shown in Figure 4-1 (c) and (d), these samples with Ag and MgO top layers were named as Si/MgO/FePt/Ag and Si/MgO/FePt/MgO.

Characterizations of these samples were carried out by SEM, AFM, AGM, and XRD.

* No Ag, MgO, FePt peaks were detected in the patterned FePt films by XRD, probably due to the depression of the XRD signal from the patterned structure. Whether they were crystalline or amorphous was not determined.

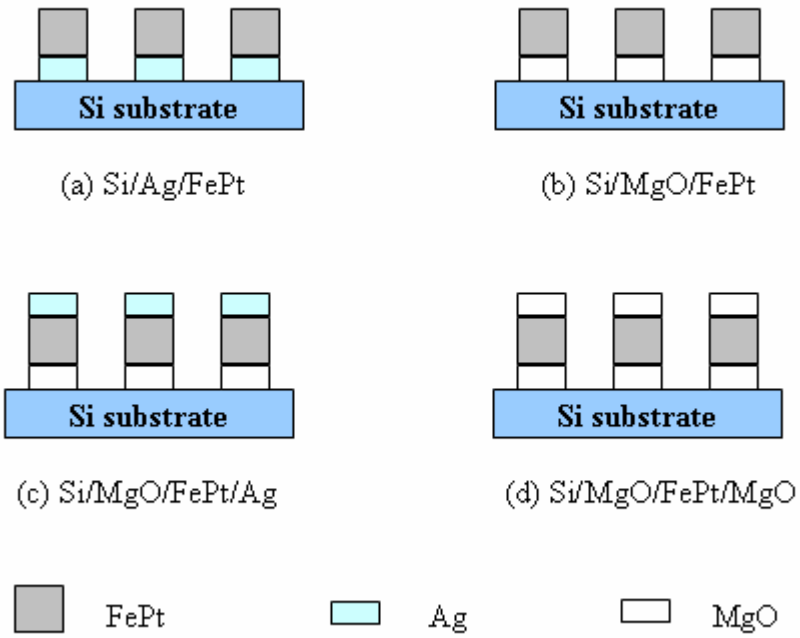

Figure 4-1 Illustration of the patterned film structures of (a) Si/Ag(20 nm)/FePt(40 nm), (b) Si/MgO(20 nm)/FePt(40 nm), (c) Si/MgO(20 nm)/FePt(40 nm)/Ag(20 nm), and (d) Si/MgO(20 nm)/FePt(40 nm)/MgO(20 nm).

4.3 Results and Discussion

Figure 4-2 shows the scanning electron micrograph of the top-view of the pre-patterned photo-resist template, which was deposited with a thin layer of gold for the convenience of SEM characterization. The SEM images revealed that a large area and uniformly distributed template structure was formed. The inset schematically illustrates the cross-sectional view of the template structure. As shown in Figure 4-2, the black dots in the top-view SEM image were the holes in the sketch, and the bright parts in the top-view SEM image were the photo-resist parts in the sketch. The diameter of the holes was ~200 nm, and the inter-hole distance was ~300 nm.

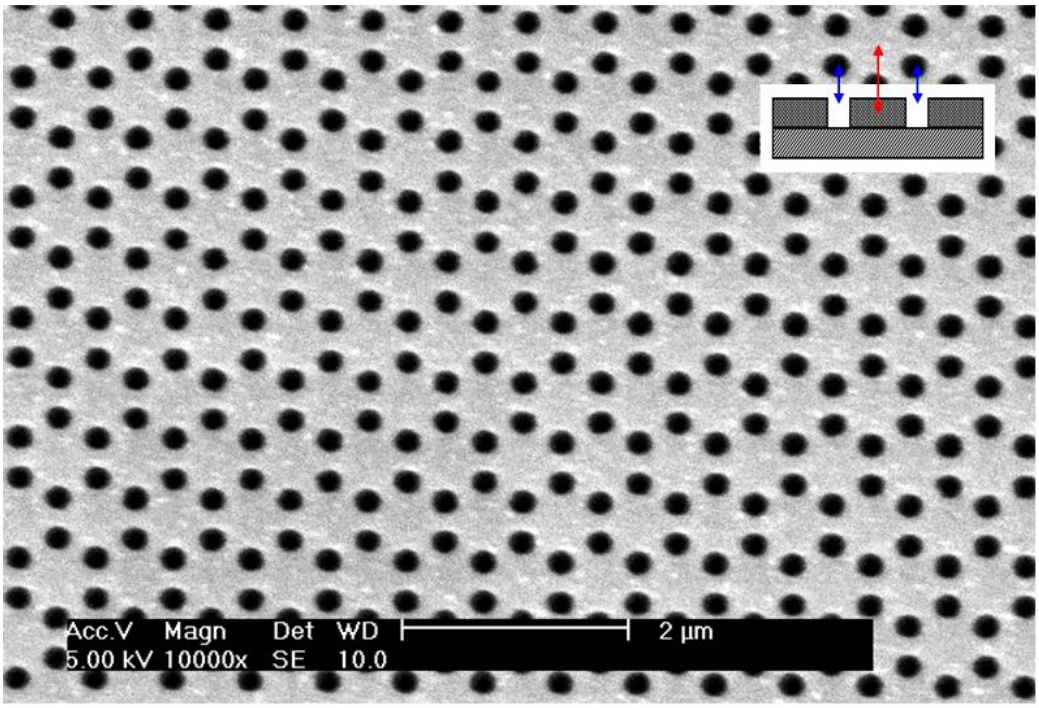

Figure 4-2 SEM image of the pre-patterned photo-resist template.

Figure 4-3 shows the scanning electron micrographs of the patterned Si/Ag/FePt films before lift-off. The inset is a schematic illustration of the cross-sectional view of the patterned Si/Ag/FePt films before lift-off. As shown in Figure 4-3, the black dots in the top-view SEM image were the holes in the sketch, and the bright parts in the top-view SEM image were the Ag/FePt films on the photo-resist parts in the sketch.

Figure 4-4 shows the scanning electron micrographs of the patterned Si/Ag/FePt films after lift-off while before post-annealing. The inset schematically illustrates the cross-sectional view of the patterned Si/Ag/FePt structure. As shown in this inset of Figure 4-4, the photo-resist parts as well as the Ag/FePt films on the photo-resist were lifted-off. Only Ag/FePt films in the holes directly deposited on the Si substrates remained. Thus, the white dots in the top-view SEM image were the Ag/FePt patterns in the sketch, and the dark parts in the top-view SEM image were the Si substrate in the sketch. As shown in Figure 4-2, Figure 4-3, and Figure 4-4 the pre-patterned photo-resist template was perfectly transferred to the patterned structure. Large-area and uniformly distributed FePt patterned structures were obtained after lift-off. The diameter of the FePt particles was ~200 nm, and the inter-particle distance was ~300 nm.

The SEM images of the other patterned samples, like the patterned Si/MgO/FePt films before and after lift-off were almost the same as Figure 4-3 and Figure 4-4, respectively.

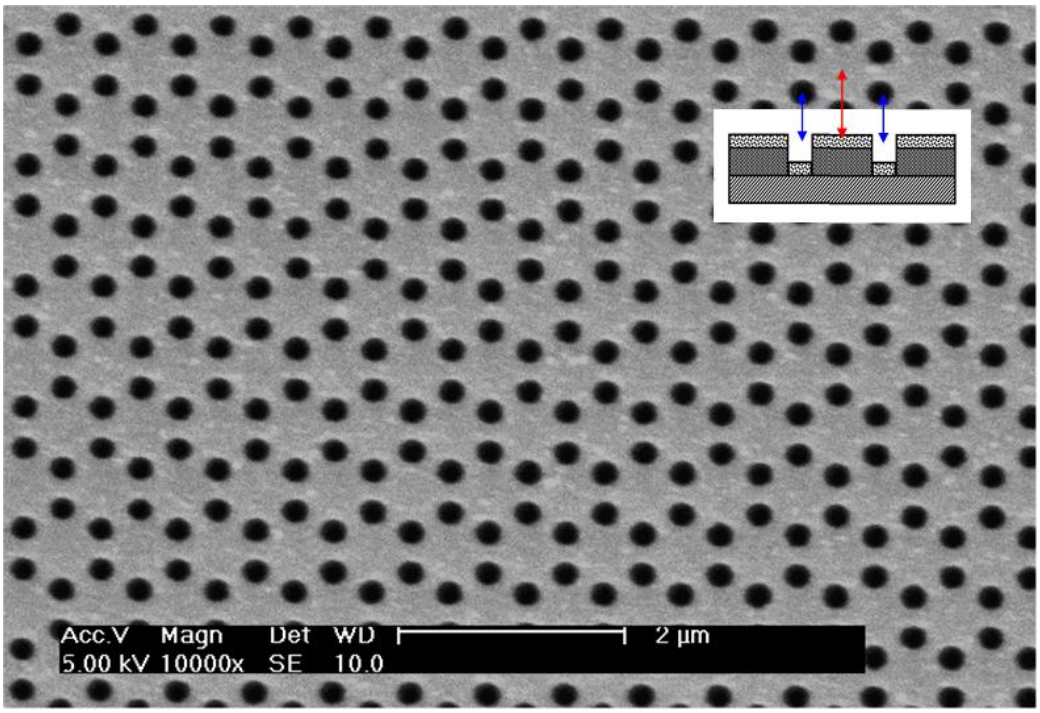

Figure 4-3 SEM image of the patterned Ag/FePt film before lift-off.

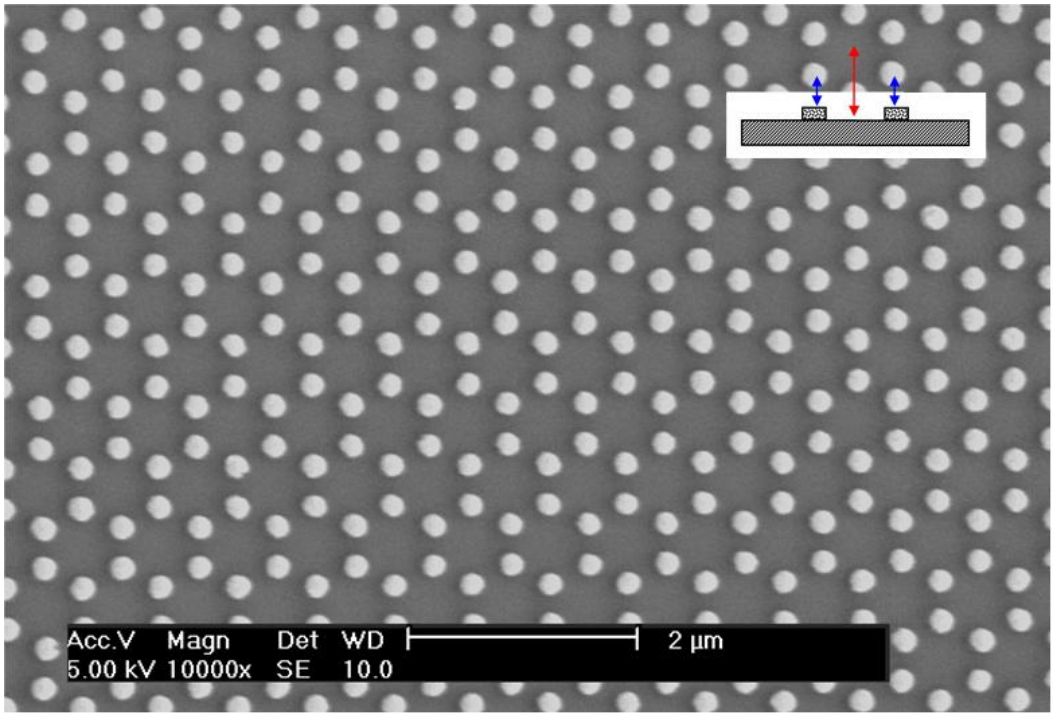

Figure 4-4 SEM image of the patterned Ag/FePt film after lift-off and before post-annealing.

4.3.1 Patterned FePt Films with Ag Underlayers

Figure 4-5 shows the SEM images of the patterned Si/Ag/FePt films after post-annealing at different temperatures. The regular patterned FePt structures could be maintained after post-annealing at lower temperatures (300-500 ^{o}C). Irregular shapes of the particles appeared after post-annealing at higher temperatures (600-800 ^{o}C). Further investigation with atomic force microscopy showed that our FePt pattern was agglomerated after post-annealing at higher temperatures. Figure 4-6 presents a typical top-view and three-dimensional AFM images of the regular FePt patterned structure. Moreover, Figure 4-7 shows the top-view and three-dimensional AFM images of the patterned Si/Ag/FePt film after post-annealing at 800 ^{o}C. From Figure 4-7, multiple peaks forming in a ring can be observed.

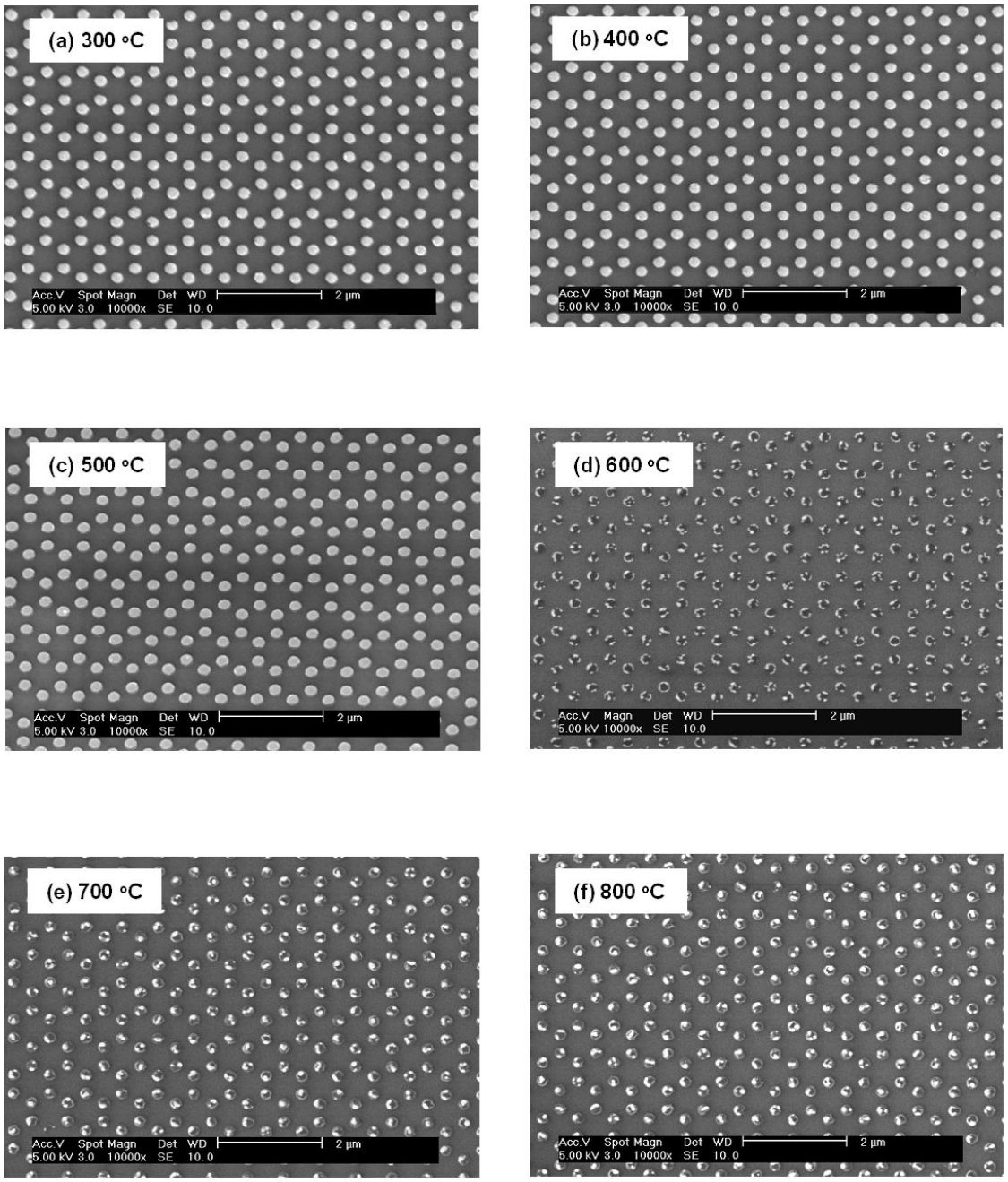

Figure 4-5 SEM images of the patterned Si/Ag/FePt films post-annealed at (a) 300 ^{o}C, (b) 400 ^{o}C, (c) 500 ^{o}C, (d) 600 ^{o}C, (e) 700 ^{o}C, (f) 800 ^{o}C.

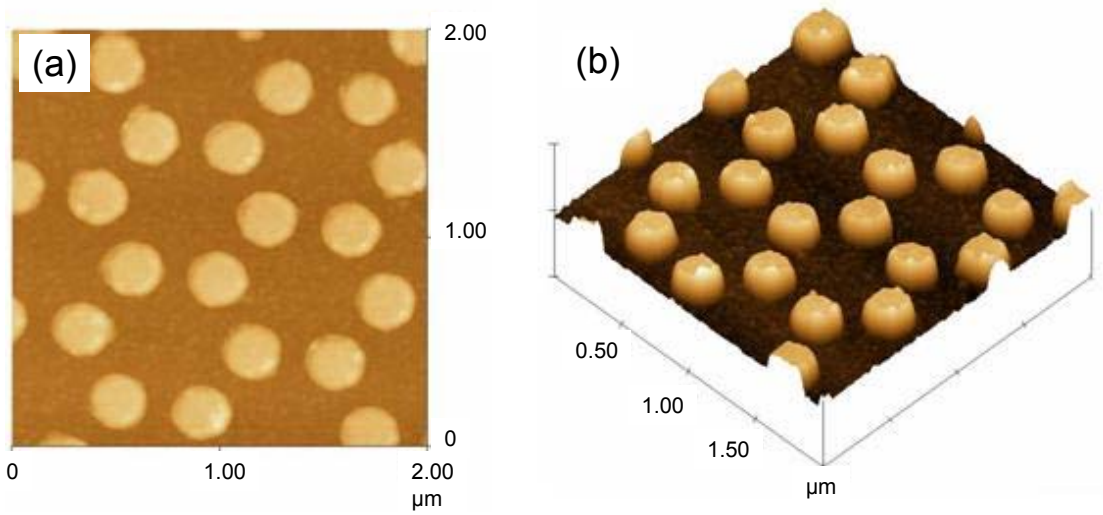

Figure 4-6 (a) Top-view and (b) three-dimensional AFM images of the patterned Si/Ag/FePt film after post-annealing at 500 ^{o}C.

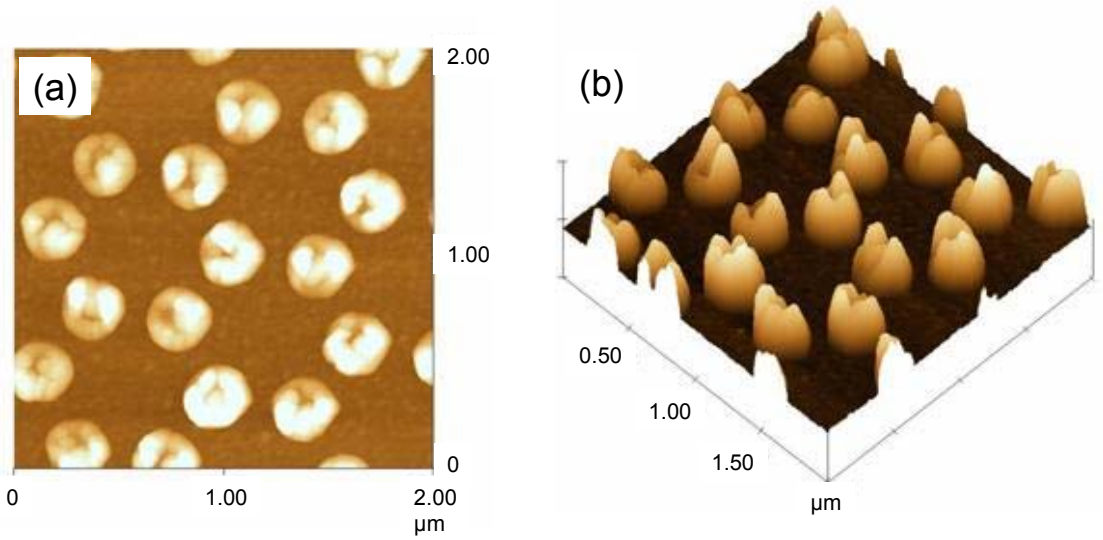

Figure 4-7 (a) Top-view and (b) three-dimensional AFM images of the patterned Si/Ag/FePt film after post-annealing at 800 ^{o}C.

The in-plane and out-of-plane normalized magnetization hysteresis loops of the patterned Si/Ag/FePt samples post-annealed at different temperatures are plotted in Figure 4-8. The samples post-annealed at 400 °C or below exhibited the soft magnetic property, as the hysteresis loops were narrow. When the post-annealing temperature increased to 500 °C, both the in-plane and out-of-plane hysteresis loops became broad, showing hard magnetic property. This result also indicated that the ordered fct FePt phase was forming. With increasing of the post-annealing temperature, the hysteresis loops became broader until 700 °C, indicating that the hard magnetic property was enhanced. Similar as to the continuous FePt films, steps in the hysteresis loops were also observed in the patterned Si/Ag/FePt samples annealed at 500 °C or above. This could also be understood that the FePt films were partially ordered and some remaining disordered fcc phase contributed to the soft magnetic property. Compared to the continuous Si/Ag/FePt films, the patterned films showed less difference between the in-plane and out-of-plane hysteresis loops, indicating less magnetic anisotropy in the patterned films.

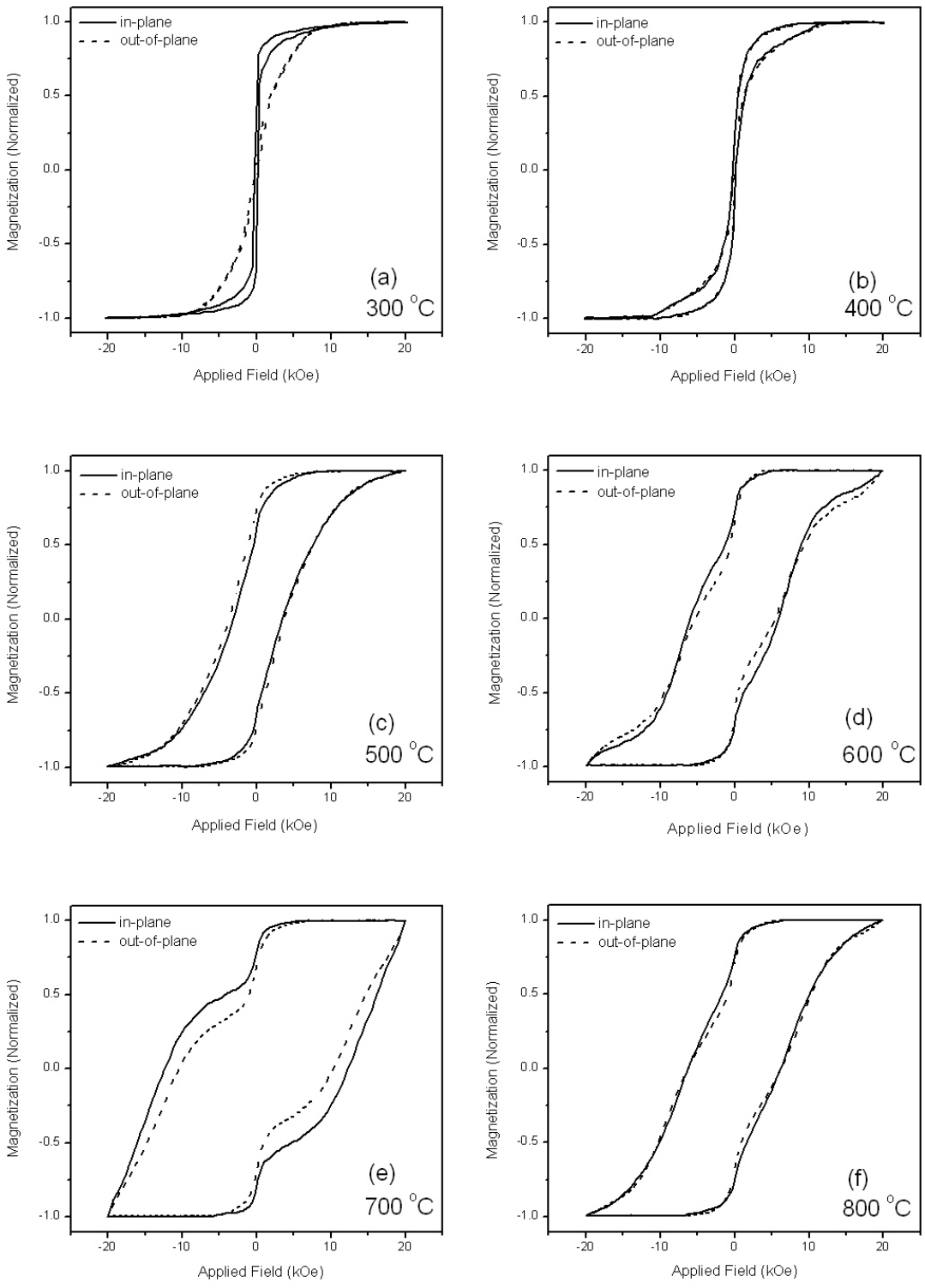

Figure 4-8 Magnetization hysteresis loops of the patterned Si/Ag/FePt samples post-annealed at (a) 300 °C, (b) 400 °C, (c) 500 °C, (d) 600 °C, (e) 700 °C, (f) 800 °C.

The values of the in-plane and out-of-plane coercivity of the patterned Si/Ag/FePt films are summarized in Table 4-1. Figure 4-9 shows the in-plane and out-of-plane coercivity as a function of the post-annealing temperature. The coercivity remained very low after post-annealing at 400 °C. When the fct phase was formed after annealing at 500 °C, the coercivity was ~3.6 kOe. Coercivity increased gradually and reached a maximum of ~13 kOe after annealing at 700 °C. The results implied that the phase transformation was considerably reduced in patterned FePt films, and that the ordering temperature was relatively higher, compared to the continuous FePt films. It had to be noted that no significant magnetic anisotropy was present in the patterned Si/Ag/FePt films.

Table 4-1 In-plane and out-of-plane coercivity of the patterned Si/Ag/FePt samples.

Temperature (^{o}C)	**$H_{c\parallel}$ (kOe)**	**$H_{c\perp}$ (kOe)**
300	0.13	0.10
400	0.21	0.11
500	3.29	3.70
600	5.98	5.50
700	12.80	10.87
800	6.22	6.51

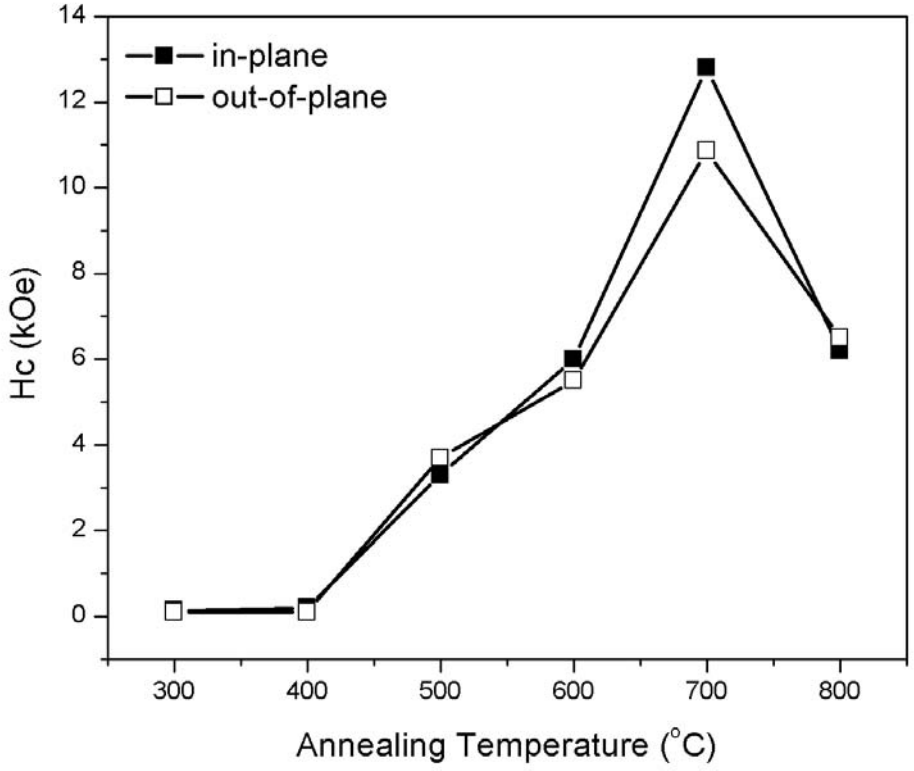

Figure 4-9 In-plane and out-of-plane coercivity of the patterned Si/Ag/FePt samples post-annealed at different temperatures.

4.3.2 Patterned FePt Films with MgO Underlayers

The SEM images of the patterned Si/MgO/FePt films after post-annealing at different temperatures are shown in Figure 4-10. The regular FePt patterned structures could be maintained even after post-annealing at 600 ^{o}C, which was better than the patterned FePt films with Ag underlayers. However, the particles shrank into the center of the particles for the patterned Si/MgO/FePt films post-annealed at 700 ^{o}C or higher. Top-view and three-dimensional AFM images showed that after post-annealing at higher temperatures, the FePt particle was agglomerated into an island in the center of the position where the original particle was (Figure 4-12). For comparison, the typical top-view and three-dimensional AFM images of the regular FePt patterned structure

are also shown in Figure 4-11.

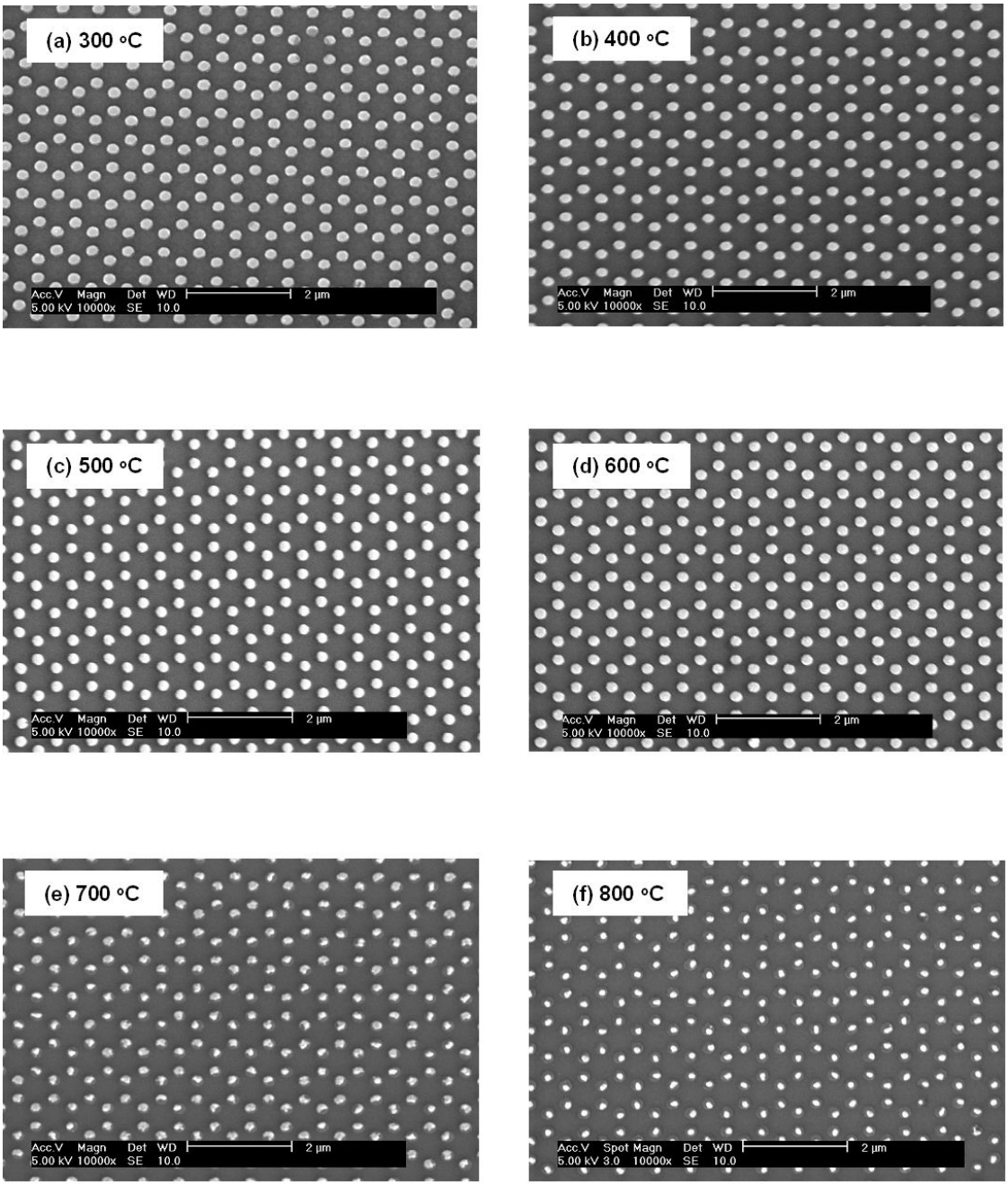

Figure 4-10 SEM images of the patterned Si/MgO/FePt films post-annealed at (a) 300 °C, (b) 400 °C, (c) 500 °C, (d) 600 °C, (e) 700 °C, (f) 800 °C.

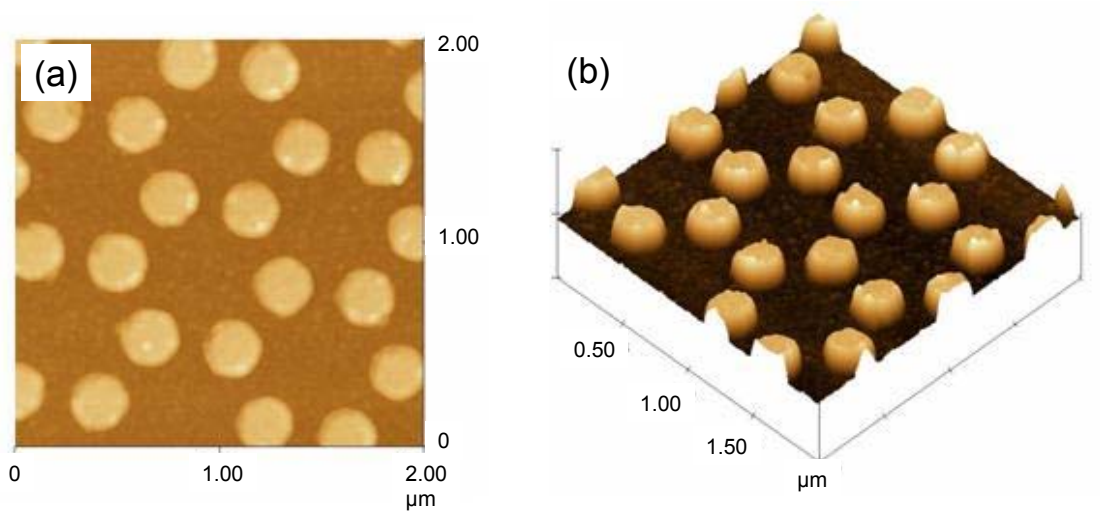

Figure 4-11 (a) Top-view and (b) three-dimensional AFM images of the patterned Si/MgO/FePt film after post-annealing at 500 ^{o}C.

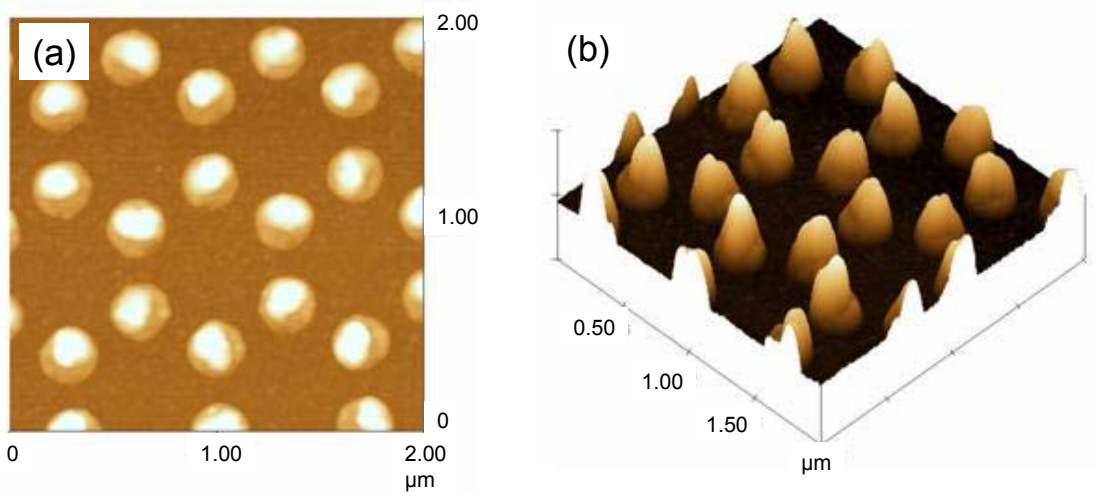

Figure 4-12 (a) Top-view and (b) three-dimensional AFM images of the patterned Si/MgO/FePt film after post-annealing at 800 ^{o}C.

Figure 4-13 shows the magnetic hysteresis loops of the patterned films with MgO as the underlayers after post-annealing at different temperatures. The patterned Si/MgO/FePt samples post-annealed at 300 °C or below were magnetically soft. For the patterned Si/MgO/FePt films after post-annealing at 400 °C, the hysteresis loops in both the in-plane and out-of-plane directions were much broader than those of the patterned samples with Ag underlayers which were also post-annealed at 400 °C. This indicated that the ordering temperature were lower for the patterned samples with MgO underlayers. With the increase of the post-annealing temperature, the samples became magnetically hard. However, the increase in the width of the hysteresis loops was slight until 800 °C. After post-annealing at 800 °C, the patterned Si/MgO/FePt films showed very broad hysteresis loops in both the in-plane and out-of-plane directions.

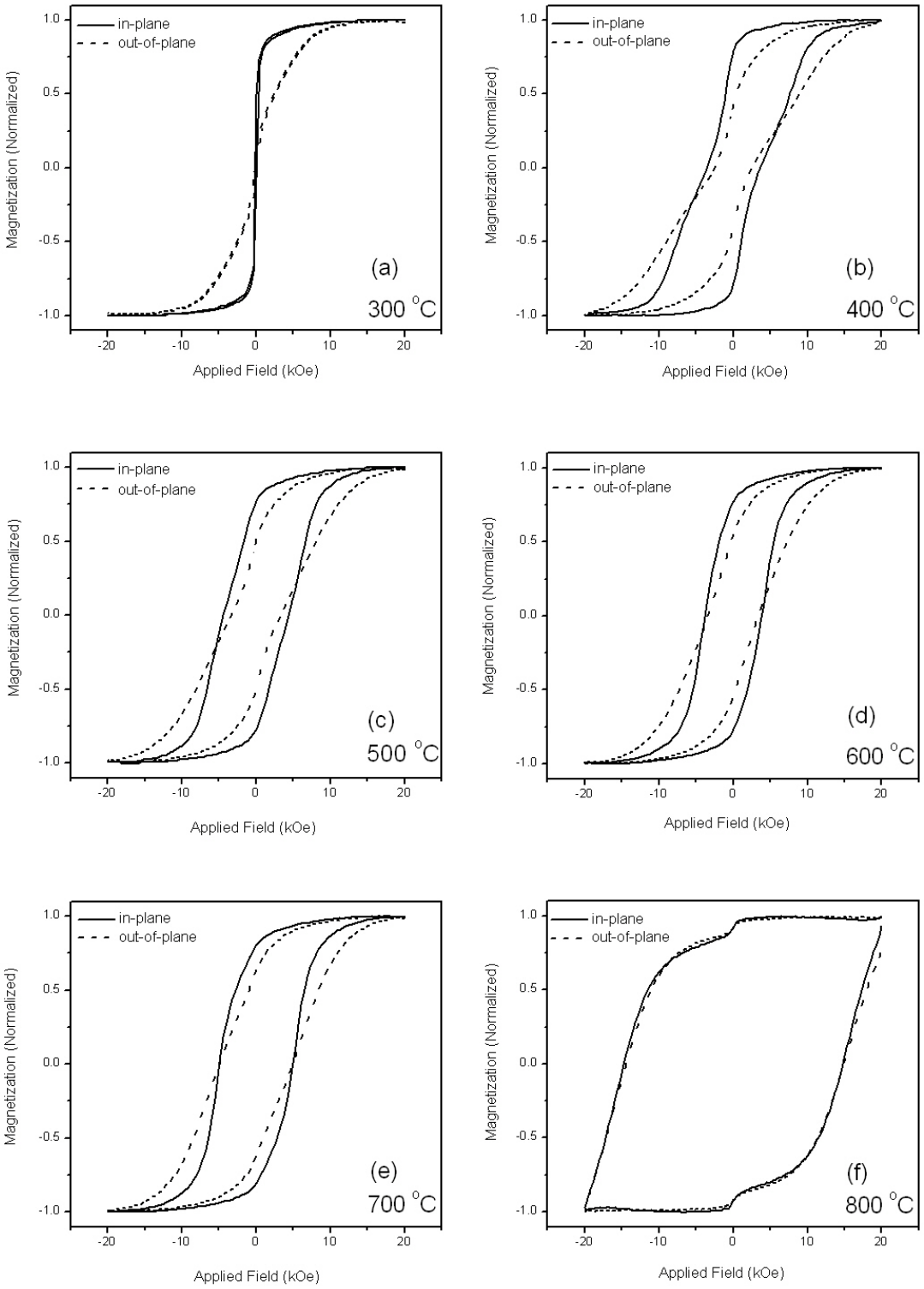

Figure 4-13 Magnetization hysteresis loops of the patterned Si/MgO/FePt samples post-annealed at (a) 300 °C, (b) 400 °C, (c) 500 °C, (d) 600 °C, (e) 700 °C, (f) 800 °C.

Table 4-2 shows the values of the in-plane and out-of-plane coercivity of the patterned Si/MgO/FePt films. The in-plane and out-of-plane coercivity as a function of post-annealing temperature for the patterned Si/MgO/FePt films is plotted in Figure 4-14. The sample post-annealed at 300 °C was magnetically soft, probably due to the predominantly FePt fcc phase. Coercivity increased to ~3 kOe for the patterned Si/MgO/FePt film post-annealed at 400 °C, indicating the formation of the ordered fct FePt phase. This ordering temperature of 400 °C for the patterned Si/MgO/FePt films was lower than that of the patterned samples with Ag underlayers (500 °C). With the further increase of the post-annealing temperature, the patterned Si/MgO/FePt samples became more magnetically hard. After post-annealing at 800°C, high coercivity over 13 kOe was obtained in both the in-plane and out-of-plane directions. This strong increase in coercivity might be associated with the agglomeration of FePt particles. Compared to the patterned Si/Ag/FePt films annealed at 800 °C, which showed the morphology of multiple peaks in a circle (Figure 4-7), the patterned Si/MgO/FePt films after annealing at 800 °C exhibited the morphology of the single island in the center (Figure 4-12). Different morphologies implied the different strain and grain size in these two samples. Furthermore, the strain and grain size had great effects on both the formation of the ordered fct FePt phase and improvement of coercivity [6,7]. Therefore, the single-island morphology in the patterned Si/MgO/FePt films after annealing at 800 °C might be related to the increase of the coercivity.

Table 4-2 In-plane and out-of-plane coercivity of the patterned Si/MgO/FePt samples.

Temperature (^{o}C)	$H_{c\parallel}$ (kOe)	$H_{c\perp}$ (kOe)
300	0.07	0.10
400	3.59	2.45
500	4.39	3.34
600	3.84	3.39
700	4.97	4.95
800	14.75	14.60

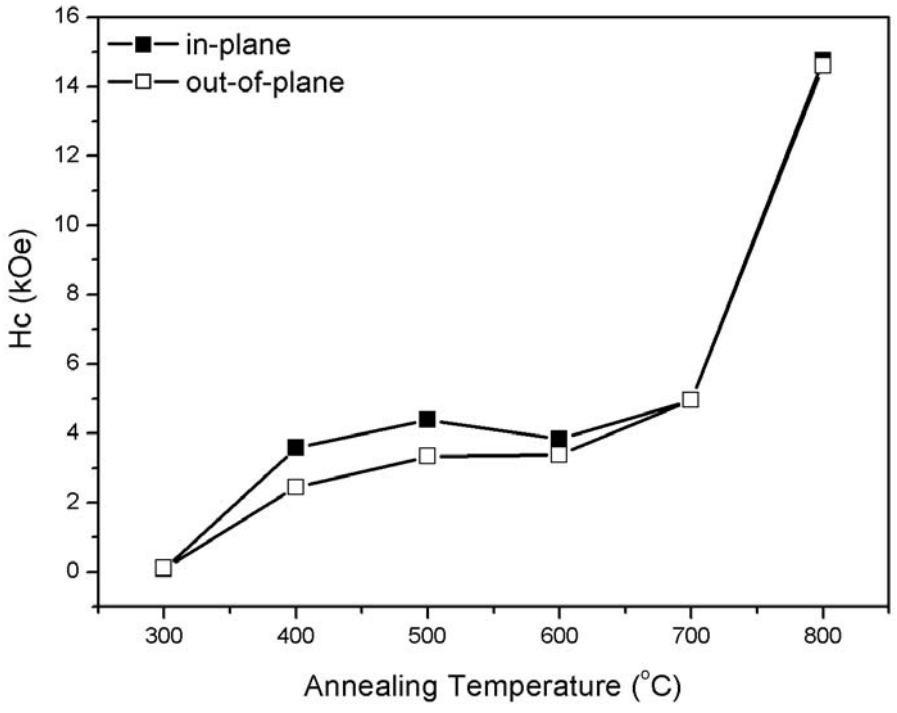

Figure 4-14 In-plane and out-of-plane coercivity of the patterned Si/MgO/FePt samples post-annealed at different temperatures.

4.3.3 FePt Films with MgO Underlayers and Ag Top Layers

Another important issue is whether the patterned FePt structure can be well maintained after the post-annealing, particularly after annealing at higher temperature for the formation of the ordered fct phase with a high coercivity. Our study has shown that the FePt pattern is well maintained after annealing at 500 °C or below for the patterned Si/Ag/FePt films (Figure 4-5 (a), (b), (c)). A higher temperature could result in damage of the FePt particles (Figure 4-5 (d), (e), (f)). For the patterned Si/MgO/FePt films, the FePt pattern could be well maintained after annealing at 600 °C or below (Figure 4-10 (a), (b), (c), (d)). In other words, the damage of the particles for the patterned Si/MgO/FePt films was retarded to 700 °C, compared to the patterned Si/Ag/FePt films. However, the Si/MgO/FePt patterned structure was still damaged after post-annealing at higher temperature for the formation of the ordered fct phase. Therefore, studies on protecting the regular patterned structure while maintaining the high coercivity by introducing Ag and MgO top layer on the patterned Si/MgO/FePt films were carried out. The two sets of samples were named as the patterned Si/MgO/FePt/Ag films and the patterned Si/MgO/FePt/MgO films, respectively.

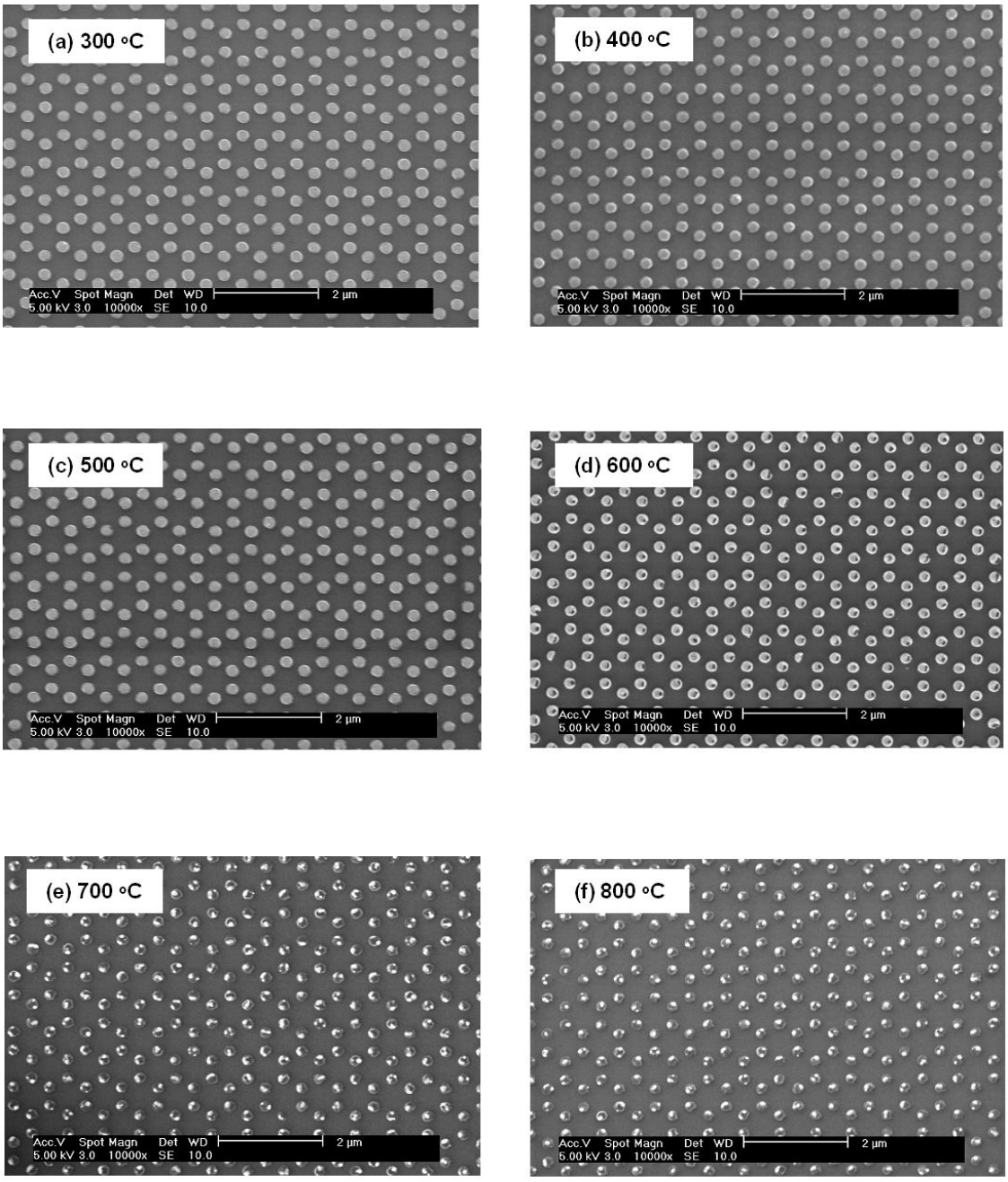

Figure 4-15 SEM images of the patterned Si/MgO/FePt/Ag films post-annealed at (a) 300 °C, (b) 400 °C, (c) 500 °C, (d) 600 °C, (e) 700 °C, (f) 800 °C.

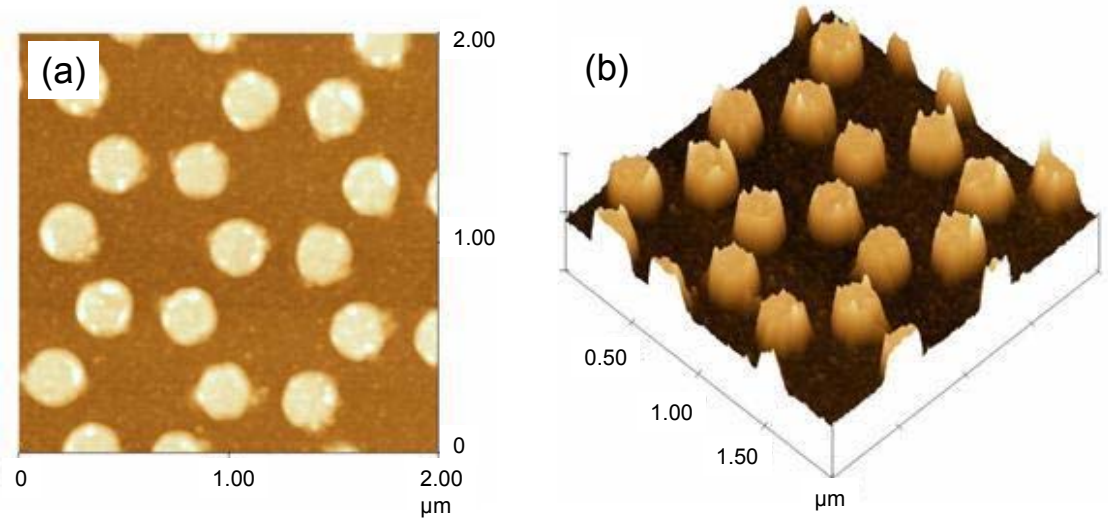

Figure 4-16 (a) Top-view and (b) three-dimensional AFM images of the patterned Si/MgO/FePt/Ag film after post-annealing at 500 ^{o}C.

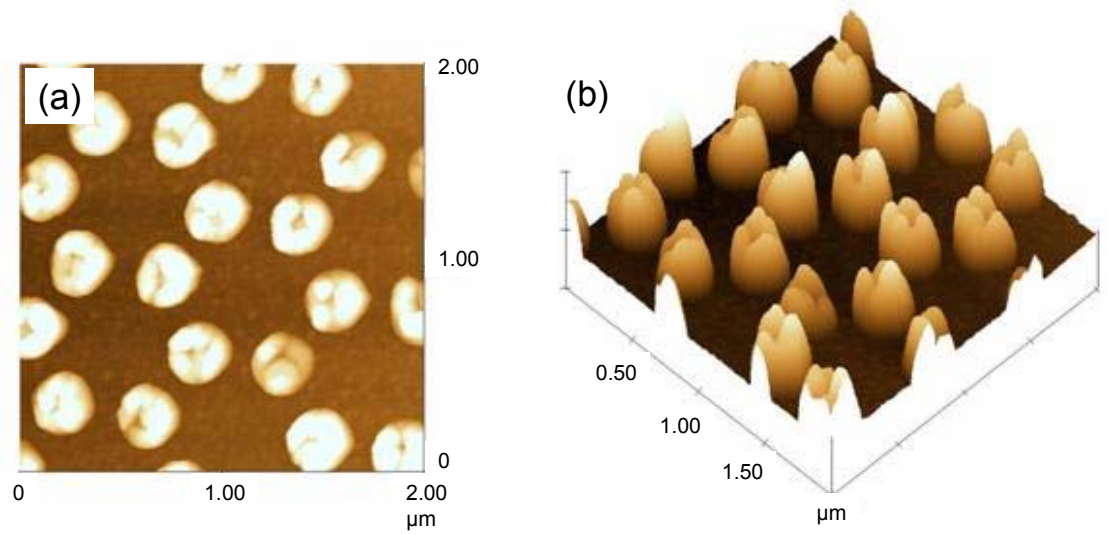

Figure 4-17 (a) Top-view and (b) three-dimensional AFM images of the patterned Si/MgO/FePt/Ag film after post-annealing at 800 ^{o}C.

The morphology for the patterned Si/MgO/FePt/Ag films after post-annealing at different temperatures is shown in Figure 4-15. It could be seen that the regular FePt patterned structure could be maintained after post-annealing at 500 ^{o}C or below. The damage of the patterned structure was accelerated by introducing a top layer of Ag, because the irregular shape appeared in Si/MgO/FePt/Ag samples after post-annealing at 600 ^{o}C. Compared to the patterned Si/MgO/FePt film, whose structure was well maintained after annealing at 600 ^{o}C, the patterned Si/MgO/FePt/Ag sample was not an improvement but deterioration.

Figure 4-16 shows typical top-view and three-dimensional AFM images of the regular patterned structure for the Si/MgO/FePt/Ag samples. Figure 4-17 shows the top-view and three-dimensional AFM images of the patterned Si/MgO/FePt/Ag film after post-annealing at 800 ^{o}C. Not like the single island structure in the patterned Si/MgO/FePt films, but similar to the patterned Si/Ag/FePt films, the patterned Si/MgO/FePt/Ag films after post-annealing at 800 ^{o}C showed several peaks forming in a ring.

Figure 4-18 shows the magnetization hysteresis loops of the patterned Si/MgO/FePt/Ag films with Ag as the top layer after post-annealing at different temperatures. The variation of the hysteresis loops showed the similar trend as that of the patterned Si/MgO/FePt samples without top layer. However, the hysteresis loops of the samples post-annealed at 500 °C – 700 °C were broader than the samples without

the top layer, which indicated the enhancement of the ordered fct phase.

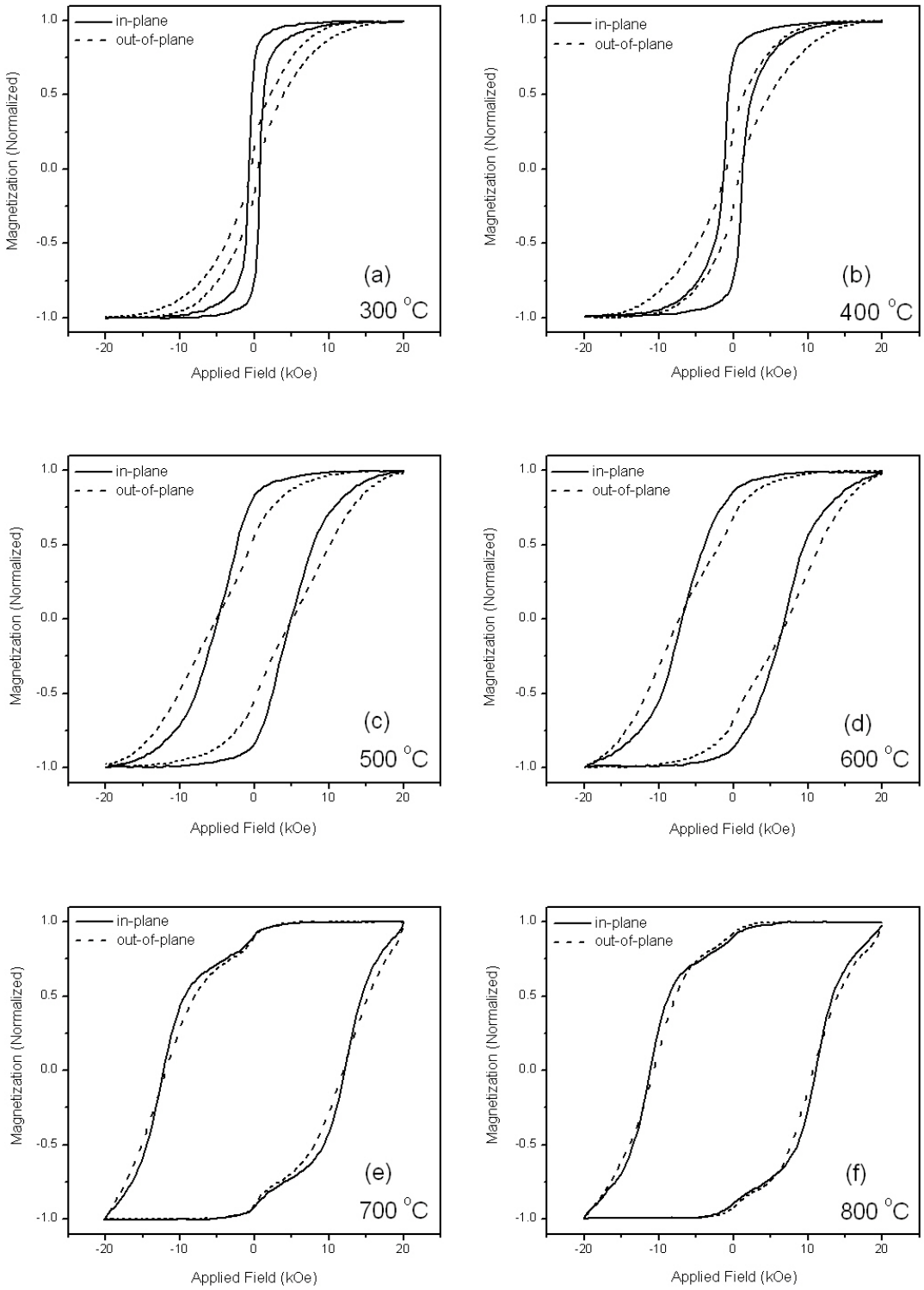

Figure 4-18 Magnetization hysteresis loops of the patterned Si/MgO/FePt/Ag samples post-annealed at (a) 300 °C, (b) 400 °C, (c) 500 °C, (d) 600 °C, (e) 700 °C, (f) 800 °C.

Table 4-3 shows the in-plane and out-of-plane coercivity of the patterned Si/MgO/FePt/Ag films post-annealed at different temperatures. Figure 4-19 shows the in-plane and out-of-plane coercivity in the dependence of the post-annealing temperature. The trend of the coercivity was similar as that of the patterned Si/Ag/FePt films. The samples post-annealed at 400 °C or below were magnetically soft. With the further increase of the annealing temperature, the samples became magnetically hard, and the coercivity increased gradually until reaching the maximum of 12 kOe at 700 °C. Compared to the patterned Si/MgO/FePt films without any top layer, the samples with the Ag top layer showed the retarded ordering in FePt and a higher ordering temperature.

Table 4-3 In-plane and out-of-plane coercivity of the patterned Si/MgO/FePt/Ag samples.

Temperature (^{o}C)	**$H_{c\parallel}$ (kOe)**	**$H_{c\perp}$ (kOe)**
300	0.74	0.44
400	1.26	0.93
500	4.92	5.09
600	6.88	7.32
700	12.16	12.13
800	11.12	10.93

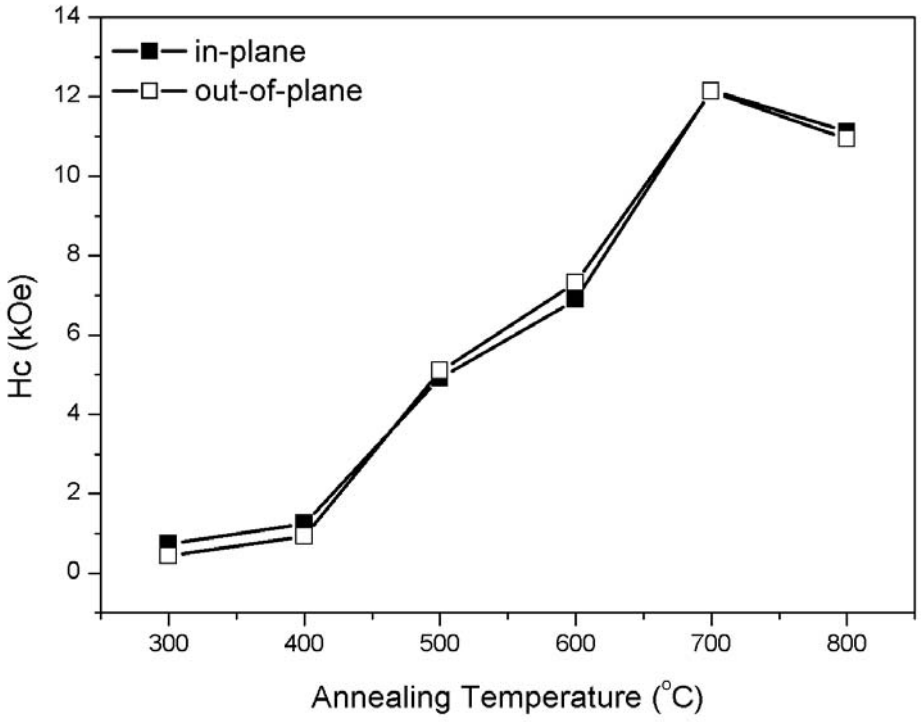

Figure 4-19 In-plane and out-of-plane coercivity of the patterned Si/MgO/FePt/Ag samples post-annealed at different temperatures.

4.3.4 FePt Films with MgO Underlayers and MgO Top Layers

Figure 4-20 shows the morphology for the patterned Si/MgO/FePt/MgO films after post-annealing at different temperatures. It should be noted that the regular FePt patterned structure is well maintained even after post-annealing at 800 ^{o}C by introducing a top layer of MgO. Further observation with AFM revealed that, though there was still some mild agglomeration for the samples annealed at 800 ^{o}C (Figure 4-22), the patterned structure was to the great extent well maintained (Figure 4-21, Figure 4-22). Compared to the Ag top layer, the MgO top layer was much more significant to protect the perfect patterned structure. This might be because the melting temperature of MgO (~2830 ^{o}C) was much larger than that of Ag (~962 ^{o}C).

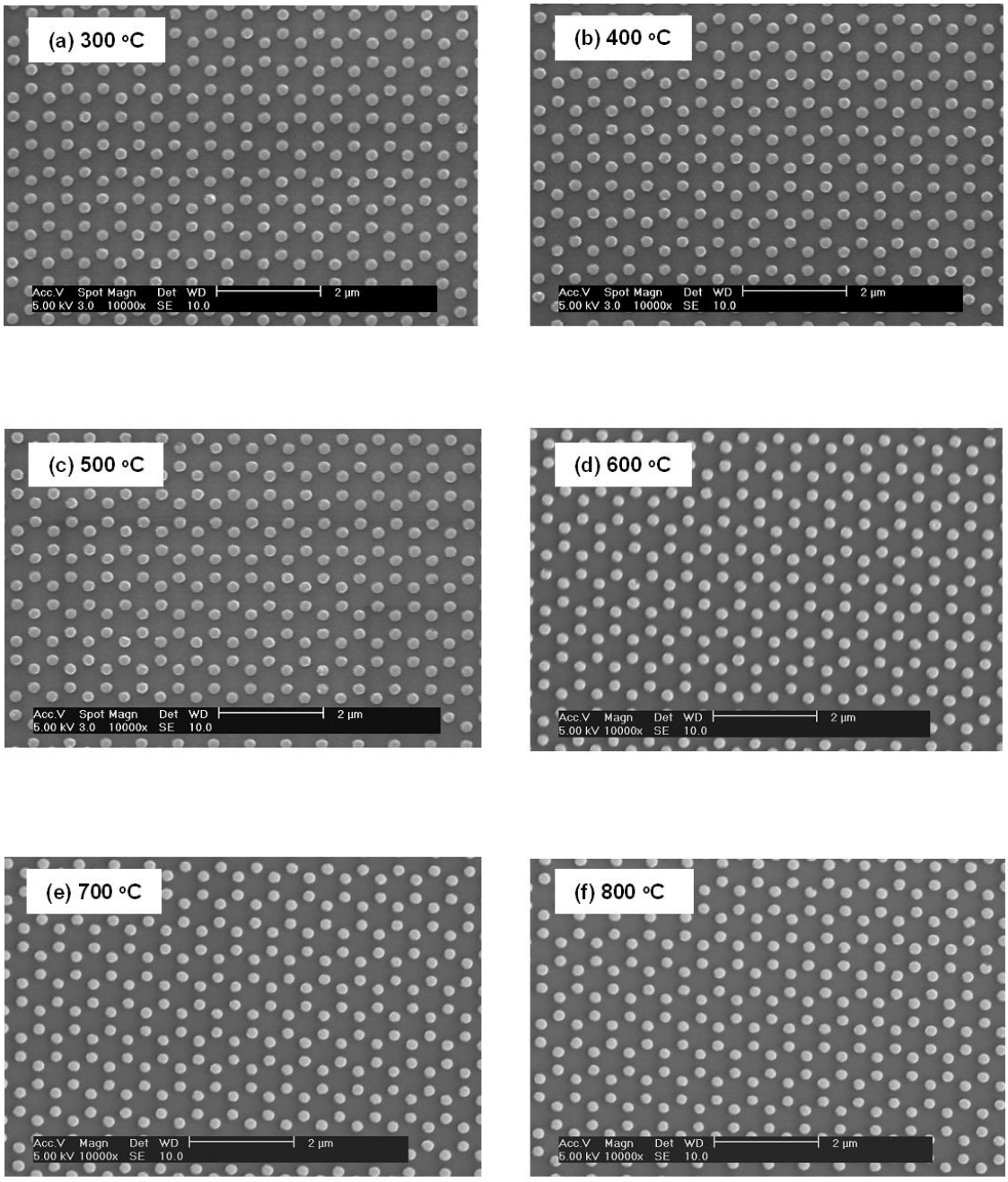

Figure 4-20 SEM images of the patterned Si/MgO/FePt/MgO films post-annealed at (a) 300 °C, (b) 400 °C, (c) 500 °C, (d) 600 °C, (e) 700 °C, (f) 800 °C.

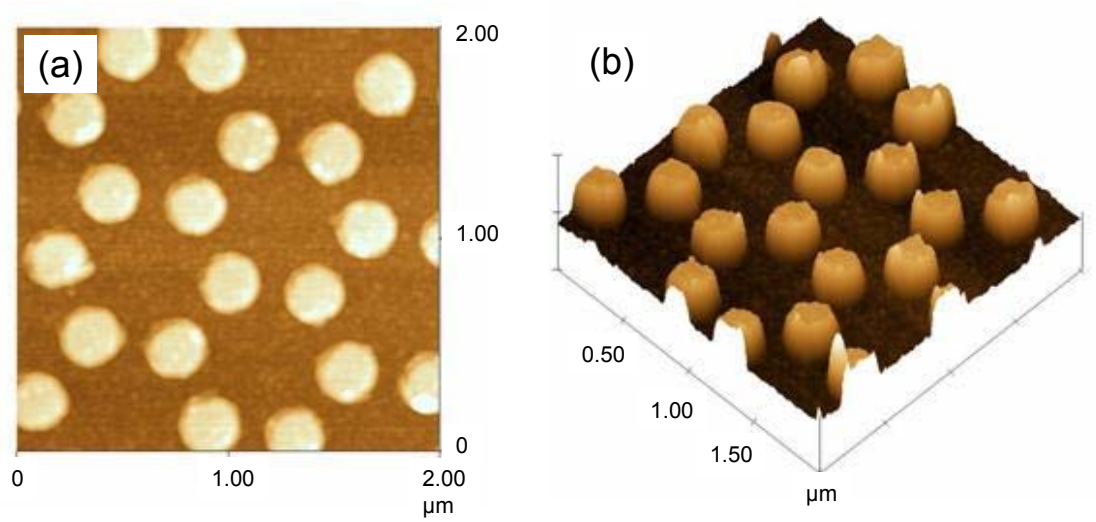

Figure 4-21 (a) Top-view and (b) three-dimensional AFM images of the patterned Si/MgO/FePt/MgO film after post-annealing at 500 °C.

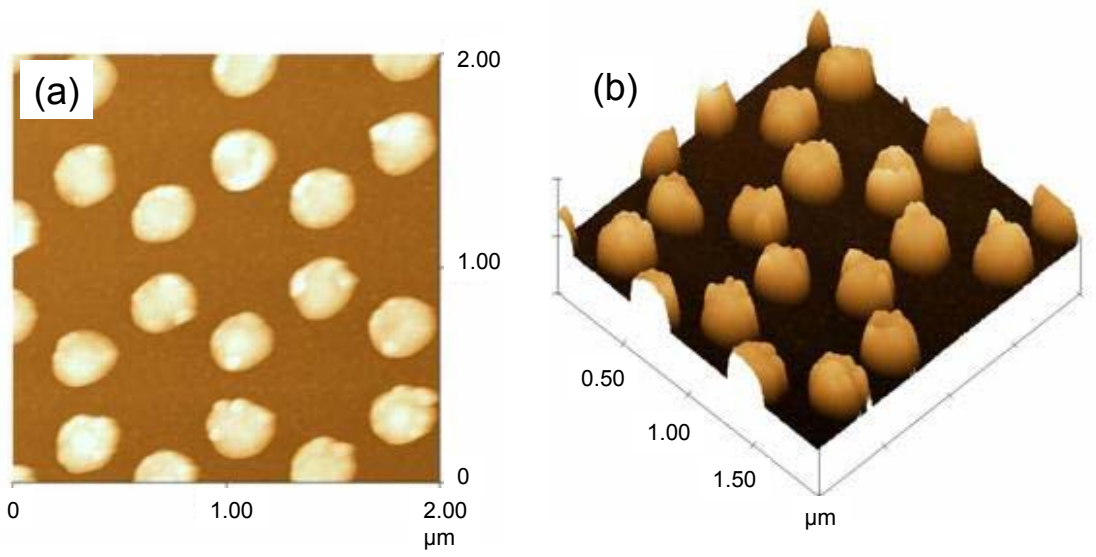

Figure 4-22 (a) Top-view and (b) three-dimensional AFM images of the patterned Si/MgO/FePt/MgO film after post-annealing at 800 °C.

Figure 4-23 shows the dependence of the hysteresis loops on the post-annealing temperature for the patterned Si/MgO/FePt/MgO samples with MgO as the top layer. The variation trend of the hysteresis loops was similar as the patterned Si/MgO/FePt/Ag samples with the Ag top layer. However, the squareness of the in-plane loop for the patterned Si/MgO/FePt/MgO sample post-annealed at 800 °C was increased. Furthermore, there was no step in the loop, which indicated that the FePt films were fully ordered.

The values of the in-plane and out-of-plane coercivity of the patterned Si/MgO/FePt/MgO samples post-annealed at different temperatures are shown in Table 4-4. Figure 4-24 shows how the in-plane and out-of-plane coercivity varied with different post-annealing temperatures. Both the in-plane and out-of-plane coercivity was low, when the samples were post-annealed at 400 °C or below, indicating the disordered fcc phase dominated in FePt. When the post-annealing temperature increased to 500 °C, the coercivity increased to 2 kOe. This indicated that the ordering transformation in the FePt pattern started to occur. Coercivity increased gradually with the increase of the post-annealing temperature. After annealing at 700 °C and 800 °C, the coercivity reached maximum of ~10 kOe. Therefore, the optimized FePt patterned structure would be the patterned Si/MgO/FePt/MgO films with a MgO top layer, as high coercivity ~10 kOe could be achieved with a well maintained FePt patterned structure.

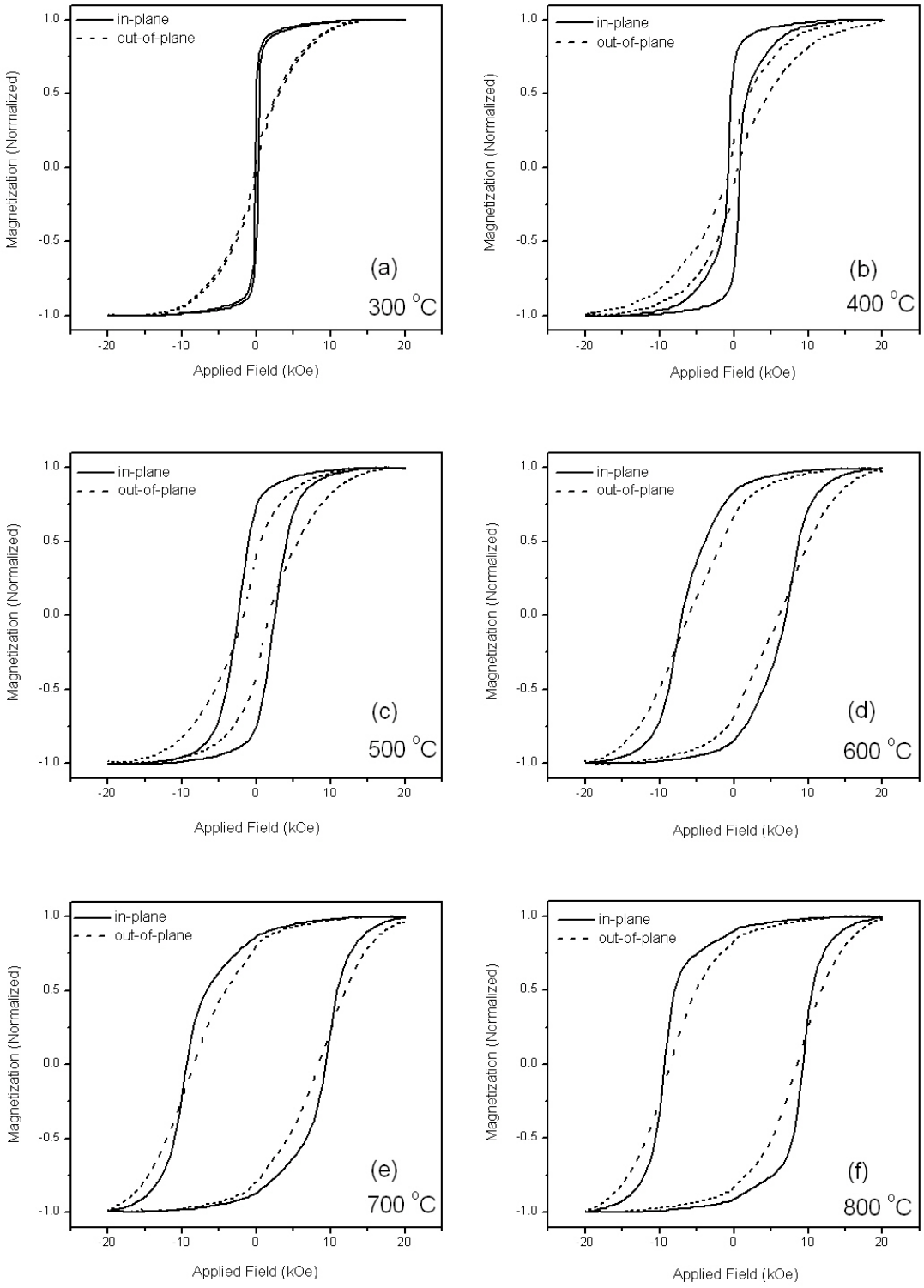

Figure 4-23 Magnetization hysteresis loops of the patterned Si/MgO/FePt/MgO samples post-annealed at (a) 300 °C, (b) 400 °C, (c) 500 °C, (d) 600 °C, (e) 700 °C, (f) 800 °C.

Table 4-4 In-plane and out-of-plane coercivity of the patterned Si/MgO/FePt/MgO samples.

Temperature (^{o}C)	$H_{c\parallel}$ (kOe)	$H_{c\perp}$ (kOe)
300	0.14	0.10
400	0.76	0.51
500	2.45	1.71
600	6.98	6.07
700	9.36	8.42
800	9.30	8.53

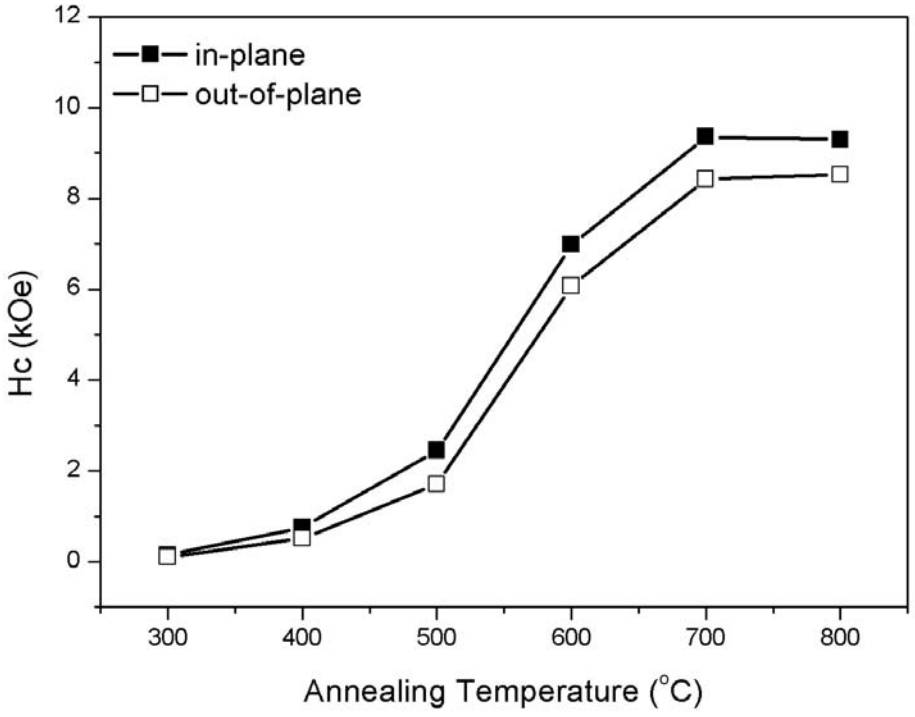

Figure 4-24 In-plane and out-of-plane coercivity of the patterned Si/MgO/FePt/MgO samples post-annealed at different temperatures.

4.4 Summary

Large area of uniform FePt patterned films were successfully fabricated on silicon (100) substrates based on the following steps: deep ultraviolet lithography with the wavelength of 248 nm, pulsed laser deposition at room temperature, lift-off, and post-annealing. Underlayers of Ag or MgO were deposited on Si substrates to prevent the chemical reaction between Si and FePt. Phase transformation from the disordered fcc phase to the ordered fct phase started after annealing at 400 ^{o}C for the continuous FePt films, while for the patterned FePt films, it was retarded to ~500 ^{o}C. However, high coercivity of 10-15 kOe has still been achieved in the patterned FePt films after post-annealing at 700 ^{o}C or higher. The maximum in-plane and out-of-plane coercivity of the patterned FePt samples with different underlayers or top layers is summarized in Table 4-5. Moreover, the MgO underlayer was found favorable for the formation of the high-coercivity fct phase in the patterned FePt films, as the ordering temperature is lower than that of the patterned samples with Ag underlayers. It was found that a top layer of MgO could result in the enhancement of coercivity with a well maintained FePt patterned structure.

Table 4-5 Summary of the maximum in-plane and out-of-plane coercivity of the patterned FePt samples with different underlayers or top layers.

Samples	**$H_{c\parallel}$ (kOe)**	**$H_{c\perp}$ (kOe)**
Si/Ag/FePt (700 ^{o}C)	13	11
Si/MgO/FePt (800 ^{o}C)	15	15
Si/MgO/FePt/Ag (700 ^{o}C)	12	12
Si/MgO/FePt/MgO (800 ^{o}C)	9	9

References:

[1] J. G. Korvink and O. Paul, *MEMS: A Practical Guide to Design, Analysis, and Applications*, Springer, Heidelberg, Germany (2006).
[2] N. V. Myung, D. Y. Park, B. Y. Yoo, and P. T. A. Sumodjo, J. Magn. Magn. Mater. 265, 189 (2003).
[3] H. J. Cho, S. Bhansali, C. H. Ahn, J. Appl. Phys. 87, 6340 (2000).
[4] O. Cugat, J. Delamare, and G. Reyne, IEEE Trans. Mag. 39, 3607 (2003).
[5] Y. Ishikawa, M. Kumezawa, R. Nuryadi, and M. Tabe, Appl. Surf. Sci. 190, 11 (2002).
[6] E. F. Kneller and F. E. Luborsky, J. Appl. Phys. 34, 656 (1963).
[7] J. H Yin, B. H. Liu, J. Ding, and Y. C. Wang, Bulletin. Mater. Sci. 29, 573 (2006).

CHAPTER 5

Conclusion

Continuous FePt thin films with thickness of 40 nm were deposited on Si (100) substrates by pulsed laser deposition (PLD) at room temperature, and post-annealed at different temperatures ranging from 300 to 800 °C. The effects of different underlayers (or substrates) have been compared via two groups of underlayers (or substrates): Amorphous underlayers (amorphous SiO_x, and amorphous MgO) and crystalline underlayers (crystalline Ag, and (100) textured MgO). Among them, crystalline Ag and textured MgO underlayers were found effective to promote the formation of the ordered fct FePt phase; it showed an ordering temperature of lower than 400 °C. High coercivity of 10-15 kOe has been achieved after post-annealing at 600 °C. Moreover, it has been found that coercivity of the 40 nm thick FePt films grown on all those underlayers increased as the annealing temperature increased until 700 °C. The coercivity of the samples post-annealed at 800 °C was smaller than those post-annealed at 700 °C. This result might be due to the oxidization of FePt at a high post-annealing temperature. Furthermore, the FePt films with textured MgO underlayers had smaller grain size, which was also a key advantage for magnetic recording application, which was stated in Chapter 1.

Thus, FePt thickness effects on magnetic properties of FePt films with different thicknesses deposited on the textured MgO underlayers were further studied. The FePt film thickness under study ranged from 5 nm to 40 nm. It was found that the ordering temperature of the FePt films decreased with increasing FePt film thickness and perpendicular magnetic anisotropy was formed in FePt films with thickness below ~10

nm.

Large-area of uniform patterned FePt films were fabricated on silicon (100) substrates based on the following steps: deep ultraviolet lithography with the wavelength of 248 nm, pulsed laser deposition at room temperature, lift-off, and post-annealing. The diameter of the FePt particles was ~200 nm, and the inter-particle distance was ~300 nm. Underlayers of Ag or MgO were deposited on Si substrates to prevent a chemical reaction between Si and FePt. Phase transformation from the disordered fcc to the ordered fct FePt phase started after annealing at 500 °C for the patterned FePt films, while for the continuous FePt films, it started at 400 °C. This indicated that a higher ordering temperature was required in the patterned FePt films. However, high coercivity of 10-15 kOe has also been achieved in the patterned FePt films after post-annealing at 700 ^{o}C or higher. Moreover, the MgO underlayer was found favorable for the formation of the high-coercivity fct phase in the patterned FePt films, as the ordering temperature is lower than that of the patterned samples with Ag underlayers. In addition, the effects of Ag and MgO top layers on the patterned structure maintenance and coercivity enhancement were also investigated. It was found that a top layer of MgO resulted in the enhancement of coercivity with a well maintained FePt patterned structure.

This work has showed that the patterned FePt thin films have many different properties, which are interested to be further investigated in the future work. To realize the

patterned FePt thin films as commercial recording media, firstly, patterned FePt films with smaller particle size should be fabricated in the future work. Secondly, it should be aimed to achieve perpendicular magnetic anisotropy in the patterned FePt films.